

TR 2005-38

**Uncertainty-based Design Optimization of Structures with
Bounded-But-Unknown Uncertainties**



Uncertainty-based Design Optimization of Structures with Bounded-But-Unknown Uncertainties

Proefschrift

ter verkrijging van de graad van doctor
aan de Technische Universiteit Delft,
op gezeg van de Rector Magnificus Prof.dr.ir. J.T. Fokkema,
voorzitter van het College voor Promoties,
in het openbaar te verdedigen
op dinsdag 13 december 2005 te 10.30 uur
door

Sham Prabhakar GURAV

Master of Technology
in Aerospace Engineering,
Indian Institute of Technology, Madras.
geboren te Rukadi, India.

Dit proefschrift is goedgekeurd door de promotor:
Prof.dr.ir. A. van Keulen

Samenstelling van de promotiecommissie:

Rector Magnificus	voorzitter
Prof.dr.ir. A. van Keulen	Technische Universiteit Delft
Prof.dr. P.J. French	Technische Universiteit Delft
Prof.dr. V.V. Toropov	University of Bradford, UK
Prof.Dr.-Ing.habil. F.J. Barthold	Universität Dortmund, Germany
Prof.dr. G.Q. Zhang	Technische Universiteit Delft
Dr.ir. L.F.P. Etman	Technische Universiteit Eindhoven
Dr.ir. J.F.L. Goosen	Technische Universiteit Delft

Published and distributed by: DUP Science

DUP Science is an imprint of
Delft University Press
P.O. Box 98
2600 MG Delft
The Netherlands
Telephone: +31 15 2785678
Telefax: +31 15 2785706
E-mail: info@library.tudelft.nl

ISBN: 90-407-2617-5

Keywords: Uncertainty, Optimization, Response Surface, Parallel Computing, MEMS

Copyright © 2005 by S.P. Gurav

All rights reserved. No part of the material protected by this copyright notice may be reproduced or utilized in any form or by any means, electronic or mechanical, including photocopying, recording or by any information storage and retrieval system, without written consent of the copyright owner.

Printed in the Netherlands

In memory of my grandfather, Shankar Gurav.



Table of Contents

1	Introduction	1
1.1	Background	1
1.1.1	Design Optimization	1
1.1.2	Uncertainty-based Design Optimization	2
1.2	Research question	3
1.3	Objectives and approach	4
1.4	Outline of the thesis	5
1.5	Guideline for the reader	5
2	Preliminaries	7
2.1	Introduction	7
2.2	Multipoint Approximation Method	7
2.2.1	Introduction	7
2.2.2	Problem formulation	7
2.2.3	Approximate Optimization Problem	8
2.2.4	Response Surface Approximations	8
2.2.5	Move Limit Strategy	9
2.2.6	Gradient Enhanced Response Surface	9
2.3	Bounded-But-Unknown Uncertainties	10
2.4	Anti-optimization	12
2.4.1	Introduction	12
2.4.2	Optimization problem formulation using BBU uncertainties	12
2.4.3	Asymptotic Method	12
2.4.4	Rigorous Anti-optimization	15
2.5	Parallel Computing	15
2.5.1	Introduction	15
2.5.2	Parallel Computing in the MAM setting	16
2.5.3	Parallel Computing Framework	16
3	Enhanced Anti-optimization	19
3.1	Introduction	19
3.2	Multipoint Approximation Method	21
3.3	Uncertainty variables	21
3.4	Bounded-but-unknown uncertainty variables	21

3.5	Clustered Uncertainty Variables	22
3.6	Asymptotic Method	22
3.7	Rigorous Method	23
3.8	Enhanced method	24
3.8.1	Anti-optimization	24
3.8.2	Main optimization	24
3.8.3	Use of database	25
3.9	Example: Corrugated Panel	25
3.9.1	Asymptotic Evaluation of the Corrugated Panel	27
3.9.2	Evaluation of the Corrugated Panel using the Enhanced Method	28
3.10	Discussion and Conclusion	32
3.11	Acknowledgment	32
4	Enhanced Anti-optimization combined with Parallel Computing	33
4.1	Introduction	33
4.2	Method	35
4.2.1	Multipoint Approximation Method	35
4.2.2	Bounded-But-Unknown Uncertainty	38
4.2.3	Anti-optimization	40
4.2.4	Enhanced Anti-optimization	41
4.2.5	Parallel Computing	43
4.3	Examples	45
4.3.1	Ten-Bar-Truss	45
4.3.2	Elastically supported beam	46
4.3.3	Embedded measurement MEMS structure	48
4.4	Discussion/Conclusion	52
4.5	Acknowledgment	52
5	Cycle-based Alternating Anti-optimization	53
5.1	Introduction	53
5.2	Design Optimization	55
5.2.1	Deterministic optimization	55
5.2.2	Uncertainty-based optimization	55
5.3	PZT Energy Reclamation Device Optimization Problem Formulation	58
5.3.1	Objective function	58
5.3.2	Mechanical Constraints	58
5.3.3	Electrical Constraints	59
5.3.4	Design Variables	59
5.3.5	Uncertainties	60
5.3.6	Material properties	60
5.4	Optimization Results	60
5.4.1	Optimization including L/b constraint	61
5.4.2	Optimization excluding L/b constraint	62

5.5	Discussion and Conclusions	63
5.6	Acknowledgment	63
6	Cycle-based Alternating Anti-optimization combined with Nested Parallel Computing	65
6.1	Introduction	65
6.2	Multipoint Approximation Method	67
6.2.1	Introduction	67
6.2.2	Optimization problem formulation	67
6.3	Bounded-But-Unknown Uncertainty	68
6.4	Uncertainty-based optimization using Anti-optimization	69
6.4.1	Anti-optimization	69
6.4.2	Lombardi-Haftka alternating anti-optimization	71
6.4.3	Cycle-based alternating Anti-optimization	71
6.4.4	Combined Cycle-based alternating and Asymptotic method	72
6.4.5	Parallel Computing	73
6.5	Applications	77
6.5.1	Elastically supported beam	77
6.6	Shape Memory Alloy Microgripper Optimization Under Uncertainty	80
6.6.1	Introduction	80
6.6.2	Microgripper model	81
6.6.3	Optimization problem formulation	82
6.6.4	Results	85
6.7	Discussion/Conclusion	90
6.8	Appendix	91
6.8.1	Material Model for Shape Memory Alloy	91
6.8.2	Additional tables	92
6.9	Acknowledgment	92
7	Anti-optimization using Combined Response Surface	93
7.1	Introduction	93
7.2	Multipoint Approximation Method	95
7.3	Bounded-But-Unknown Uncertainty	95
7.4	Uncertainty-based optimization using Anti-optimization	96
7.4.1	Anti-optimization using Combined Response Surface	96
7.5	Micro Piezoelectric Composite Energy Reclamation Device Problem Formulation	98
7.5.1	Introduction	98
7.5.2	Objective function	98
7.5.3	Mechanical Constraints	99
7.5.4	Electrical Constraints	99
7.5.5	Design Variables	99
7.5.6	Uncertainties	100
7.5.7	Material properties	101
7.6	Optimization Results	101

7.7	Discussion and Conclusions	103
7.8	Acknowledgment	103
8	Conclusions and Recommendations	105
8.1	Conclusions	105
8.1.1	Enhanced Anti-optimization	105
8.1.2	Alternating Anti-optimization	106
8.1.3	Combined Response Surface-based anti-optimization	107
8.2	Recommendations	107
8.2.1	Enhanced Anti-optimization	108
8.2.2	Cycle-based Alternating Anti-optimization	108
8.2.3	Combined Response Surface-based anti-optimization	108
8.3	Future work	108
	References	109
	Publications based on present work	113
	Summary	115
	Samenvatting	117
	Acknowledgments	119
	Curriculum Vitae	121

Chapter 1

Introduction

1.1 Background

1.1.1 Design Optimization

General Introduction

These days optimization has become a key aspect in design. This is mainly due to the increasing product requirements and market competition. For example, in automobile and aerospace industries design optimization has become vital. In case of extreme applications, such as space structures, design optimization is playing an important role in order to make such missions feasible. Due to the everlasting revolution in computer hardware and software, computerized tools are becoming more and more popular. Use of analysis software, such as Finite Element Analysis (FEA), has become a common tool in practical design processes. Because of the easy access to large computing power, extension of such computer-based tools to more than just analysis is quite obvious, for example, FEA based automated design optimization.

Several optimization techniques have been under development and are being used for design optimization. To name a few, tools based on genetic algorithms, tools based on response surface techniques, and many many others. Many of these tools require a large number of response evaluations. Because of the underlying use of expensive computational modeling, such techniques may suffer due to limitations on computing power. Due to the so called "curse of dimensionality", this problem can grow exponentially with the increase in design parameters. In addition, growing use of complicated models and nonlinear analysis in order to bring the FEA closer to reality, is making the optimization problem more and more computationally intensive. In such situations, approaches that make use of approximations in order to reduce the required FEAs are mandatory. The Multipoint Approximation Method which is based on Response Surface (RS) approximation is quite suitable for use in design optimization of practical applications.

Multipoint Approximation Method

In general, design optimization involves evaluation of response functions. Quite often these response functions are evaluated numerically using methods such as FEA. From optimization point of view, application of computational modeling can either suffer from numerical noise or the large computational times involved. In this situation direct coupling between optimizer and FEA can be disadvantageous. Here approximations to the actual response functions, which are generally explicit and very computationally inexpensive, can be used instead. Several techniques based on approximations are available in literature.

In the present thesis, the Multipoint Approximation Method (MAM), which is based on response surface approximations, is used as a basis. The MAM is presented in detail in Toropov *et al.* [1, 2] and Van Keulen and Toropov [3, 4]. A MAM-based framework for the optimization of practical

applications is described in detail in Jacobs *et al.* [5]. The main advantage in using the MAM is a reduction in computational costs and its insensitivity to noisy responses due to numerical inaccuracies, Van Keulen and Toropov [3,4]. The MAM is based on solving a sequence of approximate optimization problems. Each individual approximate optimization problem involves a mathematical programming problem using computationally inexpensive explicit functions for responses. This may result in a substantial reduction of overall computational costs. The detailed description of the MAM is given in the Preliminaries, see Chapter 2.

1.1.2 Uncertainty-based Design Optimization

Uncertainties in Structures

In general design practice, one faces the problem of uncertainties of various kinds. Some uncertainties are inherent or irreducible and have, for example, a physical origin. These type of uncertainties are also termed as aleatory uncertainties, Oberkampf *et al.* [6]. Typical examples of such uncertainties may represent loading conditions or variations in material properties. Other types of uncertainties are of different nature and can be influenced by the designer. These uncertainties, also termed as epistemic uncertainties by Oberkampf *et al.* [6], originate from the lack of information or impreciseness. A typical example is provided by manufacturing induced inaccuracies, for example in dimensions of Micro Electro Mechanical Systems (MEMS). Here, by adopting a more expensive manufacturing process or accepting higher rejection rates, the designer can influence the level of uncertainty to a certain extent.

The methods to tackle various types of uncertainties can be classified mainly in three different ways, namely probabilistic approach, fuzzy-sets-based approach, and the anti-optimization (Elishakoff *et al.* [7]). These approaches differ in the way they deal with uncertainties. Probabilistic techniques have been developed mainly to deal with random uncertainties described using statistical distributions, fuzzy-sets-based techniques originated from the vague or qualitative description of uncertainties, and anti-optimization is developed to tackle bounded uncertainties with no information on how these uncertainties vary within bounds. Probabilistic techniques typically attempt to ensure a certain amount of reliability of the structure, i.e. to make sure that the structure's response will remain below the limiting values with given probability. Fuzzy-sets-based techniques use membership function to describe uncertain variables resulting in an interval of confidence for the response at each level of the membership function. Anti-optimization accounts for the worst possible response of the structure, thus ensuring that the failure due to violation of a limit state will never occur.

Generally, fuzzy-sets-based techniques are used when uncertainties are either vague or can only be described linguistically. On the otherhand, in case of probabilistic techniques, when sufficient statistical data is available, the uncertainties can be represented by means of probabilistic distributions, Elishakoff [8]. However, probabilistic techniques require an abundance of experimental data, Elishakoff [9]. Additionally, probabilistic techniques may suffer from large errors in the computed probability of failure even with small inaccuracies in the statistical data, Elishakoff [9]. Moreover, the impreciseness of information increases with the increase in complexity of structures, Bae *et al.* [10]. In the present thesis, the case of uncertainties with bounds is considered and the associated anti-optimization technique is studied in detail.

Bounded-But-Unknown Uncertainties

As mentioned in the foregoing, in the present thesis, uncertainties are represented using the Bounded-But-Unknown (BBU) description. Typically, upper and lower bounds are specified on uncertainties, whereas the distribution within these bounds is unknown. Thus, uncertainties can be identified as belonging to some closed sets, i.e. to be of Bounded-But-Unknown (BBU) nature, Ben-Haim and Elishakoff [11] and Ben-Haim [12]. Many times, for example in preliminary design phases, even

though some experimental data is available, it is not enough to construct reliable probability distributions. However, the available data can be used, particularly in combination with engineering experience, to set tolerances or bounds on uncertainties.

Anti-optimization

To tackle optimization with BBU uncertainties, the so-called *anti-optimization* technique proposed by Elishakoff *et al.* [7] is used in the present thesis. In this technique, uncertainty-based optimization is basically split in two parts, namely, main- and anti-optimization. The main optimization is a standard optimization (minimization) problem, which searches for the best design in the design domain. The design domain is typically specified by upper- and lower limits on design variables. The anti-optimization consist of performing numerical searches for the combination of uncertainties, which yields the worst response for a given design and a particular response function. In the worst case scenario, an anti-optimization for every constraint is required. Within these anti-optimizations, the uncertainties are set as "design variables", whereas the "design domain" is specified by the bounds on the uncertainties. Thus, anti-optimizations are nested within the main optimization.

In the anti-optimization technique discussed in Elishakoff *et al.* [7], the anti-optimization consists of a systematic search along the vertices of the uncertainty domain for obtaining the worst combination of uncertainties. This makes the technique computationally efficient, but limits its application to convexity in terms of uncertainties. Often when response evaluation involves complicated FEA, for example multiphysics problems or problems involving nonlinearities, the dependency of responses on uncertainties is highly nonlinear. In such practical cases, the worst set of uncertainties may fluctuate from design to design. Moreover, interior worst cases can be found in such cases, i.e. the worst setting of uncertainties is not found as one of the vertices. For such problems, vertex checking would not be enough, rather it is essential to have a more general technique that can handle such non-convexities.

1.2 Research question

In the present thesis, it is assumed that there is no statistical data available for describing uncertainties and the uncertainties are of the BBU type. Here, the anti-optimization technique is used to tackle BBU uncertainties. On this basis, the following research questions are studied

- How to generalize the anti-optimization technique such that it can handle convex as well as non-convex uncertainties?
- How to make the anti-optimization technique computationally efficient and feasible for practical applications?

The first question deals with the generalization of anti-optimization techniques such that convexity and nonconvexity in the uncertainties can be handled easily. In case of the anti-optimization technique, the anti-optimization is nested within the main optimization. This makes it a two level optimization problem. In general, the optimization procedure needs several iterations before convergence. Each iteration involves evaluation of response functions. If these response evaluations require computationally expensive numerical calculations, then the whole optimization becomes computationally quite intensive. This problem grows exponentially with the increase in the number of design variables and uncertainties. Consequently, the anti-optimization technique involving two-level optimization can become very computationally intensive with the increase in the number of design variables as well as uncertainties. Therefore, the second research question mainly deals with the overall efficiency of the method.

1.3 Objectives and approach

Based on the research questions, the research objectives are set as follows:

- Develop a general framework that can handle convex as well as non-convex uncertainties, when there is no statistical data available except bounds on them.
- Reduce the number of computationally expensive response function evaluations required in the anti-optimization by making use of sensitivities and smart techniques such as using a database.
- Develop a Parallel Computing framework, which can be used in combination with the anti-optimization technique to spread the computational burden involved.
- Study alternative approaches for anti-optimization in order to develop computationally efficient technique.

To meet the first objective, the anti-optimization technique based on vertex checking (Elishakoff *et al.* [7]), is extended in the present thesis to a full or rigorous search on the uncertainty domain (Van Keulen *et al.* [13]). This requires a two-level optimization approach, where anti-optimization for each of the constraints is carried out for every design within the main optimization. This generalized or *Rigorous* anti-optimization technique can deal with large and non-convex uncertainties safely. However, the required number of computationally expensive function calls may become a big obstacle. In the present thesis, this *Rigorous* technique is enhanced to make it computationally efficient.

The second objective is motivated by the need for a reduction of the number of computationally expensive response function evaluations used in the *Rigorous* anti-optimization technique. In the present thesis, the *Rigorous* anti-optimization technique is enhanced by incorporating sensitivities and a database technique. In many cases of computational response analysis, gradient information can often be obtained at a fraction of the computing time as compared to the analysis itself, van Keulen *et al.* [14] and van Keulen and de Boer [15, 16]. This sensitivity information can be used in addition to the function values to construct, for example, Gradient Enhanced Response Surfaces (GERS), van Keulen and Vervenne [17, 18]. This incorporation of sensitivities can improve the quality of the response surface approximations thus improving the convergence. Alternatively, fewer response evaluations may be required to construct the response surface approximations. Consequently, using derivative information may decrease the total number of function evaluations and hence may speed up the optimization process. In addition, the anti-optimization technique is further modified to use a database technique. For this purpose, the worst sets of uncertainties obtained by the anti-optimizations are stored in a database. When there is enough data available in the database, it is used to create good starting points for the anti-optimizations. Often this can speed up the anti-optimizations significantly.

The third objective is motivated by the need for parallel evaluation in case of practical applications involving computationally expensive response evaluations. The total number of response evaluations required by the anti-optimization technique can be reduced substantially with the enhanced (sensitivities + database) anti-optimization, however, only a limited reduction can be obtained. In case of practical applications, where response evaluation is carried out using, e.g., FEA, even with these improvements the anti-optimization technique may become impractical. Use of Parallel Computing can be a solution here. Nowadays, the use of a number of powerful computers, forming a cluster, is quite common. Such computer clusters can be used to evaluate different configurations in parallel to speed up the optimization. In the present thesis, a framework for using Parallel Computing in the anti-optimization technique is developed.

The fourth objective looks at alternative formulations of the anti-optimization technique. This includes an alternating anti-optimization and a combined response surface approach. In a approach

proposed by Lombardi and Haftka [19], instead of nesting anti-optimization within the main optimization, main and anti-optimization are carried out alternately. Inspired by Lombardi and Haftka technique, a slightly modified technique, referred to as *cycle-based* alternating anti-optimization in Gurav *et al.* [20], is studied in this thesis. In this technique, anti-optimization is carried out only at the sub-optimal point, i.e. the point obtained at the end of each cycle of the main optimization. Thus, it can save a lot of intermediate response evaluations and speeds up the technique significantly. In a separate approach, a Combined Response Surface (CRS) for design variables as well as uncertainties is used as a basis for the anti-optimization. A similar approach is used by Qu *et al.* [21] for the reliability-based optimization of composite laminates with random uncertainties. This CRS-based anti-optimization technique is studied in the present thesis.

In the present thesis, the algorithms developed to carry out uncertainty-based design optimization are first studied on the basis of test examples from literature in order to compare them with existing techniques. Then, these techniques are applied to various practical applications. The latter include uncertainty-based design optimization of a car deck floor of a ferry, an embedded measurement MEMS structure, a micro piezoelectric composite energy reclamation device, and a Shape Memory Alloy (SMA) microgripper. This variety of practical problems demonstrates the applicability of present techniques to wide range of practical problems.

1.4 Outline of the thesis

The present thesis consists of eight chapters. Chapter 2 gives the detailed preliminaries for the optimization techniques used in the present research. It will serve as a basis for the remaining chapters. Chapter 3 till Chapter 7 discuss developments in the anti-optimization technique together with various applications. Chapter 3 discusses the modifications to the anti-optimization technique combining sensitivities and a database technique. The enhanced anti-optimization technique is applied to the uncertainty-based design optimization of a car deck floor of a ferry. In Chapter 4, enhanced anti-optimization is combined with parallel computing. In this chapter the technique is applied first to the test examples from literature. Then uncertainty-based design optimization of an embedded measurement MEMS structure is carried out. Chapter 5 proposes a different approach in order to save computational efforts. In this approach, alternating anti-optimization is used instead of nesting it within the main optimization. Uncertainty-based design optimization of a micro piezoelectric energy reclamation device using cycle-based alternating anti-optimization is studied in Chapter 5. In Chapter 6, the cycle-based anti-optimization technique is combined with nested parallel computing in order to improve the computational efficiency. The technique is studied on the basis of a shape memory alloy micro gripper problem. The anti-optimization is carried out using a combined response surface technique in Chapter 7. Finally, the conclusions of the present research work and recommendations for future work are presented in Chapter 8.

1.5 Guideline for the reader

The thesis is divided mainly into three parts: Part I consists of Chapter 1 and 2, the development of the methods is discussed in Part II (Chapters 3-7). Part III contains conclusion and recommendations (Chapter 8) and summary (English and Dutch). Part I serves as the basis for remaining chapters. Part II discusses the development of the method together with some applications. Chapters 3-7 are written on the basis of journal publications and/or contributions to conference proceedings. These chapters are self-contained and can be read independently. However, this may cause repetition of some of the contents. The author apologizes for this inconvenience.

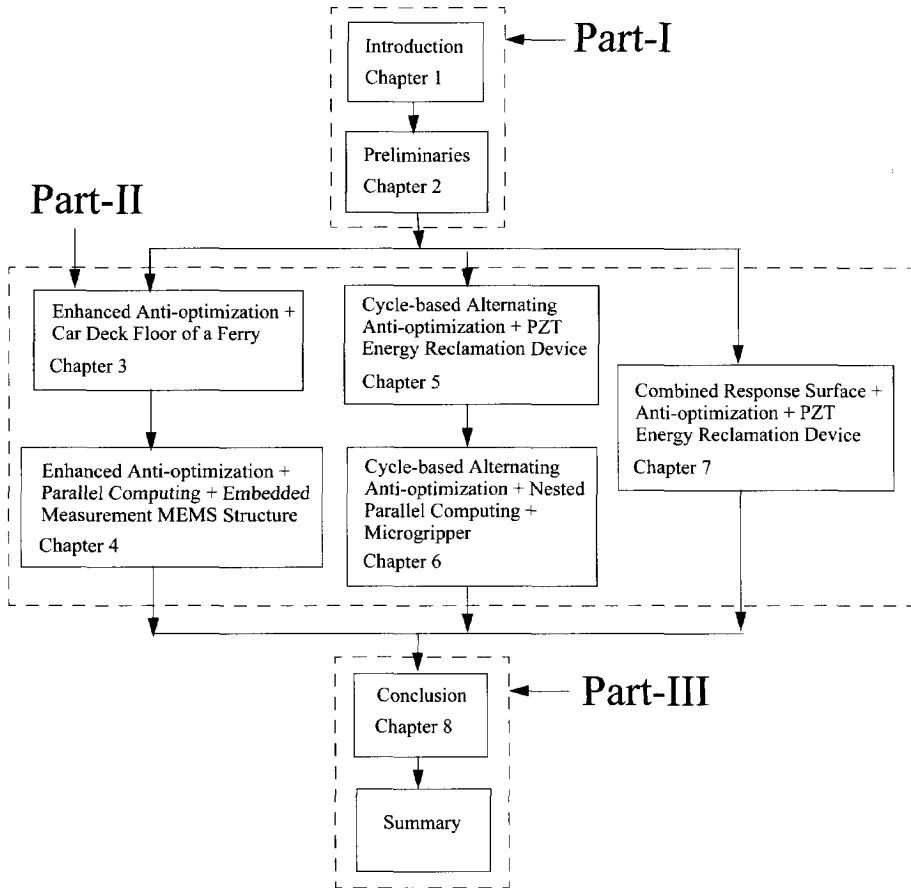


Figure 1.1: Outline of the thesis.

Chapter 2

Preliminaries

2.1 Introduction

This chapter describes preliminaries, which are prerequisite for subsequent chapters. In this chapter, the Multipoint Approximation Method (MAM) Section 2.2, Bounded-But-Unknown (BBU) Uncertainties Section 2.3, Anti-optimization technique Section 2.4, and Parallel Computing Section 2.5 are discussed in detail.

2.2 Multipoint Approximation Method

2.2.1 Introduction

In the present paper the Multipoint Approximation Method (MAM) is used as a basis for optimization. Many practical applications involve numerical evaluation of response functions. From an optimization point of view, this type of problem can either suffer from numerical noise or the large computational time involved. The MAM, which is based on sequential application of Response Surface Methodology, see the textbooks Khuri and Cornell [22] and Myers and Montgomery [23], can be applied to such problems. The interested reader is referred to the studies by Toropov *et al.* [1, 2] and Van Keulen and Toropov [3, 4]. The MAM uses a sequence of approximations to reduce the number of expensive numerical response evaluations. However, it should be noted here, that it suffers from the so-called curse of dimensionality. It becomes inefficient with the increase in dimensions (number of design variables). A MAM-based framework for the optimization of practical applications is described in detail in Jacobs *et al.* [5]. A detailed description of the MAM is given in the remainder of this section.

2.2.2 Problem formulation

Designing a structure implies that a design concept has to be selected, which subsequently has to be optimized. The latter involves the selection of design variables, which determine, among other features, the dimensions, shapes and materials. This set of n design variables is denoted as \mathbf{x} , with

$$\mathbf{x} = (x_1 \dots x_n). \quad (2.1)$$

Throughout the present paper, it is assumed that all design variables are continuous.

The behavior of the structure is described by the response functions, which depend on the design variables. These response functions are denoted as \mathbf{f} , with

$$\mathbf{f} = (f_1 \dots f_m)^T. \quad (2.2)$$

The response function may reflect, for example, weight, cost, buckling loads, maximum equivalent stress, or strain levels.

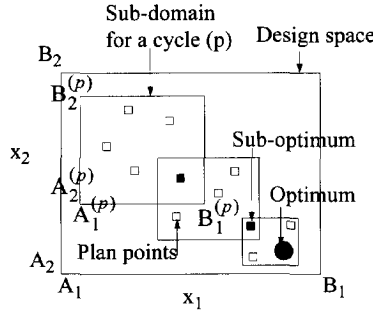


Figure 2.1: Optimization using the MAM for a problem of two design variables (x_1 and x_2).

The optimization problem can now be formulated mathematically as

$$\begin{aligned} \min_{\mathbf{x}} \quad & f_o(\mathbf{x}) \\ \text{s.t.} \quad & f_i(\mathbf{x}) \leq 1, \quad i = 1, \dots, m, \\ & A_j \leq x_j \leq B_j, \quad j = 1, \dots, n. \end{aligned} \quad (2.3)$$

Here, f_o is the objective function and f_i are constraints, whereas \mathbf{x} is a set of design variables. The design space is defined by A_j and B_j , upper and lower limits on x_j respectively, see Fig. 2.1.

2.2.3 Approximate Optimization Problem

The MAM replaces the actual optimization problem, as described by Eq. (2.3), by a sequence of approximate optimization problems. The approximate optimization problem (AOP) for a cycle p , can be formulated as

$$\begin{aligned} \min_{\mathbf{x}} \quad & \tilde{f}_o^{(p)}(\mathbf{x}) \\ \text{s.t.} \quad & \tilde{f}_i^{(p)}(\mathbf{x}) \leq 1, \quad i = 1, \dots, m, \\ & A_j^{(p)} \leq x_j \leq B_j^{(p)}, \quad j = 1, \dots, n, \\ & A_j^{(p)} \geq A_j, \quad B_j^{(p)} \leq B_j. \end{aligned} \quad (2.4)$$

Here, the response functions are replaced by approximate functions over the sub-domain for a cycle. Hence, $\tilde{f}_i^{(p)}(\mathbf{x})$ are considered as adequate approximations of $f_i(\mathbf{x})$ over the sub-domain (p) represented by the move limits $A_j^{(p)}$ and $B_j^{(p)}$, see Fig. 2.1, for the current AOP. It should be noted here that, the move limits for the initial cycle ($A_j^{(0)}$ and $B_j^{(0)}$), can be chosen either arbitrarily or based on engineering experience. Many times this can significantly influence the convergence. For example, if the initial move limits include the optimum, then the optimization may converge quite rapidly.

2.2.4 Response Surface Approximations

The MAM relies on response surface approximations of the true responses in order to limit the number of expensive numerical evaluations. Typically, inexpensive-to-evaluate explicit approximations are used. To construct the approximate response surfaces, first a plan of numerical experiments is generated in the sub-domain of the current cycle, see Fig. 2.1. In the present study, space filling technique is used for generating plans of experiments, for details see Toropov *et al.* [2] and Van Keulen and Toropov [3, 4]. Approximate response surfaces are fitted through the numerical evaluations of plan points using a weighted least squares (WLS) method, see Toropov *et al.* [2] and Van Keulen

and Toropov [3, 4], that is

$$\min_{\beta} \sum_{s=1}^S w_i^s \left[f_i(\mathbf{x}_s) - \tilde{f}_i^{(p)}(\mathbf{x}_s) \right]^2, \quad (2.5)$$

$$\text{with } \tilde{f}_i^{(p)}(\mathbf{x}_s) = f_i^{(p)}(\mathbf{x}_s)\beta_i, \quad i = 0, \dots, m,$$

where s represents a plan point and S is the total number of plan points in the current plan of experiments. Here, $\tilde{f}_i^{(p)}(\mathbf{x}_s)$ represent the response surface approximations for the true functions $f_i(\mathbf{x}_s)$ over the current sub-domain (p), whereas $f_i^{(p)}(\mathbf{x}_s)$ contains the approximation functions and β_i represent corresponding regression coefficients, see Khuri and Cornell [22] and Myers and Montgomery [23]. Moreover, it has been assumed that the approximations are linear in the regression coefficients. In the minimization problem, β_i , which are unknowns, are used as tuning parameters in order to get the approximations $\tilde{f}_i^{(p)}(\mathbf{x})$, as close as possible to the true functions $f_i(\mathbf{x})$. The weight factors w_i , used here to combine the data from different points in the WLS method, reflect the relative importance of the function values (and their derivatives if available) to the optimization process. The selection of the weight factors is made based on mainly the objective function value and the location of a plan point relative to the boundary between feasible and infeasible design space. This selection of the weight factors, affects significantly the efficiency of the method, see for details Van Keulen and Toropov [4] and Toropov *et al.* [2].

2.2.5 Move Limit Strategy

At the end of every optimization cycle the Move limit strategy checks, if the solution has converged and if not, it defines the AOP for the next cycle. Here, the approximate optimum (sub-optimum), obtained by solving the nonlinear minimization programming (NMP) for the current AOP given by Eq. (2.4), is evaluated for the true response. In order to define the location and size of the sub-domain for the next cycle, several indicators are computed based on the assessment of the current sub-optimum, see for details Van Keulen and Toropov [4]. The procedure is summarized here shortly.

The first indicator is based on the largest relative error in the approximations for the sub-optimum. Depending on this indicator, the approximations are termed as "bad", "average" or "good". The second indicator is based on the location of the sub-optimum in the sub-domain for the current cycle. When none of the current movelimits is active, the solution is considered "internal", or otherwise "external". The next two indicators are based on the angle between the move vectors of the last two sub-optimums. Depending on this the movement of the optimum is termed as "straight", "curved", "backward" or "forward". The fifth indicator denotes the size of the current sub-domain as "small" or "large" and is used in the termination criteria. Depending on the most active constraint value, the sixth indicator labels the current solution as "close" or "far" from the boundary of the feasible and infeasible regions of the design space.

A factor to resize the current sub-domain is chosen based on these indicators. For example, if the quality of the approximations is "bad", then the size of the sub-domain will be reduced and *vice versa*. Furthermore, the reduction factor changes depending on the move direction, such as in case of the "curved" move, higher reduction is expected. Similarly, if the solution is indicated as "close", the sub-domain will be reduced substantially. In case of "internal" solution, if the size of the sub-domain is "small", then the optimization is terminated. A detailed description of the move limit strategy is given in Van Keulen and Toropov [4]. The whole process is repeated until convergence.

2.2.6 Gradient Enhanced Response Surface

In case both function and derivative values are available, then Gradient Enhanced Response Surfaces (GERS) have been constructed using both data entities as discussed in Van Keulen and Vervenne

[17]. Derivative information can often be obtained at a fraction of the computing time as compared to the analysis itself, see van Keulen *et al.* [14] and van Keulen and de Boer [15, 16]. Use of sensitivities can benefit the optimization in two ways. First, it can improve the quality of the response surfaces affecting the convergence. Second, fewer response evaluations may be required to construct the approximations resulting in a reduction in the total number of function evaluations. This is particularly advantageous when higher order approximations are used. Alternatively, it can allow the inclusion of more design variables in the optimization. The technique used for the construction of GERS using both the function values and the design sensitivities, is described in detail in Van Keulen and Vervenne [17]. A short summary is included here for self-containment.

The response function (f_{0j}) and the corresponding derivatives (f_{ij}) associated with the point \mathbf{x}_j are given here as

$$\begin{aligned} f_{0j} &= f_0(\mathbf{x}_j), \\ f_i &= \frac{\partial f_0}{\partial x_i}, \\ f_{ij} &= f_i(\mathbf{x}_j), \end{aligned} \quad (2.6)$$

where $i = 1, \dots, n$ and $j = 1, \dots, S$. These are represented using a compact notation as

$$\mathbf{y}_j = [f_{0j} \dots f_{nj}], \quad j = 1, \dots, S. \quad (2.7)$$

The response surfaces for function and derivatives are represented as

$$\begin{aligned} \tilde{f}_0 &= f_0(\mathbf{x})\boldsymbol{\beta}, \\ \tilde{f}_i &= \frac{\partial \tilde{f}_0}{\partial x_i} = f_i(\mathbf{x})\boldsymbol{\beta}, \quad i = 1, \dots, n, \end{aligned} \quad (2.8)$$

where $f_i(\mathbf{x})$ contains approximation functions and $\boldsymbol{\beta}$ denote corresponding regression coefficients, which are to be determined, see Khuri and Cornell [22] and Myers and Montgomery [23]. Thus, the response surface approximations for the response function and derivatives are given as

$$\begin{aligned} \tilde{\mathbf{y}}_j &= [\tilde{f}_{0j} \dots \tilde{f}_{nj}], \quad j = 1, \dots, S \\ &= [f_0(\mathbf{x}_j) \dots f_n(\mathbf{x}_j)]\boldsymbol{\beta} \\ &= \mathbf{F}_j\boldsymbol{\beta}. \end{aligned} \quad (2.9)$$

The error in the actual function value and derivatives (\mathbf{y}_j) and the corresponding approximations ($\tilde{\mathbf{y}}_j$) can be given as

$$\mathbf{r}_j = \tilde{\mathbf{y}}_j - \mathbf{y}_j = \mathbf{F}_j\boldsymbol{\beta} - \mathbf{y}_j, \quad j = 1, \dots, S. \quad (2.10)$$

The norm of the error using WLS method, in order to combine all the errors with different weights assigned to them, can be given as

$$e_j^2 = \langle \mathbf{r}_j; \mathbf{r}_j \rangle = \mathbf{r}_j^T \mathbf{W}_j \mathbf{r}_j, \quad j = 1, \dots, S, \quad (2.11)$$

where \mathbf{W}_j is a matrix of weight coefficients, see Van Keulen and Vervenne [17]. The unknown parameters $\boldsymbol{\beta}$ are determined as the minimizers of the total error as

$$\min_{\boldsymbol{\beta}} e^2 = \sum_{j=1}^S e_j^2. \quad (2.12)$$

2.3 Bounded-But-Unknown Uncertainties

If the problem at hand is non-deterministic, i.e. there are uncertainties that play a non-negligible role, the response functions also depend on the uncertainties. The set of uncertainty variables will be denoted $\boldsymbol{\alpha}$, with

$$\boldsymbol{\alpha} = (\alpha_1 \dots \alpha_u). \quad (2.13)$$

Consequently, the response functions depend on both design variables and uncertainties, hence $f(\mathbf{x}, \boldsymbol{\alpha})$.

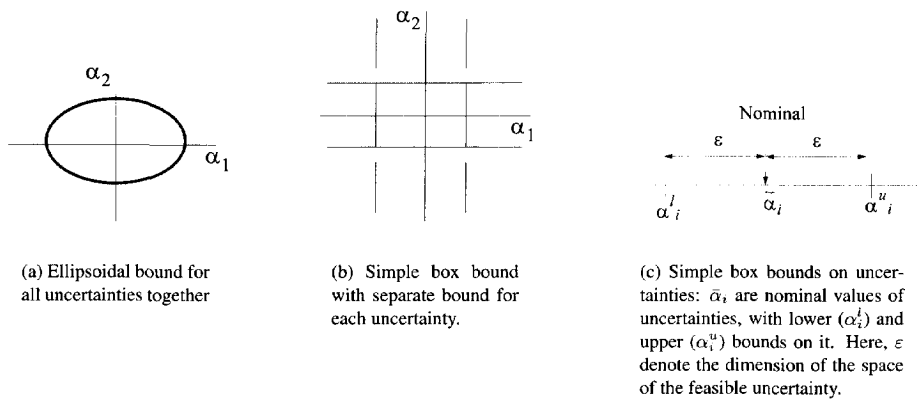


Figure 2.2: Bounds on uncertainties.

In the present paper, uncertainties are modeled using BBU approach. In this, several bounds can be introduced, each providing a bound for a group of uncertainty variables or all uncertainty variables simultaneously, for example see Fig. 2.2. At the same time we may want to measure the amount of uncertainty. Thus, measures for the dimensions of the subspace containing all possible selections of uncertainty variables are desired. This can be cast into a mathematical framework as follows. Assuming a set with b bounds, then a possible or *feasible* selection of $\boldsymbol{\alpha}$ satisfies, see Van Keulen *et al.* [13];

$$B_i(\boldsymbol{\alpha}, \boldsymbol{\varepsilon}) \leq 0, \quad \text{for } i = 1, \dots, b. \quad (2.14)$$

Otherwise the selection of the uncertainty variables $\boldsymbol{\alpha}$ is *infeasible*.

In the present paper, simple box bounds, see Fig. 2.2(b & c), are used to specify uncertainties as

$$(\alpha_i - \bar{\alpha}_i)^2 - \varepsilon^2 \leq 0. \quad (2.15)$$

These type of bounds generally come from a tolerance specified on a nominal value, for example, due to the manufacturing induced inaccuracies. These bounds can be alternatively represented in terms of lower (α_i^l) and upper bounds (α_i^u) on uncertainties as

$$\begin{aligned} \alpha_i^l &= \bar{\alpha}_i - \varepsilon, \\ \alpha_i^u &= \bar{\alpha}_i + \varepsilon. \end{aligned} \quad (2.16)$$

Here, the components of $\boldsymbol{\varepsilon}$ are used to specify the dimensions of the space of feasible uncertainty variables. We will therefore refer to these components as the *levels of uncertainty*. Here, the components of $\boldsymbol{\varepsilon}$ are used to specify the dimensions of the space of feasible uncertainty variables. We will therefore refer to these components as the *levels of uncertainty*. As we use these levels of uncertainties to describe the dimensions of a space, each of the components will be non-negative, i.e.

$$\varepsilon_j \geq 0, \quad \text{for } j = 1, \dots, r. \quad (2.17)$$

Note that the number of components of $\boldsymbol{\varepsilon}$, r , is not necessarily equal to the number of bounds, b , being introduced.

It seems natural to assume that if the dimensions of the space of uncertainty variables have become zero, the uncertainty variables become deterministic. In other words, if $\boldsymbol{\varepsilon} = \mathbf{0}$ then there is

only a single solution $\alpha = \bar{\alpha}$ such that

$$B_i(\bar{\alpha}, \mathbf{0}) \leq 0, \quad \text{for } i = 1, \dots, b. \quad (2.18)$$

Moreover, for $\alpha = \bar{\alpha}$ the equal sign holds true.

2.4 Anti-optimization

2.4.1 Introduction

In order to anticipate the effect of uncertainties on the response of structure, the anti-optimization technique determines the worst-case scenario for the response. It basically checks the response of the structure for the worst possible combination of uncertainties in order to ensure that the structure will not fail for any combination of uncertainties. In the technique, uncertainty-based optimization is basically split in two parts, namely, main- and anti-optimization. The main optimization is treated as a standard minimization problem, which searches for the best design in the design domain, whereas the anti-optimization consist of performing numerical searches for the combination of uncertainties, which yields the worst response for a given design and a particular response function. In the worst case scenario, an anti-optimization for every constraint is required.

2.4.2 Optimization problem formulation using BBU uncertainties

The anti-optimization problem using BBU uncertainties can be formulated mathematically as:

$$\begin{aligned} \min_{\mathbf{x}} \quad & f_o(\mathbf{x}) \\ \text{s.t.} \quad & f_i(\mathbf{x}; \alpha_i^*) \leq 1, \quad i = 1, \dots, m, \end{aligned} \quad (2.19)$$

where α_i^* is the maximizer of

$$\begin{aligned} \max_{\alpha_i} \quad & f_i^*(\mathbf{x}; \alpha_i) \\ \text{s.t.} \quad & B_j(\alpha_i, \varepsilon) \leq 0, \quad j = 1, \dots, b. \end{aligned} \quad (2.20)$$

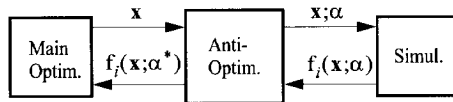


Figure 2.3: Anti-optimization Technique: Anti-optimization is carried out at every design (\mathbf{x}) for each constraint (f_i) to obtain corresponding worst set of uncertainties (α^*).

Here, $f_o(\mathbf{x})$ is the objective function and $f_i(\mathbf{x}, \alpha_i)$ are constraints, whereas $B_j(\alpha_i, \varepsilon)$ are bounds on uncertainties. The minimization as defined in Eq. (2.19) will be referred to as the main optimization. Notice that, in general, the evaluation of the constraints involves, for each set of design variables, anti-optimization of the individual constraints. This anti-optimization is reflected by Eq. (2.20). The anti-optimization technique as represented by Eq. (2.19) and Eq. (2.20) is depicted in Fig. 2.3

2.4.3 Asymptotic Method

The anti-optimization (Eq. (2.20)) to find the worst response for a given design is approximated in this method with the use of Taylor series. This approximation limits the applicability of the technique to the problems with uncertainties of small magnitude. Nevertheless it provides computationally efficient way for the worst estimation of uncertainties.

Approximate bounds

The first approximations that will be introduced are related to the bounds (\mathbf{B}). As a basis for these approximations we develop the bounds around the nominal uncertainties ($\alpha = \bar{\alpha}, \varepsilon = 0$), where $\bar{\alpha}$ refers to the values of uncertainty variables if the levels of uncertainty have become zero. Introducing $\Delta\alpha = \alpha - \bar{\alpha}$ leads to

$$B_i(\alpha, \varepsilon) = \bar{B}_i + \frac{\partial \bar{B}_i}{\partial \varepsilon_k} \Delta \varepsilon_k + \frac{\partial \bar{B}_i}{\partial \alpha_k} \Delta \alpha_k + \frac{1}{2} \frac{\partial^2 \bar{B}_i}{\partial \alpha_k \partial \alpha_l} \Delta \alpha_k \Delta \alpha_l + \frac{\partial^2 \bar{B}_i}{\partial \alpha_k \partial \varepsilon_l} \Delta \alpha_k \Delta \varepsilon_l + \frac{\partial^2 \bar{B}_i}{\partial \varepsilon_k \partial \varepsilon_l} \Delta \varepsilon_k \Delta \varepsilon_l + \dots, \quad (2.21)$$

here the over bar denotes evaluation for $\alpha = \bar{\alpha}$ and $\varepsilon = 0$. Note, that summation convention has been applied for repeated indices. As for ($gv\alpha = \bar{\alpha}, \varepsilon = 0$) the equal sign in Eq. (2.18) holds true, the first term in the right hand side of Eq. (2.21) is zero. In many cases the bounds \mathbf{B} will be constructed in such a way that mixed derivatives, for example $\frac{\partial^2 \bar{B}_i}{\partial \alpha_k \partial \varepsilon_l}$, become also zero. This restriction will also be adopted here, leading to

$$B_i(\alpha, \varepsilon) = \frac{\partial \bar{B}_i}{\partial \varepsilon_k} \Delta \varepsilon_k + \frac{\partial^2 \bar{B}_i}{\partial \varepsilon_k \partial \varepsilon_l} \Delta \varepsilon_k \Delta \varepsilon_l + \frac{\partial \bar{B}_i}{\partial \alpha_k} \Delta \alpha_k + \frac{\partial^2 \bar{B}_i}{\partial \alpha_k \partial \alpha_l} \Delta \alpha_k \Delta \alpha_l \dots \quad (2.22)$$

We shall now introduce another simplification. As we have stated that for $\varepsilon = 0$, there is only a single solution which satisfies Eq. (2.18), it is for most cases correct to take $\frac{\partial \bar{B}_i}{\partial \alpha_k} = 0$. If there is only a single bound or several bounds that each depend on a different set of uncertain variables, then this simplification seems justified. If several bounds are functions of (partially) the same uncertain variables, then this simplification may not be valid. After having adopted the foregoing simplification and retaining the most important terms in Eq. (2.22), $B_i(\alpha, \varepsilon)$ can be approximated by

$$B_i(\alpha, \varepsilon) = \frac{1}{2} \Delta \alpha^T J_i \Delta \alpha - \mathbf{g}_i^T \varepsilon \quad (2.23)$$

with

$$J_i = \begin{pmatrix} \frac{\partial^2 \bar{B}_i}{\partial \alpha_1 \partial \alpha_1} & \dots & \frac{\partial^2 \bar{B}_i}{\partial \alpha_1 \partial \alpha_u} \\ \vdots & & \vdots \\ \frac{\partial^2 \bar{B}_i}{\partial \alpha_u \partial \alpha_1} & \dots & \frac{\partial^2 \bar{B}_i}{\partial \alpha_u \partial \alpha_u} \end{pmatrix} \quad (2.24)$$

and

$$\mathbf{g}_i^T = \left(-\frac{\partial \bar{B}_i}{\partial \varepsilon_1}, \dots, -\frac{\partial \bar{B}_i}{\partial \varepsilon_r} \right). \quad (2.25)$$

If all bounds are functions of different sets of uncertainties, then, since $gv\alpha = \bar{\alpha}$ is a unique solution of Eq. (2.18) for $\varepsilon = 0$, the matrices J_i must be positive semi-definite. In the subspace of uncertainties that affect a single bound, the latter can be interpreted as an ellipsoid with the coordinates of its center determined by $\bar{\alpha}$. To stress this type of interpretation we introduce

$$R_i^2 = 2\mathbf{g}_i^T \varepsilon \quad (2.26)$$

and the approximate bounds can be written as

$$B_i(\alpha, \varepsilon) = \frac{1}{2} (\Delta \alpha^T J_i \Delta \alpha - R_i^2). \quad (2.27)$$

The representation of the bounds as given by Eq. (2.27) has been constructed on the basis of a series of assumptions and approximations as outlined above. It may be that a particular problem does not permit the application of this simplified bounds. However, for many cases the approximate representation Eq. (2.27) will be adequate and becomes exact for linear dependencies. In the sequel of this paper we shall restrict ourselves to those cases for which Eq. (2.27) is adequate. Moreover, we shall, as discussed above, also assume that the matrices J_i are all positive semi-definite.

Linearizing of response functions

Approximation for responses is constructed here using Taylor series around $gv\alpha = \bar{\alpha}$ for a given design $v\alpha$. These Taylor series read

$$\Delta f_i = \frac{\partial \bar{f}_i}{\partial \alpha_k} \Delta \alpha_k + \frac{1}{2} \frac{\partial^2 \bar{f}_i}{\partial \alpha_k \partial \alpha_l} \Delta \alpha_k \Delta \alpha_l + \dots, \quad (2.28)$$

with

$$\Delta f_i = f_i(\mathbf{x}, \boldsymbol{\alpha}) - \bar{f}_i = f_i(\mathbf{x}, \boldsymbol{\alpha}) - f_i(\mathbf{x}, \bar{\boldsymbol{\alpha}}) \quad (2.29)$$

It is important to emphasize that it is not always possible to construct the above Taylor series. This is, for example, the case when a response function is continuous but its derivatives are discontinuous. If the above Taylor series can be created, then first-order approximations for the response functions are obtained by dropping all higher-order terms, giving

$$\Delta f_i = \frac{\partial \bar{f}_i}{\partial \alpha_k} \Delta \alpha_k. \quad (2.30)$$

It is important to realize that the derivatives of the response functions with respect to the uncertain variables are relatively inexpensive to calculate, provided efficient algorithms for sensitivity analysis are available.

Approximate maximization problem

Combination of the approximations for the bounds and the response functions, which are given by Eq. (2.27) and Eq. (2.30), respectively, leads to the maximization problem

$$\begin{aligned} \max_{\Delta \boldsymbol{\alpha}} \quad & \mathbf{h}_j^T \Delta \boldsymbol{\alpha} \\ \text{s.t.} \quad & \Delta \boldsymbol{\alpha}^T J_i \Delta \boldsymbol{\alpha} - R_i^2 \leq 0, \quad j = 1, \dots, b, \end{aligned} \quad (2.31)$$

with

$$\mathbf{h}_j^T = \left(\frac{\partial \bar{f}_j}{\partial \alpha_1}, \dots, \frac{\partial \bar{f}_j}{\partial \alpha_u} \right). \quad (2.32)$$

This approximation is entirely based on Taylor series approximations of the actual optimization problem and is therefore referred to as an asymptotical formulation. These Taylor series have been developed around the point $\bar{\boldsymbol{\alpha}}$, which is the set of uncertainty variables if the levels of uncertainty equal zero. Clearly, the approximate optimization problem has been solved by truncation. The approximate optimization problem can be solved inexpensively and gives an asymptotic estimate of the uncertainty variables $\boldsymbol{\alpha}^{(k)}$.

The asymptotic analytical method entirely hinges on the fact that derivatives are available and that a sufficient approximation can be constructed on the basis of this information. Clearly if the effect of the uncertainty variables becomes large, then one has to expect that truncation errors may become too large. Another critical issue is whether the derivatives can be retrieved at all. First, one may not have the possibility to carry out inexpensive sensitivity analysis at all. Second, derivatives may exhibit discontinuities and may therefore become inadequate for the present setting.

2.4.4 Rigorous Anti-optimization

In case of problems involving large uncertainties, the asymptotic method can make large errors while predicting the worst response. For such problems more general or *Rigorous* anti-optimization technique, in which the anti-optimization as given by Eq. (2.20) involves full or exhaustive search for the worst sets of uncertainties.

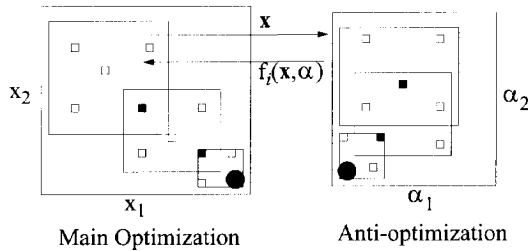


Figure 2.4: Anti-optimization technique in the MAM setting for a problem of two design variables (x_1 and x_2) and two uncertainties (α_1 and α_2). The big boxes indicate the search (sub-) domains. The small open boxes indicate sets of design variables (left) or uncertainty variables (right) for which function evaluations are carried out. The small solid boxes indicate solutions of the approximate optimization problems.

The *Rigorous* anti-optimization technique is depicted in Fig. 2.4 in the MAM setting. It consists of an anti-optimization for every design point in the main optimization and for every constraint. The main optimization, Eq. (2.19), is treated as a standard minimization problem, which searches for the best design in the design domain. The design domain is specified by upper- and lower bounds on the design variables. The anti-optimizations, Eq. (2.20), consist of performing numerical searches for the worst sets of uncertainty variables while keeping all design variables constant. Thus, the anti-optimizations are maximization problems searching for the worst combinations of uncertainty variables for a given set of design variables. These searches are restricted by the bounds on the uncertainty variables.

The anti-optimization technique, as sketched above, can handle large uncertainties safely. Moreover, it can account for discontinuities if any exist. The price paid for this flexibility is the large amount of computing efforts required for anti-optimization processes. Significant computational costs can be saved if the anti-optimization problem is convex. In that case, the worst set of uncertainty variables will be located at the bound. Often the anti-optimization can be reduced to a systematic search along the vertices of the domain of feasible uncertainty variables, Elishakoff et al. [7]. In the present thesis this assumption has not been adopted and the intention is to focus on methods that can be applied to more general problems, i.e. for which maximizers of Eq. (2.20) turn out not to be the vertices of the uncertainty domain.

2.5 Parallel Computing

2.5.1 Introduction

In general, response evaluations using FEA are computationally expensive. For applications involving such expensive FEAs, even application of an enhanced (sensitivities and database) anti-optimization technique for uncertainty-based optimization can become impractical. For such problems, the use of parallel computing is essential to make the anti-optimization technique computationally feasible. Computer clusters combining several fast computers can be utilized to evaluate

expensive FEAs in parallel in order to speed up the optimization process. In the present thesis, a Parallel Computing Tool (PCT) developed using PYTHON, Lutz [24], is used for response evaluations involving FEA.

2.5.2 Parallel Computing in the MAM setting

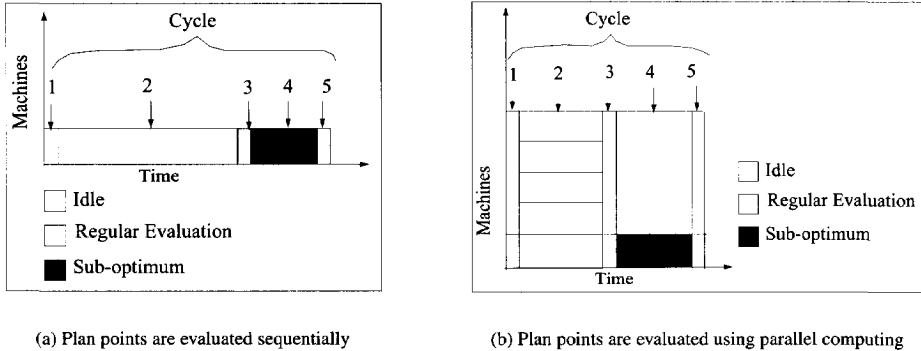


Figure 2.5: A cycle in optimization using the MAM: Steps involved are 1: Planning, 2: Evaluation of plan points, 3: NMP, 4: Evaluation of sub-optimum, 5: Move limit strategy.

Optimization using the MAM, involves various steps such as planning of experiments, response evaluation, response surface approximation, nonlinear minimization problem and movelimit strategy, see Section 2.2. The computing times required for these steps of a typical optimization are represented approximately in Fig. 2.5 (a). It can be clearly seen here, that evaluation of the plan points is computationally the most expensive phase, whereas the nonlinear minimization programming (NMP) problem and move limit strategy are relatively computationally very cheap. However, if multiple processors are available for computation, they can be utilized easily to improve the efficiency of the method as shown in see Fig. 2.5 (b), see Van Keulen and Toropov [25].

It should be noted here that an additional response evaluation is required at the end of the cycle to evaluate the sub-optimum of the AOP. In the present setting for response evaluation, splitting of the individual response evaluation is not possible, therefore every response can only be evaluated by a single processor. Because of this, during the evaluation of the sub-optimum only a single processor can be utilized, keeping the other processors idle. This increases the overall idle time significantly.

2.5.3 Parallel Computing Framework

The parallel computing framework used in the present research is developed in PYTHON, see the textbook Lutz [24]. To start multiple threads in parallel, the Threading module from PYTHON is used in the current framework. This framework is depicted in Fig. 2.6. Here, each job involves evaluation of response function using, for example FEA. The number of such jobs that can be started at a time in parallel, depends on the number of processors available for computation.

During the evaluation of an individual job, first the design parameters are sent to the remote processor, see Fig. 2.6. Then the actual evaluation of responses, for example by using FEA, is started on the remote processor by the associated thread. When the evaluations for the job are finished, corresponding responses are received back and are associated with the job. As soon as the processor finishes a response evaluation and becomes available for computation, the next job in the queue is submitted to it. The procedure is repeated until all the jobs are evaluated.

It should be mentioned here, that the communication between the master and slaves, is through files containing data, for example, flags indicating whether the submitted job is finished or not. The communication using files does increase the overhead time, however in practical cases this is negligible compared to the time required for an individual response evaluation.

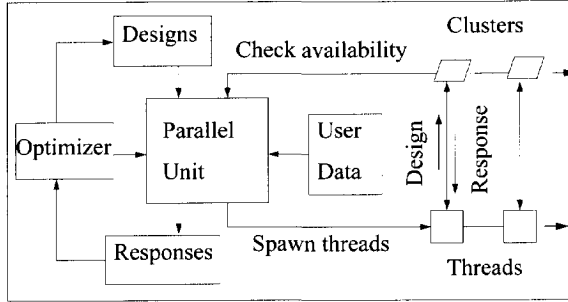


Figure 2.6: A framework for the parallel computing using the Threading module of PYTHON.



Chapter 3

Enhanced Anti-optimization

In the present chapter, uncertainties in the design process are dealt with by searching for the combination of uncertainties which yield the worst response. A description of uncertainties via bounds on the uncertainty variables is adopted. This work is the evolutionary sequel of [13] in which focus was placed on analytic, asymptotic first-order approximations, herewith inherently assuming the effect of uncertainties is relatively small. These approximations are based on first-order derivatives with respect to uncertainty variables. If the effects of uncertainties are large, a numerical method was proposed using a rigorous anti-optimization process. Both methods were embedded in a structural optimization setting using the Multipoint Approximation Method. Both the asymptotic analytical and the rigorous method were shown to have their drawbacks. The first method suffered from a lack of consistency when uncertainties have a large impact. The second method takes a very large number of evaluations, but can deal safely with uncertainties which have large effects. This chapter will combine the analytical method with the rigorous method by using sensitivity information in both main and anti-optimization, thereby decreasing the number of evaluations while retaining the desired level of accuracy.

Key words: Unknown-but-bounded uncertainties, sensitivities, optimization, anti-optimization.

3.1 Introduction

In general design practice, one faces the problem of uncertainties of various kinds. Some uncertainties may have a physical origin. Typical examples are fluctuations in material properties and uncertainties in loading conditions due to environmental effects. One could visualize that these uncertainties are inherently connected to the problem at hand, i.e. these uncertainties cannot be influenced by the designer. Typical examples could be loading conditions and material properties. Other uncertainties are of different nature and can be influenced by the designer. A typical example is provided by manufacturing induced inaccuracies. Clearly, by adopting a more expensive manufacturing process or accepting higher rejection rates, the designer can influence these uncertainties at least to a certain extent.

One way to deal with uncertainties, is to use probability density functions for the uncertainty variables. But in many practical situations the available experimental data is insufficient to warrant reliable probabilistic analysis. An alternative way is to identify uncertainties as belonging to some closed sets, i.e. to be of unknown-but-bounded nature. The optimization is treated here as an ordinary minimization problem, searching for the best design in the design domain, and will be referred to as main optimization. On the other hand it includes numerical searches for the worst set of uncertainty variables keeping all design variables constant. This search will be referred to as *anti-optimization* (a term dubbed by [26]). The anti-optimization is treated as a maximization problem searching for the worst responses for certain combinations of uncertainty variables in the domain defined by the bounds on uncertainties. Here the anti-optimization is carried out for every

response evaluation in the main optimization, thus nesting main optimization with anti-optimization. This approach was adopted by [7]. A similar approach is taken by [19] for the design of laminated composites under load uncertainties. Except that instead of using nested optimization, which is very expensive, a techniques used alternating between optimization and anti-optimization.

In the present chapter the uncertainty variables, are treated as unknown-but-bounded. This chapter adopts the *Multipoint Approximation Method* (MAM) developed by [1], [3] and [2] as the optimization algorithm of choice. The basic idea is to find for each evaluation of every goal function and every constraint function the corresponding set of uncertainties which yields the worst response, i.e. in terms of design considerations the most pessimistic set of uncertainty values. This can be accomplished in multiple ways. In [13] two methods have been proposed, namely:

1. Asymptotic method for uncertainties that have small effects;
2. Rigorous method for uncertainties with large impact.

The asymptotic method uses first-order derivatives of the response functions and first- and second-order derivatives of the uncertainty bounds to estimate the worst combination of uncertainty variables and the corresponding values for the response functions. This method has the advantage of being inexpensive in terms of computational effort, as expensive anti-optimization is avoided. However, it is not always possible to calculate the first-order derivatives with respect to the uncertainties for all of the response functions, which restricts its application. Moreover, even if information on sensitivities with respect to uncertainties can be generated, approximations on this basis may turn out to be handicapped by too large truncation errors.

In contrast to the asymptotic method, the second method on the other hand can be used virtually always for both small and large uncertainties. Moreover, depending on the anti-optimization used, even discontinuities may be accounted for. In this method rigorous anti-optimizations are carried out for each design to be evaluated within the main optimization. This immediately reveals its severe drawback, that is the large computational effort.

This chapter intends to relieve the drawbacks of both the asymptotic method regarding the incapability to handle large uncertainties as well as the rigorous method concerning the large number of evaluations by combining the methods. This is done as follows. In case of numerical analysis gradient information can be obtained often at a fraction of the computing time as compared to the analysis itself. The required sensitivities will be calculated using the so-called refined semi-analytical formulation [15, 16]. This sensitivity information can be used in addition to the function values to construct response surfaces as being used within the MAM. This incorporation of sensitivities can be used to improve the quality of the response surfaces. Alternatively, less response evaluations may be required to construct the approximations. Thus, using derivative information may decrease the total number of function evaluations and hence may speed up the numerical optimization process. In this way the advantages of the asymptotic and the rigorous method are combined.

In literature several methods to include derivative information in response surface approximations can be found. In [27] and [28] sensitivities are included in the response surface by an enhanced weighted least squares formulation. A two step blending approach is described by [18]. In this approach, gradient information is incorporated using the weighted least squares method but now formulated in terms of a multi-objective optimization problem. Extending this idea further, a single step scheme is described by [17]. In the sequel, following [17], we shall refer to response surfaces based on both function values and derivatives as Gradient Enhanced Response Surfaces (GERS).

The main goal of this chapter is to explain and demonstrate the combined method in a structural optimization setting. The fitting of response surfaces to both design sensitivities as well as to function values is one of the aspects exploited here. Further, differences of incorporating uncertainties as part of the anti-optimization process as opposed to a regular optimization process can be found in the fact that data from previous anti-optimizations is available. These data have been used to interact with the function evaluations and sensitivities in order to speed up the anti-optimization process even

more. The ideas put forward are studied on the basis of a numerical example using a finite element model of a section of a car-deck floor of a ferry.

3.2 Multipoint Approximation Method

In the present chapter the Multipoint Approximation Method has been used for optimization and anti-optimization. The interested reader is referred to the studies by Toropov *et al.* [1, 2] and Van Keulen and Toropov [3, 4]. The basic idea is that in a sub-domain of the search domain approximating response surfaces are constructed as a function of the design variables. For this, within a sub-domain of the design space a plan of experiments is generated using a space filling technique. The construction of the response surfaces is carried out using a weighted least-squares fit. The weights reflect the relative importance of the data to the optimization process. The minimization problem for the approximated response surface is solved to get a sub-optimal solution in the corresponding sub-domain. Based on the quality of sub-optimal solution of the current sub-domain the direction and size of a new search sub-domain is defined. This process is repeated until convergence has occurred.

In case both function values and derivative values are available, then the response surfaces have been constructed using both data entities. The technique used for this construction is described in detail in [17]. The basic idea is to use a weighted least square formulation, though this is loaded upon as a multi-objective optimization problem as first proposed in [18].

3.3 Uncertainty variables

Designing a structure implies that a design concept has to be selected which has to be optimized subsequently. The latter involves the selection of design variables which determine, among other features, the dimensions, shapes and materials. In the sequel, this set of n design variables is denoted \mathbf{x} , with

$$\mathbf{x}^T = (x_1, \dots, x_n). \quad (3.1)$$

Throughout the present chapter, it is assumed that all design variables are continuous.

The behavior of the structure is described by the response functions which are functions of the design variables. These response functions, are denoted as \mathbf{f} with

$$\mathbf{f}^T = (f_1, \dots, f_m), \quad (3.2)$$

which may reflect, for example, weight, cost, buckling loads, maximum equivalent stress, or strain levels. If the problem at hand is non-deterministic, i.e. there are uncertainties that play a non-negligible role, the response functions also depend on the uncertainty variables. The set of uncertainty variables will be denoted $\boldsymbol{\alpha}$, with

$$\boldsymbol{\alpha}^T = (\alpha_1, \dots, \alpha_u). \quad (3.3)$$

Consequently, the response functions depend on both design variables and uncertainty variables, hence $\mathbf{f} = \mathbf{f}(\mathbf{x}, \boldsymbol{\alpha})$.

3.4 Bounded-but-unknown uncertainty variables

Even though insufficient information is available in order to perform a probabilistic analysis, it may be possible to determine reasonable bounds on the uncertainties. In general, several bounds are introduced, each providing a bound for a group of uncertainty variables or all uncertainty variables simultaneously. At the same time we may want to measure the amount of uncertainty. Thus, measures for the dimensions of the subspace containing all possible selections of uncertainty variables

are desired. This can be cast into a mathematical framework as follows. Assuming a set with b bounds, then a possible or *feasible* selection of α satisfies

$$B_i(\alpha, \varepsilon) \leq 0, \quad \text{for all } i = 1 \dots b, \quad (3.4)$$

otherwise the selection of the uncertainty variables α is *infeasible*. The components of ε are used to specify the dimensions of the subspace of feasible uncertainty variables. We will therefore refer to these components as the *levels of uncertainty*. As we use these levels of uncertainty to describe the dimensions of a subspace, each of the components will be non-negative, i.e.

$$\varepsilon_j \geq 0, \quad \text{for } j = 1, \dots, r. \quad (3.5)$$

Note that the number of components of ε is not necessarily equal to the number of bounds being introduced.

It seems natural to assume that if the dimensions of the space of uncertainties have become zero, the uncertainty variables become deterministic. In other words, if $\varepsilon = \mathbf{0}$ then there is only a single solution $\alpha = \bar{\alpha}$ such that

$$B_i(\bar{\alpha}, \mathbf{0}) \leq 0, \quad \text{for all } i = 1 \dots b. \quad (3.6)$$

Moreover, for $\alpha = \bar{\alpha}$ the equal sign holds true.

3.5 Clustered Uncertainty Variables

As can be seen from Eq. (3.4) all uncertainty variables are coupled through the bounds $B(\alpha, \varepsilon)$. Often this fully coupled description is too general as the uncertainty variables are often *clustered*. This implies that we can group the uncertainty variables in such a manner that for each cluster a corresponding set of bounds can be identified. A cluster of uncertainty variables will be denoted $\alpha^{(k)}$ with $k = 1, \dots, d$. Here d denotes the number of clusters one may identify. The number of uncertainty variables belonging to the k -th cluster is denoted u_k . Thus, the entire set of uncertainty variables is

$$\alpha^T = \left((\alpha^{(1)})^T, \dots, (\alpha^{(d)})^T \right). \quad (3.7)$$

As mentioned, we can identify a corresponding set of bounds and uncertainty levels for each cluster, if the clusters of uncertainty variables are decoupled. Hence, a feasible selection for the k -th cluster satisfies

$$B_i^{(k)}(\alpha^{(k)}, \varepsilon^{(k)}) \leq 0, \quad \text{for all } i = 1 \dots b_k, \quad (3.8)$$

with

$$\varepsilon^T = \left((\varepsilon^{(1)})^T, \dots, (\varepsilon^{(d)})^T \right). \quad (3.9)$$

Here the number of bounds introduced for the k -th cluster is denoted b_k , whereas the number of uncertainty levels is r_k .

3.6 Asymptotic Method

The problem now is to find, for a given design \mathbf{x} , the set of uncertainty variables which is feasible and which leads to the worst possible value of the function f_j . Thus we need to find

$$\begin{aligned} & \max_{\alpha} f_j(\mathbf{x}; \alpha) \\ & \text{subject to: } B_i(\alpha; \varepsilon) \leq 0, \\ & \text{for all } i = 1 \dots b. \end{aligned} \quad (3.10)$$

Clearly this optimization may be costly. Therefore following [13] these maximization problems are approximated by:

$$\begin{aligned} \max_{\Delta\alpha} \quad & (\mathbf{h}_j^{(1)})^T \Delta\alpha^{(1)} + \dots + (\mathbf{h}_j^{(d)})^T \Delta\alpha^{(d)} \\ \text{subject to:} \quad & (\Delta\alpha^{(k)})^T \mathbf{J}_i^{(k)} \Delta\alpha^{(k)} - (R_i^{(k)})^2 \leq 0 \\ & \text{with } i = 1 \dots b_k, \quad k = 1 \dots d, \end{aligned} \quad (3.11)$$

with

$$\mathbf{J}_i^{(k)} = \begin{pmatrix} \frac{\partial^2 \bar{B}_i^{(k)}}{\partial \alpha_1^{(k)} \partial \alpha_1^{(k)}} & \dots & \frac{\partial^2 \bar{B}_i^{(k)}}{\partial \alpha_1^{(k)} \partial \alpha_{u_k}^{(k)}} \\ \vdots & & \vdots \\ \frac{\partial^2 \bar{B}_i^{(k)}}{\partial \alpha_{u_k}^{(k)} \partial \alpha_1^{(k)}} & \dots & \frac{\partial^2 \bar{B}_i^{(k)}}{\partial \alpha_{u_k}^{(k)} \partial \alpha_{u_k}^{(k)}} \end{pmatrix}. \quad (3.12)$$

Further, $R_i^{(k)}$ is defined by:

$$(R_i^{(k)})^2 = 2 \left(-\frac{\partial \bar{B}_i^{(k)}}{\partial \varepsilon_1^{(k)}}, \dots, -\frac{\partial \bar{B}_i^{(k)}}{\partial \varepsilon_{r_k}^{(k)}} \right) \mathbf{e}^{(k)}. \quad (3.13)$$

and

$$(\mathbf{h}_j^{(k)})^T = \left(\frac{\partial \bar{f}_j}{\partial \alpha_1^{(k)}}, \dots, \frac{\partial \bar{f}_j}{\partial \alpha_{u_k}^{(k)}} \right). \quad (3.14)$$

Here the over bar denotes quantities evaluated for $\alpha = \bar{\alpha}$. The solution is written as,

$$\alpha^{(k)} = \bar{\alpha}^{(k)} + \Delta\alpha^{(k)}. \quad (3.15)$$

This approximation is entirely based on Taylor series approximations of the actual optimization problem and is therefore referred to as an asymptotical formulation. These Taylor series have been developed around the point $\bar{\alpha}$, which is the set of uncertainty variables if the levels of uncertainty equal zero. Clearly, the approximate optimization problem has been solved by truncation. The approximate optimization problem can be solved inexpensively and gives an asymptotic estimate of the uncertainty variables $\alpha^{(k)}$.

The asymptotic analytical method entirely hinges on the fact that derivatives are available and that a sufficient approximation can be constructed on the basis of this information. Clearly if the effect of the uncertainty variables becomes large, then one has to expect that truncation errors may become too large. Another critical issue is whether the derivatives can be retrieved at all. First, one may not have the possibility to carry out inexpensive sensitivity analysis at all. Second, derivatives may exhibit discontinuities and may therefore become inadequate for the present setting.

Notice, that in the present approach the formulation of the bounds has to be done carefully in order to avoid difficulties. That is, the bounds have to be formulated in such a form that the first order derivatives with respect to the uncertainty variables are zero and that second order derivatives can be evaluated.

3.7 Rigorous Method

The concept of the rigorous method is similar to the asymptotic method. For every response function and every set of deterministic design variables to be evaluated, the corresponding set of uncertainties is to be determined. Contrary to the asymptotic method, which uses approximations constructed on the basis of gradient information, the rigorous method consists of a straight-forward anti-optimization of every response function. Each of the response functions in turn will fulfill the

role of goal function during this anti-optimization, while the boundaries $B_i(\alpha, \epsilon)$ become the constraints. Hence the rigorous method tends to solve Eq. (3.10).

Contrary to the asymptotic method, the worst set of uncertainties can be everywhere on and within the bounds. Moreover, the anti-optimization can be carried out even when no gradient information is available. The price paid for this flexibility is the large amount of computing time required for anti-optimization processes.

In [13] the rigorous method has also been used. In order to speed up the anti-optimization processes, estimates of the uncertainty variables have been constructed using response surfaces. These estimates have been used as starting points, for the anti-optimization. In this way the number of optimization cycles, required for the anti-optimization, has been reduced.

3.8 Enhanced method

If design sensitivities can be obtained at low computational cost, they can be used in two ways. The first is to increase the information available to obtain a higher order fit, potentially resulting in higher accuracy approximations used in the MAM. The second way is to reduce the necessary number of function evaluations to obtain a function fit of a certain order and accuracy. These strategies can be used in both the main and the anti-optimization.

3.8.1 Anti-optimization

Anti-optimization is done for every design point in the main optimization. As such, in case of anti-optimization the main design variables are kept constant. Thus the design variables during the anti-optimization are the uncertainty variables α , whereas one of the response functions becomes the goal function. The constraint functions are formed by the corresponding boundary function $B_i(\alpha, \epsilon)$. The design variables of the main optimization \mathbf{x} become nothing but constants.

Extending this procedure further, sensitivities with respect to uncertainties can be incorporated while building the GERS for the response functions. This can improve the accuracy of the response surfaces, affecting the convergence of the anti-optimization process in one way. Alternatively, a lesser number of function evaluations is required to build the response surfaces with the same complexity. Obtaining sensitivities of response functions with respect to uncertainties is much easier and straightforward as compared to obtaining sensitivities of responses with respect to main design variables in case of main-optimization as will be explained later.

The bounds can be included as constraint functions. Often the bounds come as upper and lower limits on the uncertainty variables. In those cases the anti-optimizations can be formulated as unconstrained optimization with only the response function as goal function. In the numerical example presented in the present chapter this has been the case.

3.8.2 Main optimization

The main optimization search for the best design, which minimizes the objective function while satisfying the constraint functions. First, for every design point $\bar{\mathbf{x}}$ and every response function anti-optimization is carried out to get the worst set of response functions. Thus, the anti-optimization processes for a certain design point $\bar{\mathbf{x}}$ hence results in the worst response function values f_i and their corresponding uncertainty variables.

The response functions which have been obtained on the basis of anti-optimization will be used in the MAM. As described before, the function values form the basis for the construction of response surfaces. In case information on derivatives is also available, then this information can be used to build GERS. A problem at the stage of the main optimization is that the uncertainty variables may be an implicit function of the design variables. This problem will be addressed below.

The objective function and/or the constraint functions in the main optimization are functions of the design variables \mathbf{x} as well as the uncertainty variables $\boldsymbol{\alpha}$, i.e.

$$\mathbf{f} = \mathbf{f}(\mathbf{x}; \boldsymbol{\alpha}). \quad (3.16)$$

However, the uncertainty variables $\boldsymbol{\alpha}^*$ that maximize a response function are implicit functions of main design variables, $\boldsymbol{\alpha}_j^* = \boldsymbol{\alpha}_j^*(\mathbf{x})$.

Consequently, sensitivities of response functions must be calculated as follows

$$\frac{\partial f_j}{\partial x_i} = \frac{\partial f_j}{\partial x_i} + \frac{\partial f_j}{\partial \alpha_k^*} \frac{\partial \alpha_{jk}^*}{\partial x_i}, \quad (3.17)$$

It is clear from the above equation that in addition to the sensitivities of response functions with respect to the main design variables we need sensitivities of response functions with respect to the uncertainty variables and sensitivities of uncertainty variables with respect to the main design variables. Obtaining sensitivities of uncertainty variables with respect to the main design variables is not straightforward as compared to the other sensitivities in equation Eq. (3.17).

In the present chapter the availability of response surface techniques prompted the idea to approximate the required derivatives of $\boldsymbol{\alpha}_j^*$ using response surfaces. Thus, after enough data on previous anti-optimization has been collected, the derivatives $\frac{\partial \alpha_{jk}^*}{\partial x_i}$ are approximated using response surfaces, giving approximation to $\boldsymbol{\alpha}_j^*(\mathbf{x})$.

Thus, as soon as sufficient data is available, GERS constructed over the current sub-domain can be used to obtain the new suboptimal point. The basic idea here is that a lesser number of experiments is required to construct the response surface at an equal level of accuracy as compared to the original rigorous method. Notice, that each additional design point means additional anti-optimizations, as such using a lesser number of design points can save a large number of function evaluations. Thus, incorporation of sensitivities in the main optimization can reduce the total number of function evaluations and increase the overall efficiency substantially.

3.8.3 Use of database

As explained previously, the primary purpose of creating a database is to get sensitivities of uncertainty variables with respect to the design variables. Another potential use of the database is to speed up the anti-optimization processes. In the beginning of optimization there is not enough data contributed in the database to fit response surfaces. Here normal anti-optimizations are carried out which automatically contribute to the database. Once there is enough data available, response surfaces can be fitted for uncertainties as a function of the design variables. As mentioned earlier, these can be used to estimate the required derivatives in the main optimization. Moreover, these can also be used to provide estimates for good starting points for the anti-optimizations.

3.9 Example: Corrugated Panel

As an example, a realistic optimization problem is stated and studied. The problem consists of the mass optimization of atypical section of the car deck floor of a ferry. The floor section is a so-called corrugated panel consisting of an upper and lower aluminum surface at distance (h) connected by two webs under a certain angle (β), see Fig. 3.1. The thickness of the upper and lower plates is t_1 , while the webs have thickness t_2 . The dimensions for the panel are listed in Table 3.9 and are depicted in Fig. 3.1. The whole structure has been made of aluminum (Young's modulus = 70 GPa, Poisson's ratio = 0.35, density = 2640 kg/m³). The lower plate of the panel has been welded to the surrounding frames at its front and backside. The floor is loaded by a car wheel the location of which can be all over the floor panel. The wheel print has a length $w_l = 160$ mm and width $w_b = 140$ mm and is assumed to produce a uniform pressure of $p = 138$ kPa.

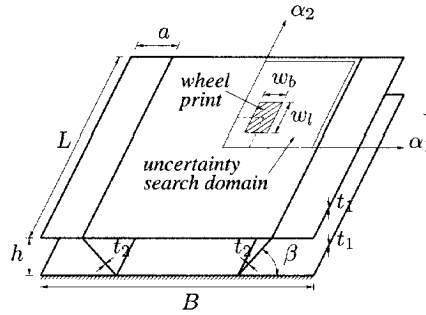


Figure 3.1: Corrugated floor panel.

Table 3.1: Dimensions of the corrugated panel.

L	= 1200	mm	β	= 0.785	rad
B	= 800	mm	w_b	= 140	mm
a	= 50	mm	w_l	= 160	mm
h	= 50	mm			

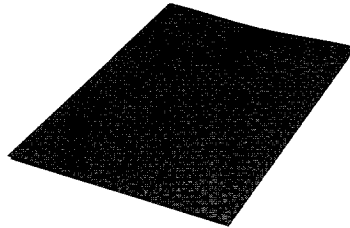


Figure 3.2: Deformation of the corrugated panel.

The purpose here is to minimize the mass (m) of the panel subject to the constraint that the deflection δ of the panel must be less than 25 mm. The plate thicknesses t_1 and t_2 are the design variables, while the α_1 - and α_2 -coordinates of the center of the wheel print are taken as the uncertainty variables. The goal of the optimization is to find the best design for minimum weight which exhibits least maximum deflection on the one hand and to find the location of the wheel print that exhibits the largest deflection for the chosen design on the other hand. As such, the final design should be corresponding to the best response and for the worst combination of uncertainty variables.

In order to perform the optimization, a finite element model of the floor section has been used, see Fig. 3.2. The mesh of the model is dependent on the location of the wheel print, hence on the uncertainty variables. Thin shell elements [29] have been used for both the surfaces and the webs. The model has been parameterized in order to be able to move the position of the wheel print over the upper surface. Due to this parameterization a small region is necessary between the wheel print and the edge of the surface. Consequently, the wheel print can not reach the edges completely. Because of symmetry the search region of the uncertainty variables has been limited to only one quarter of the upper surface. This puts an upper bound $B_1^{(1)}$ on uncertainty α_1 and $B_1^{(2)}$ on α_2 . The corresponding lower bounds are zero. The search region is indicated in Fig. 3.1.

3.9.1 Asymptotic Evaluation of the Corrugated Panel

The asymptotic method requires a linearization of the boundary functions and the response functions.

The uncertainty variables in the corrugated panel optimization can be split into two clusters ($d = 2$). To each cluster belongs only a single uncertainty variable ($b_1 = b_2 = 1$). Since the boundary function for each cluster can be described by a single level of uncertainty ($r_1 = r_2 = 1$), they have been selected as

$$\begin{aligned} B_1^{(1)}(\boldsymbol{\alpha}, \boldsymbol{\varepsilon}) &= \left(\alpha_1^{(1)} - \bar{\alpha}_1 \right)^2 - \varepsilon_1^{(1)} \leq 1, \\ B_1^{(2)}(\boldsymbol{\alpha}, \boldsymbol{\varepsilon}) &= \left(\alpha_1^{(2)} - \bar{\alpha}_2 \right)^2 - \varepsilon_1^{(2)} \leq 1, \end{aligned} \quad (3.18)$$

with $\bar{\alpha}_1$ and $\bar{\alpha}_2$ equal to half the width and height of the search domain, respectively. Hence $\bar{\boldsymbol{\alpha}}$ corresponds to the center of the search domain for the uncertainty variables. Equations Eq. (3.12) and Eq. (3.13) then reduce to scalars

$$\mathbf{J}_1^{(1)} = 2 \quad \mathbf{J}_1^{(2)} = 2, \quad (3.19)$$

and

$$(R_1^{(1)})^2 = 2 \varepsilon_1^{(1)} \quad (R_1^{(2)})^2 = 2 \varepsilon_1^{(2)}. \quad (3.20)$$

The deflection constraint is formulated as

$$g_1 : \frac{\delta}{\delta_{max}} \leq 1 \quad (3.21)$$

with $\delta_{max} = -25 \text{ mm}$. The gradient vectors $(\mathbf{h}_1^{(k)})^T = \left(\frac{\partial \bar{g}_1}{\partial \alpha_1^{(k)}} \right)$ and $(\mathbf{h}_2^{(k)})^T = \left(\frac{\partial \bar{g}_1}{\partial \alpha_2^{(k)}} \right)$ are obtained from finite element calculations based on the refined semi-analytical formulation [16]. The gradients have been calculated in the center of the uncertainty search domain.

Table 3.2: Results of the asymptotic analytical optimization of the corrugated panel.

Method	Wheel print location	$\Delta\alpha_1$ mm	$\Delta\alpha_2$ mm	t_1 mm	t_2 mm	f kg	g_1 -	number of evaluations
Asymptotic	Center	-135	255	4.652	0.253	23.69	1.000	172
Verification	Left-top	-135	255	4.652	0.253	23.69	1.379	-
Verification	Right-top	135	255	4.652	0.253	23.69	0.378	-
Verification	Left-bottom	-135	-255	4.652	0.253	23.69	0.814	-
Verification	Right-bottom	135	-255	4.652	0.253	23.69	0.344	-

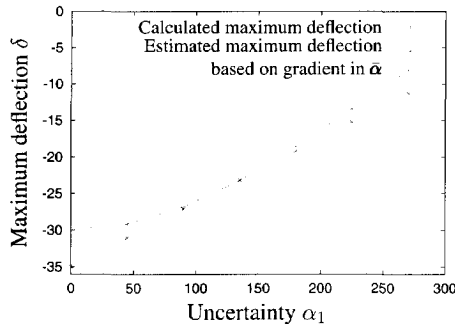


Figure 3.3: Maximum deflection δ as a function of uncertainty α_1 for uncertainty $\alpha_2 = \bar{\alpha}_2$.

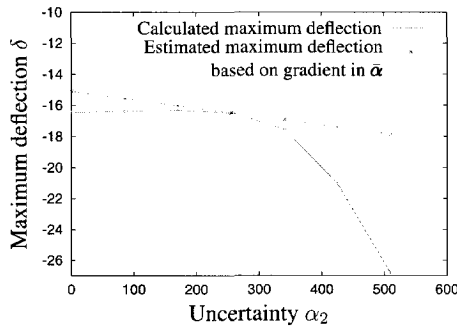


Figure 3.4: Maximum deflection δ as a function of uncertainty α_2 for uncertainty $\alpha_1 = \bar{\alpha}_1$.

The results obtained using the asymptotic method are included in Table 3.2. To verify the results, the wheel print has been placed manually in the four edges of the uncertainty search region, using the values for t_1 and t_2 resulting from the optimization. The corresponding constraint values are also listed in Table 3.2. It is seen that if the wheel print is placed in the location corresponding to the worst case, an error of roughly 40% is made. This constraint violation has been overlooked by the asymptotic method. Fig. 3.2 depicts the deflection due to this setting.

To investigate this aspect further, the maximum deflection δ as a function of α_1 and α_2 is plotted versus the corresponding asymptotic approximations. The results have been depicted in Fig. 3.3 and Fig. 3.4. It is again demonstrated that huge errors are introduced by the asymptotic method. What is however well represented is the settings of $\Delta\alpha$ for which the worst response is obtained.

3.9.2 Evaluation of the Corrugated Panel using the Enhanced Method

The example is studied in steps as follows. First the anti-optimization is studied in detail. Particularly the use of derivatives to speed up the anti-optimization is one of the main aspects. This study is carried out for arbitrarily selected settings of the design variables. Second, the effect of the use of sensitivities in the main optimization is studied, without taking into account the effect of uncertainty variables. Finally, the complete optimization is carried out with and without the use of a database.

Calculations are carried out including and excluding sensitivity information, both using linear and quadratic approximations in the MAM. Different settings in the MAM are used depending on the type of approximations and the use of sensitivity information, such as when using linear approximations a lesser number of plan points is included in the plan of experiments, whereas a larger number of plan points is used in case of quadratic approximations. In case of using sensitivity information even fewer points are used as more data is then available in terms of sensitivities.

Anti-optimization

This example studies the anti-optimization for the design variables $t_1 = 5.0 \text{ mm}$ and $t_2 = 0.5 \text{ mm}$. This is done in two ways. Results for the anti-optimization using linear approximations are shown in Fig. 3.5 (a) and the results when using quadratic approximations are shown in Fig. 3.5 (b). Here the objective function, which is maximum deflection, corresponding to each step in the anti-optimization is plotted against the number of steps.

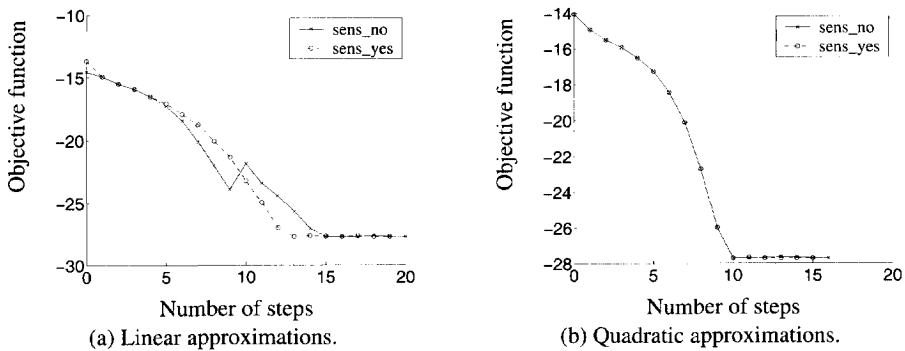


Figure 3.5: Anti-optimization for the panel. Curves with and without sensitivities have been included.

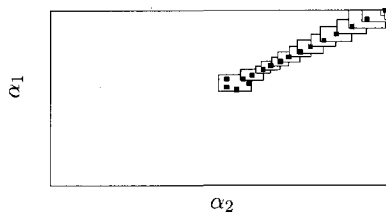


Figure 3.6: The history of anti-optimization for the panel with linear approximations and using sensitivity. The white rectangles indicate the move limits used, whereas the gray ones are the plan points.

Table 3.3: Results of the anti-optimization of the corrugated panel.

Approximation	sensitivity used	$\Delta\alpha_1$ mm	$\Delta\alpha_2$ mm	t_1 mm	t_2 mm	δ mm	number of evaluations
Linear	No	0.0	510.0	5.0	0.5	27.7097	64
Linear	Yes	0.0	510.0	5.0	0.5	27.7097	24
Quadratic	No	0.64	510.0	5.0	0.5	27.7029	67
Quadratic	Yes	0.0	510.0	5.0	0.5	27.7097	49

Results obtained using the sensitivity information in the anti-optimization are in accordance with the results obtained without using the sensitivity information. It is observed that the accuracy of the approximations is better when sensitivities are used. Table 3.3 shows that fewer function evaluations (roughly factor 2) are required when sensitivities are included in the anti-optimization, thus making it more efficient. The history of optimization in terms of move limits is shown in Fig. 3.6. Each of the boxes represents the search sub-domain as used in an optimization cycle. The location of the plan points is indicated using small rectangles.

Main optimization

The main optimization is first studied separately by keeping the worst set of uncertainties ($\alpha_1 = 0 \text{ mm}$ and $\alpha_2 = 510 \text{ mm}$), constant. Results for the main optimization, using linear approximations are shown in Fig. 3.7 (a) and Fig. 3.7 (b). Similar results based on quadratic approximations are shown in Fig. 3.8 (a) and Fig. 3.8 (b). Here the objective function (mass of the structure) and constraint function (Eq. (3.21)) corresponding to each step in the main-optimization are plotted

against the number of steps. Notice that by keeping the uncertainty variables as constants, the corresponding contribution to the sensitivities disappears.

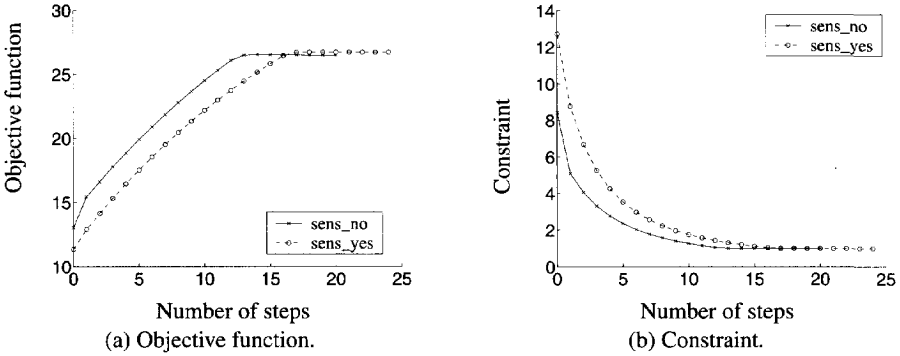


Figure 3.7: Main optimization for the panel using linear approximation for responses. Curves with and without sensitivities have been included.

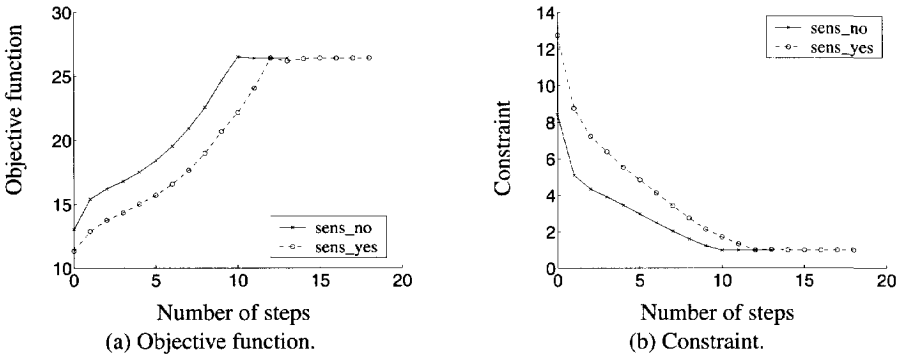


Figure 3.8: Main optimization for the panel using quadratic approximation for responses. Curves with and without sensitivities have been included.

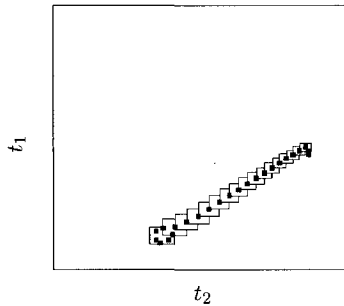


Figure 3.9: The history of main optimization for the panel with linear approximations and using sensitivity. The white rectangles indicate the move limits used, whereas the gray ones are the plan points.

Table 3.4: Results of the main-optimization of the corrugated panel

Approximation	sensitivity used	$\Delta\alpha_1$ mm	$\Delta\alpha_2$ mm	t_1 mm	t_2 mm	f kg	g_1 -	number of evaluations
Linear	No	0	510	5.1723	0.6354	26.5038	9.9998-01	64
Linear	Yes	0	510	5.1577	1.3221	26.7388	1.0000	30
Quadratic	No	0	510	5.1869	0.2837	26.4189	1.0000	68
Quadratic	Yes	0	510	5.1962	0.1944	26.4258	1.0000	41

Results obtained using the sensitivity information in the optimization are in accordance with the final results obtained without using the sensitivity information. The accuracy of the approximations is better when using sensitivities. Table 3.4 shows that a lesser number of function evaluations (roughly factor 2) are required when sensitivities are included, thus making the optimization more efficient. The optimization history in terms of move limits is depicted in Fig. 3.9.

Complete optimization

In this study, the anti-optimization is done inside the main optimization. That is, for every design point in the main optimization an anti-optimization is carried out to get the corresponding worst set of uncertainties. Note, in this example only a single response function has to be maximized. It is quite clear that this process becomes very expensive in terms of function evaluations necessary to perform the optimization.

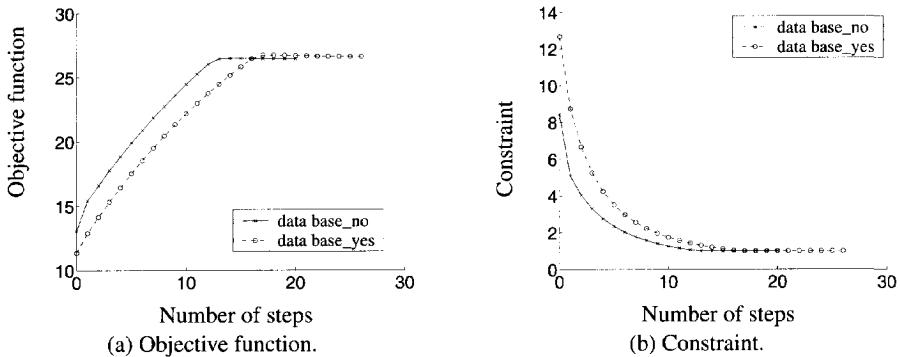


Figure 3.10: Complete optimization of the panel for Cases 1 and 4 in Table 3.5.

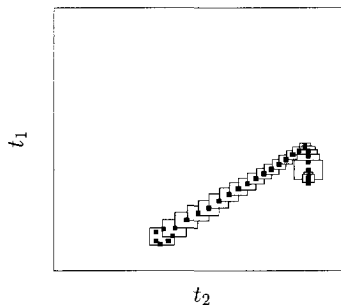


Figure 3.11: The history of complete optimization for the panel using database. The white rectangles indicate the move limits used, whereas the gray ones are the plan points.

Table 3.5: Results of the complete-optimization of the corrugated panel. The number of function evaluations required for Cases 2 and 3 have been estimated.

Cases	Type of optimization	Sensitivity used	Database used	t_1 mm	t_2 mm	f kg	g_1 -	Total no of evaluations
1	Main Anti	Yes Yes	Yes Yes	5.1647	1.0019	26.6299	1.0000	481
2	Main Anti	No Yes	No Yes	-	-	-	-	1200
3	Main Anti	No Yes	No No	-	-	-	-	1625
4	Main Anti	No No	No No	5.1758	0.4897	26.4557	1.0000	5417

The entire optimization strategy has been compared for different settings, i.e with and without database and/or the use of sensitivities. The history of the corresponding optimization processes is depicted in Fig. 3.10 (a) and Fig. 3.10 (b). Results for the corresponding design variables and response functions are provided in Table 3.5. The number of function evaluations required for the entire optimization are given in Table 3.5. Optimization history in terms of move limits is depicted in Fig. 3.11. It can be observed from this test example that the use of a database and sensitivities pays off significantly.

3.10 Discussion and Conclusion

In the present chapter a method is given to deal with uncertainties in structural design. It is based on bounded-but-unknown uncertainties. For that purpose anti-optimization, which is nothing but searching for the worst combination of uncertainties, is studied. The main focus is on reducing the number of function evaluations which is prohibiting the use of the method. The approach is to use sensitivity information to make the optimization more efficient.

As is the case with anti-optimization, the main optimization itself incorporates sensitivities as well. This is not so straightforward due to the interdependence between design variables and uncertainty variables. For this purpose, a database is made to store the history of the anti-optimization. With the use of the database, sensitivities of the uncertainty variables with respect to the design variables can be calculated, thus making it possible to use sensitivity information in anti- as well as in main optimization. The use of sensitivity in total seems to be very effective in terms of reduction of the number of function evaluations.

The database, created as a necessity while using sensitivities in the main optimization, has been used to reduce the number of function evaluations further. That is, the database is used to make a rough estimate of the uncertainties, which can be used as a starting point for anti-optimization. This effectively reduces the number of function evaluations.

3.11 Acknowledgment

This research is supported by the Technology Foundation STW, applied science division of NWO and the technology programme of the Ministry of Economic Affairs, The Netherlands.

Chapter 4

Enhanced Anti-optimization combined with Parallel Computing

In the present chapter uncertainty-based design optimization of structures is carried out. A description of uncertainties via bounds on the uncertainty variables is adopted. An anti-optimization technique, which searches for the combinations of uncertainties yielding the worst responses, is used to tackle these Bounded-But-Unknown uncertainties of non convex or discontinuous nature. This anti-optimization technique is computationally very expensive and can become impractical for real world applications, in particularly when expensive numerical response evaluations are involved. In order to reduce the number of expensive numerical response evaluations, a modified anti-optimization technique is proposed in the present chapter. This *enhanced* anti-optimization technique incorporates design sensitivities and database technique and is further modified to use parallel computing in order to increase the computational efficiency. The enhanced anti-optimization technique is studied on the basis of test examples from literature and a Microelectromechanical Systems (MEMS) structure. A comparison between results for the examples, clearly shows an improvement in computational efficiency for the anti-optimization technique, due to the use of sensitivities, database and parallel computing. The enhanced anti-optimization technique can be applied efficiently to general problems involving uncertainties of non convex or discontinuous nature.

Key words: Optimization, Anti-optimization, Bounded-But-Unknown, Uncertainties, Design Sensitivities, Parallel Computing, MEMS.

4.1 Introduction

In general design practice, one faces the problem of uncertainties of various kinds. Some uncertainties have a physical origin. Typical examples are loading conditions or variations in material properties. These uncertainties are inherently connected to the problem at hand, i.e. these uncertainties cannot be influenced by the designer. Other uncertainties are of a different nature and can be influenced by the designer. A typical example is provided by manufacturing induced inaccuracies, for example in dimensions of MEMS (Micro Electro Mechanical Systems). Clearly, by adopting a more expensive manufacturing process or accepting higher rejection rates, the designer can influence the level of uncertainty at least to a certain extent. Particularly when dealing with MEMS, because of their small dimensions, tolerances on shapes are *relatively* high, Clark *et al.* [30] and Pister *et al.* [31]. These variations in dimensions of MEMS structures can have a significant effect on their mechanical behavior. Therefore, it is quite essential to consider uncertainties while designing MEMS structures.

One way to deal with uncertainties, is to use probabilistic methods, Elishakoff [8]. However, probabilistic methods require an abundance of experimental data, Elishakoff [9]. Furthermore, even small inaccuracies in the statistical data can lead to large errors in the computed probability of

failure to meet structural requirements, Elishakoff [9]. Many times, for example in preliminary design phases, even though some experimental data is available, it is not enough to construct reliable probability distributions. However, the available data can be used, particularly in combination with engineering experience, to set tolerances or bounds on uncertainties. Consequently, uncertainties will be identified as belonging to some closed sets, i.e. to be of Bounded-But-Unknown (BBU) nature, see Ben-Haim and Elishakoff [11] and Ben-Haim [12].

To tackle such BBU uncertainties, a technique based on *anti-optimization* (a term dubbed by Elishakoff [26]) is proposed by Elishakoff *et al.* [7]. In this technique, uncertainty-based optimization is basically split in two parts, namely, main- and anti-optimization. The main optimization is treated as a standard minimization problem, which searches for the best design in the design domain. The design domain is typically specified by upper- and lower bounds on design variables. The anti-optimization consist of performing numerical searches for the combination of uncertainties, which yields the worst response for a given design and a particular response function. In the worst case scenario, an anti-optimization for every constraint is required. Within these anti-optimizations, the uncertainties are set as “design variables”, whereas the “design domain” is specified by the bounds on the uncertainties. Thus, anti-optimizations are nested within the main optimization, making it a two-level optimization problem, which can be computationally very intensive. In the method discussed in Elishakoff *et al.* [7], the searches for the worst combination of uncertainties, are replaced with systematic searches along the vertices of the uncertainty domain. This makes it computationally efficient, but limits its application to convex modelling of uncertainties.

Recent work demonstrates that the anti-optimization technique can be applied to uncertainty-based design optimization of practical applications. Optimization of composite structures considering load uncertainties is carried out using the anti-optimization technique by Faria *et al.* [32] and Adali *et al.* [33]. It is used by Lombardi and Haftka [19] for the design of laminated composites and Van Keulen *et al.* [13] and Gurav *et al.* [34] used it for the design optimization of a car deck floor of a ferry. Uncertainty-based design optimization of MEMS is carried out by Gurav *et al.* [20] using anti-optimization.

In many practical cases, even though the assumption of convex modelling for uncertainties applies often, it is essential to have a more general technique available that can handle non-convex uncertainties. Such an approach is adopted in Van Keulen *et al.* [13] and Gurav *et al.* [20, 34]. In this approach, anti-optimizations are treated as standard maximizations. This method is versatile in dealing with uncertainties, but it is computationally very intensive and impractical for large numbers of design variables and uncertainties. In the present chapter, the anti-optimization technique is modified to make it computationally more efficient. This includes the use of sensitivities, a database technique and parallel computing. Throughout this chapter, intensive use will be made of optimization techniques that rely on response surface (RS) approximations.

In many cases of computational response analysis, gradient information can often be obtained at a fraction of the computing time as compared to the analysis itself, van Keulen and de Boer [15, 16]. This sensitivity information can be used in addition to the function values to construct Gradient Enhanced Response Surfaces (GERS), van Keulen and Vervenne [17, 18]. This incorporation of sensitivities can improve the quality of the response surfaces. Alternatively, fewer response evaluations may be required to construct the approximations. Thus, using derivative information may decrease the total number of function evaluations and hence may speed up the numerical optimization process.

The anti-optimization technique is further modified to use a database technique. For this purpose, the worst sets of uncertainties obtained by anti-optimizations are stored in a database. When there is enough data available in the database, it is used to create starting points for the anti-optimizations. Often this can speed up the anti-optimizations significantly.

In many practical applications, analytical solutions for response functions are unavailable, and numerical solutions, such as using Finite Element Method (FEM), are often used to evaluate the response functions. In general, response evaluations using FEM for practical applications are computationally expensive. For such applications, even application of an enhanced (sensitivities and

database) anti-optimization technique for uncertainty-based optimization can become impractical. The use of parallel computing can be a solution here. Nowadays, the use of a number of powerful computers, forming a cluster, is quite common. Such computer clusters can be used to evaluate expensive response functions in parallel. This can speed up the optimization process significantly. In the present chapter, a parallel computing tool developed using PYTHON, Lutz [24], is used for response evaluations. It is combined with the anti-optimization technique and applied to a practical application from MEMS.

In the present chapter, the Ten-Bar-Truss example (Elishakoff *et al.* [7]) is used to illustrate the proposed anti-optimization technique. An elastically supported beam example (Lombardi and Haftka [19]) is used here to test the technique in the presence of nonlinearities. Additionally it demonstrates that a worst set of uncertainties may not be always found at the vertices of the uncertainty domain. The anti-optimization technique is applied to the uncertainty-based design optimization of an embedded measurement MEMS structure (van Drieënhuizen *et al.* [35] and Goosen *et al.* [36]). The purpose of this microstructure is to obtain information on the strain state of certain layers in a MEMS device.

Uncertainty-based design optimization technique using BBU uncertainties is described in Section 4.2. In Section 4.3, the anti-optimization technique is studied on the basis of various examples and the results for the uncertainty-based optimization are compared with those for the deterministic optimization. Final discussion and conclusion are the subject of Section 4.4.

4.2 Method

4.2.1 Multipoint Approximation Method

In the present chapter the Multipoint Approximation Method (MAM) is used as a basis for optimization. Many times practical applications involve numerical evaluation of response functions. From a optimization point of view, this type of problem can either suffer from numerical noise or the large computational time involved. The MAM, which is based on Response Surface Methodology, see Khuri and Cornell [22] and Myers and Montgomery [23], can be applied to such problems. The interested reader is referred to the studies by Toropov *et al.* [1, 2] and Van Keulen and Toropov [3, 4]. The MAM uses approximations for the responses in order to reduce the number of expensive numerical response evaluations. However, it should be noted here, that it suffers from the so-called curse of dimensionality. It becomes inefficient with the increase in dimensions (number of design variables). A MAM-based framework for the optimization of practical applications is described in detail in Jacobs *et al.* [5]. For self-containment, a short description of the MAM is given in the remainder of this section.

Optimization problem

Designing a structure implies that a design concept has to be selected, which subsequently has to be optimized. The latter involves the selection of design variables, which determine, among other features, the dimensions, shapes and materials. This set of n design variables is denoted as \mathbf{x} , with

$$\mathbf{x} = (x_1 \dots x_n). \quad (4.1)$$

Throughout the present chapter, it is assumed that all design variables are continuous.

The behavior of the structure is described by the response functions, which are functions of the design variables. These response functions are denoted as \mathbf{f} with

$$\mathbf{f} = (f_1 \dots f_m), \quad (4.2)$$

which may reflect, for example, weight, cost, buckling loads, maximum equivalent stress, or strain levels.

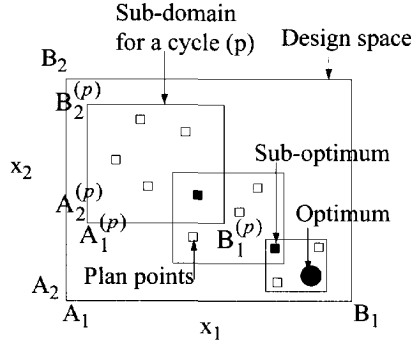


Figure 4.1: Optimization using the MAM for a problem of two design variables (x_1 and x_2).

The optimization problem using the MAM can now be formulated mathematically as

$$\begin{aligned} \min_{\mathbf{x}} \quad & f_o(\mathbf{x}) \\ \text{s.t.} \quad & f_i(\mathbf{x}) \leq 1, \quad i = 1, \dots, m, \\ & A_j \leq x_j \leq B_j, \quad j = 1, \dots, n. \end{aligned} \quad (4.3)$$

Here, f_0 is the objective function and f_i are constraints, whereas \mathbf{x} is a set of design variables. The design space is represented by A_j and B_j , upper and lower limits on x_j respectively, see Fig. 4.1.

Approximate Optimization Problem

The MAM is based on a replacement of the actual optimization problem, as described by Eq. (4.3), by a series of approximate optimization problems. The approximate optimization problem (AOP) for a cycle p , can be formulated as

$$\begin{aligned} \min_{\mathbf{x}} \quad & \tilde{f}_o^{(p)}(\mathbf{x}) \\ \text{s.t.} \quad & \tilde{f}_i^{(p)}(\mathbf{x}) \leq 1, \quad i = 1, \dots, m, \\ & A_j^{(p)} \leq x_j \leq B_j^{(p)}, \quad j = 1, \dots, n, \\ & A_j^{(p)} \geq A_j, \quad B_j^{(p)} \leq B_j. \end{aligned} \quad (4.4)$$

Here, the true response functions are replaced with approximate functions over the sub-domain for a cycle. Here, $\tilde{f}_i^{(p)}(\mathbf{x})$ are considered as adequate approximations of $f_i(\mathbf{x})$ over the sub-domain (p) represented by the move limits $A_j^{(p)}$ and $B_j^{(p)}$, see Fig. 4.1, for the current AOP. It should be noted here that, the move limits for the initial cycle ($A_j^{(0)}$ and $B_j^{(0)}$), can be chosen either arbitrarily or based on engineering experience. Many times this can significantly influence the convergence. For example, if the initial move limits include the optimum, then the optimization can converge quite rapidly.

Response Surface Approximations

The MAM relies on response surface approximations of the true responses in order to limit the number of expensive numerical evaluations. To construct approximate response surfaces for responses, first a plan of numerical experiments is generated in the sub-domain of the current cycle, see Fig. 4.1. In the present study, space filling technique is used for generating plan of experiments, for details see Toropov *et al.* [2]. Approximate response surfaces for response functions are fitted through the

numerical evaluations of plan points using weighted least squares (WLS) method, see Van Keulen and Toropov [3, 4], as

$$\min \sum_{s=1}^S w_i^s \left[f_i(\mathbf{x}_s) - \tilde{f}_i^{(p)}(\mathbf{x}_s) \right]^2, \quad (4.5)$$

$$\text{with } \tilde{f}_i^{(p)}(\mathbf{x}_s) = f_i^{(p)}(\mathbf{x}_s)\beta_i, \quad i = 0, \dots, m,$$

where s represents a plan point and S is the total number of plan points in the current plan of experiments. Here, $\tilde{f}_i^{(p)}(\mathbf{x}_s)$ represent the response surface approximations for the true functions $f_i(\mathbf{x}_s)$ over the current sub-domain (p), whereas $f_i^{(p)}(\mathbf{x}_s)$ contains the approximation functions and β_i represent corresponding regression coefficients, see Khuri and Cornell [22] and Myers and Montgomery [23]. In the minimization problem, β_i , which are unknowns, are used as tuning parameters in order to get the approximations $\tilde{f}_i^{(p)}(\mathbf{x})$, as close as possible to the true functions $f_i(\mathbf{x})$. The weight factors w_i , used here to combine the data from different points in the WLS method, reflect the relative importance of the function values (and their derivatives if available) to the optimization process. The selection of the weight factors is made based on mainly the objective function value and the location of a plan point relative to the boundary between feasible and infeasible design space. This selection of the weight factors, affect significantly the efficiency of the method, see for details Van Keulen and Toropov [4] and Toropov *et al.* [2].

Move Limit Strategy

At the end of every cycle the Move limit strategy checks, if the solution has converged and if not, it defines the AOP for the next cycle. Here, the approximate optimum (sub-optimum), obtained by solving the nonlinear minimization programming (NMP) for the current AOP given by Eq. (4.4), is evaluated for the true response. In order to define the location and size of the sub-domain for the next cycle, several indicators are computed based on the assessment of the current sub-optimum, see for details Van Keulen and Toropov [4]. The procedure is summarized here shortly.

The first indicator is based on the largest relative error in the approximations for the sub-optimum. Depending on this indicator, the approximations are termed as “bad”, “average” or “good”. The second indicator is based on the location of the sub-optimum in the sub-domain for the current cycle. When none of the current movelimits is active, the solution is considered “internal”, or otherwise “external”. The next two indicators are based on the angle between the move vectors of the last two sub-optimums. Depending on this the movement of the optimum is termed as “straight”, “curved”, “backward” or “forward”. The fifth indicator denotes the size of the current sub-domain as “small” or “large” and is used in the termination criteria. Depending on the most active constraint value, the sixth indicator labels the current solution as “close” or “far” from the boundary of the feasible and infeasible regions of the design space.

A factor to resize the current sub-domain is chosen based on these indicators. For example, if the quality of the approximations is “bad”, then the size of the sub-domain will be reduced and vice versa. Further more, the reduction factor changes depending on the move direction, such as in case of the “curved” move, higher reduction is expected. Similarly, if the solution is indicated as “close”, the sub-domain will be reduced substantially. In case of “internal” solution, if the size of the sub-domain is “small”, then the optimization is terminated. Detailed description of the move limit strategy is given in Van Keulen and Toropov [4]. The whole process is repeated until the convergence.

Gradient Enhanced Response Surface

In case both function and derivative values are available, then Gradient Enhanced Response Surfaces (GERS) have been constructed using both data entities as discussed in Van Keulen and Vervenne

[17]. Derivative information can often be obtained at a fraction of the computing time as compared to the analysis itself, see van Keulen and de Boer [15, 16]. Use of sensitivities can benefit the optimization in two ways. First, it can improve the quality of the response surfaces affecting the convergence. Second, fewer response evaluations may be required to construct the approximations resulting in a reduction in the total number of function evaluations. This is particularly advantageous when higher order approximations are used. Alternatively, it can allow the inclusion of more design variables in the optimization. The technique used for the construction of GERS using both the function values and the design sensitivities, is described in detail in Van Keulen and Vervenne [17]. A short summary is included here for self-containment.

The response function (f_{0j}) and the corresponding derivatives (f_{ij}) associated with the point \mathbf{x}_j are given here as

$$\begin{aligned} f_{0j} &= f_0(\mathbf{x}_j), \\ f_i &= \frac{\partial f_0}{\partial x_i}, \\ f_{ij} &= f_i(\mathbf{x}_j), \end{aligned} \quad (4.6)$$

where $i = 1, \dots, n$ and $j = 1, \dots, S$. These are represented using a compact notation as

$$\mathbf{y}_j = [f_{0j} \dots f_{nj}], \quad j = 1, \dots, S. \quad (4.7)$$

The response surfaces for function and derivatives are represented as

$$\begin{aligned} \tilde{f}_0 &= f_0(\mathbf{x})\boldsymbol{\beta}, \\ \tilde{f}_i &= \frac{\partial \tilde{f}_0}{\partial x_i} = f_i(\mathbf{x})\boldsymbol{\beta}, \quad i = 1, \dots, n, \end{aligned} \quad (4.8)$$

where $f_i(\mathbf{x})$ contains approximation functions and $\boldsymbol{\beta}$ denote corresponding regression coefficients, which are to be determined, see Khuri and Cornell [22] and Myers and Montgomery [23]. Thus, the response surface approximations for the response function and derivatives are given as

$$\begin{aligned} \tilde{\mathbf{y}}_j &= [\tilde{f}_{0j} \dots \tilde{f}_{nj}], \quad j = 1, \dots, S \\ &= [f_0(\mathbf{x}_j) \dots f_n(\mathbf{x}_j)]\boldsymbol{\beta} \\ &= \mathbf{F}_j\boldsymbol{\beta}. \end{aligned} \quad (4.9)$$

The error in the actual function value and derivatives (\mathbf{y}_j) and the corresponding approximations ($\tilde{\mathbf{y}}_j$) can be given as

$$\mathbf{r}_j = \tilde{\mathbf{y}}_j - \mathbf{y}_j = \mathbf{F}_j\boldsymbol{\beta} - \mathbf{y}_j, \quad j = 1, \dots, S. \quad (4.10)$$

The norm of the error using WLS method, in order to combine all the errors with different weights assigned to them, can be given as

$$e_j^2 = \langle \mathbf{r}_j; \mathbf{r}_j \rangle = \mathbf{r}_j^T \mathbf{W}_j \mathbf{r}_j, \quad j = 1, \dots, S, \quad (4.11)$$

where \mathbf{W}_j is a matrix of weight coefficients, see Van Keulen and Vervenne [17]. The unknown parameters $\boldsymbol{\beta}$ are determined as the minimizers of the total error as

$$\min_{\boldsymbol{\beta}} e^2 = \sum_{j=1}^S e_j^2. \quad (4.12)$$

4.2.2 Bounded-But-Unknown Uncertainty

If the problem at hand is non-deterministic, i.e. there are uncertainties that play a non-negligible role, the response functions also depend on the uncertainty variables. The set of uncertainty variables will be denoted $\boldsymbol{\alpha}$, with

$$\boldsymbol{\alpha} = (\alpha_1 \dots \alpha_u). \quad (4.13)$$

Consequently, the response functions depend on both design variables and uncertainty variables, hence $f(\mathbf{x}, \boldsymbol{\alpha})$.

Even though insufficient information is available in order to perform a probabilistic analysis, it may be possible to determine or specify reasonable bounds on the uncertainties. In general, several bounds can be introduced, each providing a bound for a group of uncertainty variables or all uncertainty variables simultaneously. At the same time we may want to measure the amount of uncertainty. Thus, measures for the dimensions of the subspace containing all possible selections of uncertainty variables are desired. This can be cast into a mathematical framework as follows. Assuming a set with b bounds, then a possible or *feasible* selection of $\boldsymbol{\alpha}$ satisfies, see Van Keulen *et al.* [13];

$$B_i(\boldsymbol{\alpha}, \boldsymbol{\varepsilon}) \leq 0, \quad \text{for } i = 1, \dots, b. \quad (4.14)$$

Otherwise the selection of the uncertainty variables $\boldsymbol{\alpha}$ is *infeasible*.

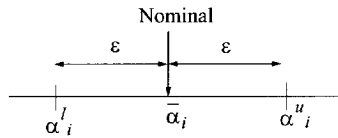


Figure 4.2: Simple box bounds on uncertainties: $\bar{\alpha}_i$ are nominal values of uncertainties, whereas α_i^l and α_i^u denote lower and upper bounds on uncertainties respectively. Here, ε denote the dimension of the space of the feasible uncertainty.

For example, in case of simple box bounds, see Fig. 4.2, the bounds on uncertainties can be specified as

$$(\alpha_i - \bar{\alpha}_i)^2 - \varepsilon^2 \leq 0. \quad (4.15)$$

These type of bounds generally come from a tolerance specified on a nominal value, for example, due to the manufacturing induced inaccuracies. In case of applications, where a very high performance is required against failure, such sharp bounds become practical. These bounds can be alternatively represented in terms of lower (α_i^l) and upper bounds (α_i^u) on uncertainties as

$$\begin{aligned} \alpha_i^l &= \bar{\alpha}_i - \varepsilon, \\ \alpha_i^u &= \bar{\alpha}_i + \varepsilon. \end{aligned} \quad (4.16)$$

Here, the components of $\boldsymbol{\varepsilon}$ are used to specify the dimensions of the space of feasible uncertainty variables. We will therefore refer to these components as the *levels of uncertainty*. As we use these levels of uncertainties to describe the dimensions of a space, each of the components will be non-negative, i.e.

$$\varepsilon_j \geq 0, \quad \text{for } j = 1, \dots, r. \quad (4.17)$$

Note that the number of components of $\boldsymbol{\varepsilon}$, r , is not necessarily equal to the number of bounds, b , being introduced.

It seems natural to assume that if the dimensions of the space of uncertainty variables have become zero, the uncertainty variables become deterministic. In other words, if $\boldsymbol{\varepsilon} = \mathbf{0}$ then there is only a single solution $\boldsymbol{\alpha} = \bar{\boldsymbol{\alpha}}$ such that

$$B_i(\bar{\boldsymbol{\alpha}}, \mathbf{0}) \leq 0, \quad \text{for } i = 1, \dots, b. \quad (4.18)$$

Moreover, for $\boldsymbol{\alpha} = \bar{\boldsymbol{\alpha}}$ the equal sign holds true.

4.2.3 Anti-optimization

The optimization problem using BBU uncertainties can be formulated mathematically as:

$$\begin{aligned} \min_{\mathbf{x}} \quad & f_o(\mathbf{x}) \\ \text{s.t.} \quad & f_i(\mathbf{x}; \boldsymbol{\alpha}_i^*) \leq 1, \quad i = 1, \dots, m, \end{aligned} \tag{4.19}$$

where $\boldsymbol{\alpha}_i^*$ is the maximizer of

$$\begin{aligned} \max_{\boldsymbol{\alpha}_i} \quad & f_i^*(\mathbf{x}; \boldsymbol{\alpha}_i) \\ \text{s.t.} \quad & B_j(\boldsymbol{\alpha}_i, \varepsilon) \leq 0, \quad j = 1, \dots, b. \end{aligned} \tag{4.20}$$

Here, $f_o(\mathbf{x})$ is the objective function and $f_i(\mathbf{x}, \boldsymbol{\alpha}_i)$ are constraints, whereas $B_j(\boldsymbol{\alpha}_i, \varepsilon)$ are bounds on uncertainties. For the applications studied in the present chapter, uncertainties through simple box bounds are adopted. Therefore the constrained maximization problem, as defined by Eq. (4.20), reduces to an unconstrained maximization problem as

$$\begin{aligned} \max_{\boldsymbol{\alpha}_i} \quad & f_i^*(\mathbf{x}; \boldsymbol{\alpha}_i) \\ \text{s.t.} \quad & \boldsymbol{\alpha}_i^l \leq \boldsymbol{\alpha}_i \leq \boldsymbol{\alpha}_i^u. \end{aligned} \tag{4.21}$$

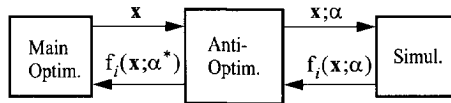


Figure 4.3: Anti-optimization Technique: Anti-optimization is carried out at every design (\mathbf{x}) for each constraint (f_i) to obtain corresponding worst set of uncertainties ($\boldsymbol{\alpha}^*$).

The minimization as defined in Eq. (4.19) will be referred to as the main optimization. Notice that, in general, the evaluation of the constraints involves, for each set of design variables, anti-optimization of the individual constraints. This anti-optimization is reflected by Eq. (4.20). The anti-optimization technique as defined in Eq. (4.19) and Eq. (4.20), is depicted by Fig. 4.3.

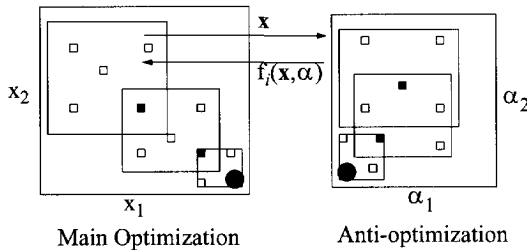


Figure 4.4: Anti-optimization technique in the MAM setting for a problem of two design variables (x_1 and x_2) and two uncertainties (α_1 and α_2). The big boxes indicate the search (sub-) domains. The small open boxes indicate sets of design variables (left) or uncertainty variables (right) for which function evaluations are carried out. The small solid boxes indicate solutions of the approximate optimization problems.

The anti-optimization technique is depicted in Fig. 4.4 in the MAM setting. It consists of an anti-optimization for every design point in the main optimization and for every constraint. The

main optimization, Eq. (4.19), is treated as a standard minimization problem, which searches for the best design in the design domain. The design domain is specified by upper- and lower bounds on the design variables. The anti-optimizations, Eq. (4.20), consist of performing numerical searches for the worst sets of uncertainty variables while keeping all design variables constant. Thus, the anti-optimizations are maximization problems searching for the worst combinations of uncertainty variables for a given set of design variables. These searches are restricted by the bounds on the uncertainty variables.

The anti-optimization technique, as sketched above, can handle large uncertainties safely. Moreover, it can account for discontinuities if any exist. The price paid for this flexibility is the large amount of computing efforts required for anti-optimization processes. Significant computational costs can be saved if the anti-optimization problem is convex. In that case, the worst set of uncertainty variables will be located at the bound. Often the anti-optimization can be reduced to a systematic search along the vertices of the domain of feasible uncertainty variables, Elishakoff et al. [7]. In the present chapter this assumption has not been adopted and the intention is to focus on methods that can be applied to more general problems, i.e. for which maximizers of Eq. (4.20) turn out not to be the vertices of the uncertainty domain.

In case of MEMS, due to their small dimensions, tolerances on shapes are *relatively* high, see Clark *et al.* [30] and Pister *et al.* [31]. In order to account for such manufacturing induced inaccuracies, uncertainties can be introduced as tolerances on design variables. The present anti-optimization technique can handle these uncertainties equally well. Uncertainty-based optimization of a Piezoelectric Energy Reclamation Device is carried out in Gurav *et al.* [37], where uncertainties in design variables are included. In the present chapter, a MEMS application is studied, where the dimensional uncertainty influences the design variable.

4.2.4 Enhanced Anti-optimization

The anti-optimization technique as discussed previously, can become inefficient for large number of design variables and uncertainties in case of practical problems. In order to reduce the total number of expensive numerical response evaluations, the anti-optimization technique is modified in the present chapter to exploit database technique and sensitivities.

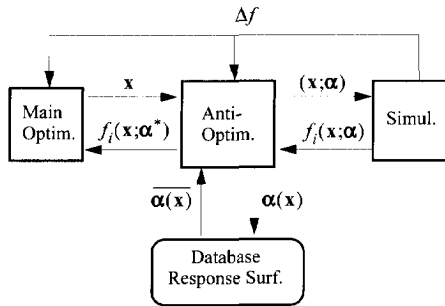


Figure 4.5: Enhanced Anti-optimization: worst uncertainties obtained by anti-optimization are stored in the database and used later to get starting points for anti-optimization. Gradient information, if available, can be used in both main- and anti-optimization.

Database Technique

As already discussed, in the anti-optimization technique for every design, worst value of every constraint is obtained by a separate anti-optimization. It should be noted here that, in the present setting

of the method, individual anti-optimization is also carried out using the MAM. Therefore, as mentioned earlier, see Section 4.2.1, the selection of proper move limits for the initial cycle can speed up the anti-optimization significantly. In the present technique, the move limits chosen for the initial cycle of the anti-optimization are based on a prediction of the corresponding worst uncertainties with the use of a database. This database stores the worst uncertainties from previous anti-optimizations.

In the database technique, a separate database is constructed for every constraint. In this, corresponding worst sets of uncertainties obtained by the anti-optimizations, $\alpha(\mathbf{x})$ see Fig. 4.5, are stored as a function of design variables. Notice, that different sets of uncertainties are stored for the individual constraints. The database can be used later to predict the worst set of uncertainties for a given design by fitting a response surface, $\alpha(\mathbf{x})$, see Fig. 4.5.

In the beginning of the optimization there is not enough data in the database to fit sufficiently accurate response surfaces. Here normal anti-optimizations are carried out, which automatically contribute to the database. Once there is enough data available, response surfaces for uncertainties as a function of the design variables, $\alpha(\mathbf{x})$, can be fitted. In turn, these response surfaces can be exploited to predict the worst uncertainties for the given design. This estimation of uncertainties is used as a starting point for the anti-optimization, and move limits that surround the predicted worst uncertainties are used as the starting move limits for the anti-optimization. This speeds up the anti-optimization, resulting in a significant reduction in the number of response function evaluations, see Gurav *et al.* [20, 34].

Sensitivities

If sensitivity information is available, it can also be used to speed up the optimization. In general, if sensitivity information is available then relatively fewer response function evaluations are required to fit a GERS, see Van Keulen and Vervenne [17, 18], or the quality of the response surface can be improved. Thus, use of sensitivities in optimization can result in better convergence and a reduction in the number of response function evaluations. In the enhanced anti-optimization technique, sensitivities are used in both main and anti-optimization.

Anti-optimization: In case of anti-optimization, using sensitivities of response functions with respect to uncertainties is quite straightforward. The goal of the anti-optimization, Eq. (4.20), is to maximize the constraint $f_i(\mathbf{x}, \alpha)$ with respect to uncertainties (α) for a given design \mathbf{x} . While constructing the response surface for the constraint function, both the function value f_i and its derivatives with respect to uncertainties (α), f_{ij} , are used as discussed in Section 4.2.1. Here, $f_{ij} = (\partial f_i / \partial \alpha_j)$ with $j = 1, \dots, u$. Including sensitivities with respect to uncertainties while building the GERS for the response functions improves the accuracy of the response surfaces, affecting the convergence of the anti-optimization process. Alternatively, a lower number of function evaluations can be used to build the response surfaces with the same complexity.

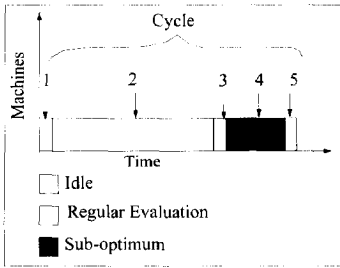
Main-optimization: In case of the main optimization, each additional design point implies additional anti-optimizations. Consequently, using fewer design points can save a large number of function evaluations. Thus, incorporation of sensitivities in the main optimization can reduce the total number of function evaluations and increase the overall efficiency substantially. Here, while constructing the GERS, function value, f_i , and its derivatives, f_{ij} , where $f_{ij} = (\partial f_i / \partial x_j)$ with $j = 1, \dots, n$, are used as discussed in Section 4.2.1. Notice here, that the response functions are functions of the design variables \mathbf{x} as well as the uncertainties α , i.e. $f_i = f_i(\mathbf{x}; \alpha)$. However, the uncertainties α^* that maximize a response function, see Eq. (4.20), are implicit functions of the design variables, $\alpha^* = \alpha(\mathbf{x})$. Consequently, sensitivities of response functions must be calculated as:

$$\frac{df_i}{dx_j} = \frac{\partial f_i}{\partial x_j} + \frac{\partial f_i}{\partial \alpha_k} \frac{\partial \alpha_k^*}{\partial x_j}, \quad (4.22)$$

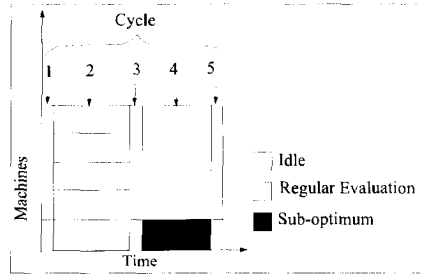
Here $i = 1, \dots, m$; $j = 1, \dots, n$; $k = 1, \dots, u$, and we have introduced $(d \cdot \cdot / dx_j)$ to denote total derivatives with respect to the independent design variable x_j . It is clear from Eq. (4.22), that in addition to the sensitivities of response functions with respect to the design variables, we need sensitivities of response functions with respect to the uncertainties and sensitivities of uncertainties with respect to the design variables. The derivatives $(\partial f_i / \partial x_j)$ and $(\partial f_i / \partial \alpha_k)$ can be obtained from an arbitrary sensitivity analysis. Evaluation of $(\partial \alpha_{ik}^* / \partial x_j)$ is troublesome. One option is to construct an approximation using response surfaces that are constructed using the data contained in the database. This requires sufficient data available in the database. In many situations, when the uncertainties α_i^* remain approximately constant in subsets of the design space, the second term in Eq. (4.22), i.e. $(\partial f_i / \partial \alpha_k^*) \cdot (\partial \alpha_{ik}^* / \partial x_j)$, can be ignored. When this is not the case, exclusion of these terms can influence the quality of response surfaces resulting in slower convergence. In the present chapter the second term in Eq. (4.22), i.e. $(\partial f_i / \partial \alpha_k^*) \cdot (\partial \alpha_{ik}^* / \partial x_j)$, is ignored, however it can be exploited in the future research work.

4.2.5 Parallel Computing

Optimization using Parallel Computing



(a) Plan points are evaluated sequentially



(b) Plan points are evaluated using parallel computing

Figure 4.6: A cycle in optimization using the MAM: Steps involved are 1: Planning, 2: Evaluation of plan points, 3: NMP, 4: Evaluation of sub-optimum, 5: Move limit strategy.

Optimization using the MAM involves the planning of experiments, leading to response evaluations for given sets of designs. If these function evaluations involve expensive finite element calculations, then the method can become computationally very intensive. However, if multiple processors are available for computation, they can be utilized easily to improve the efficiency of the method Van Keulen and Toropov [25].

The computing times required for various steps of a typical optimization using the MAM is represented approximately in Fig. 4.6 (a). It can be clearly seen here that, evaluation of plan points is the computationally most expensive phase, whereas the nonlinear minimization programming (NMP) problem and move limit strategy are relatively very cheap. When several processors are available for computation, they can be used in parallel to evaluate the expensive response evaluations in the planning phase, see Fig. 4.6 (b). It should be noted here that, an additional response evaluation is required at the end of the cycle to evaluate the sub-optimum of the AOP, see Section 4.2.1. In the present setting for response evaluation, splitting of the individual response evaluation is not possible, therefore every response can only be evaluated by a single processor. Because of this, during the evaluation of the sub-optimum only a single processor can be utilized keeping the other processors idle. This can increase the overall idle time significantly.

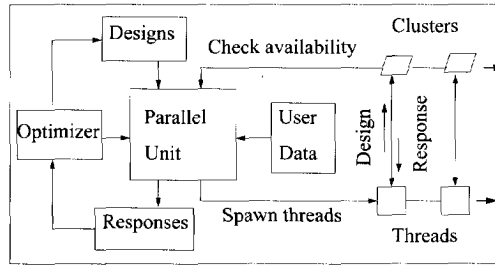
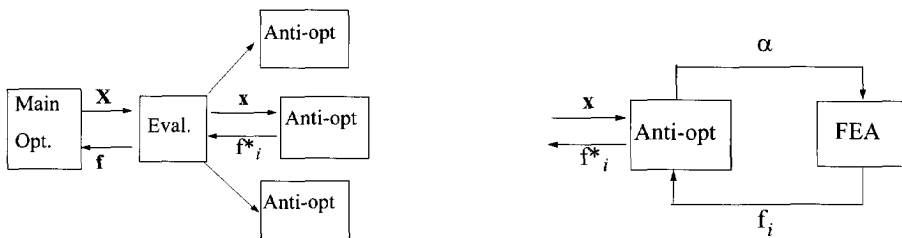


Figure 4.7: A framework for the parallel computing using the Threading module of PYTHON.

The parallel computing tool used for the present work is developed in PYTHON, see the textbook Lutz [24]. The framework for the tool is depicted in Fig. 4.7. Here, set of designs to be evaluated for responses, is given as an input to the Parallel Unit. This Parallel Unit uses the Threading module in PYTHON to start multiple threads in parallel. The number of threads, that can be started at a time in parallel, depends on the number of processors available for computation. Here, the main process first checks for the availability of the processors for computation. For example, every processor can be checked for its load average over some specified time. Then, jobs equal to the number of available processors are started in parallel with the Threading module from PYTHON. Remaining jobs are put in the queue. If any of the processors finishes a job started on it, it gets the next job in the que.

In the present setting, the programs and all the necessary data, other than the design parameters needed by the individual response evaluation, are ported to every processor before starting the jobs in parallel. Once the initialization is done, all the jobs to be evaluated are put in the que. Then the threads are spawned corresponding to the number of processors available for computation. Individual threads communicate with the remote processors associated to them through the files containing necessary data, for example, flags indicating whether the submitted job is finished or not. The communication using files does increase the overhead time, however, it is negligible as compared to the time required for an individual response evaluation. During the evaluation of an individual job, first the design parameters are send to the remote processor, see Fig. 4.7. Then the actual evaluation of responses, for example by using FEA, is started on the remote processor by the associated thread. When the evaluations for the job are finished, corresponding responses are received back and are associated with the job. Once a processor becomes available, the next job in the que is submitted to it. The procedure is repeated until all the jobs are evaluated.

Uncertainty-based Optimization using Parallel Computing



(a) Anti-optimizations are started in parallel

(b) Anti-optimization involves sequential evaluation of responses using FEA.

Figure 4.8: Parallel computing in the uncertainty-based design optimization

Uncertainty-based optimization involves anti-optimization nested within the main optimization. That is, for every design (\mathbf{x}) in the main optimization an anti-optimization is carried out for every constraint (f_i). This situation implies that there are many different options for parallel computing. As a compromise between computational efficiency and ease of implementation, each function evaluation started in parallel, actually carries out anti-optimizations for every constraint sequentially, see Fig. 4.8 (a) and Fig. 4.8 (b). It should be noted here that for the present approach, evaluation of sub-optimum points can increase the overall idle time substantially.

4.3 Examples

4.3.1 Ten-Bar-Truss

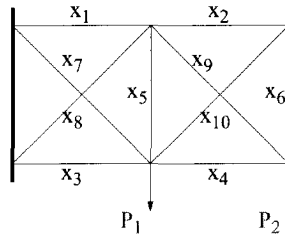


Figure 4.9: Optimization problem formulation for Ten-Bar-Truss example: Here, design variables, x_i , are cross sectional areas of bars, whereas P_i are uncertain loads.

The Ten-Bar-Truss example was used by Elishakoff *et al.* [7] to illustrate uncertainty-based optimization using BBU. However, expensive anti-optimizations are replaced by a systematic search along the vertices of the domain of feasible uncertainty variables. Here we shall use the example to test the proposed more general algorithms.

In the Ten-Bar-Truss problem, see Fig. 4.9, the goal is to minimize the weight of the structure, whereas constraints are imposed on the stresses in the bars. Here, the cross sectional areas of the bars (\mathbf{x}) are the design variables. Additionally, 10% uncertainty is introduced in the applied loads P_1 and P_2 , such that the bounds on uncertainties can be given as

$$\begin{aligned} \varepsilon &= 0.1\bar{P}_i, \\ P_i^l &= \bar{P}_i - \varepsilon = 0.9\bar{P}_i, \\ P_i^u &= \bar{P}_i + \varepsilon = 1.1\bar{P}_i. \end{aligned} \tag{4.23}$$

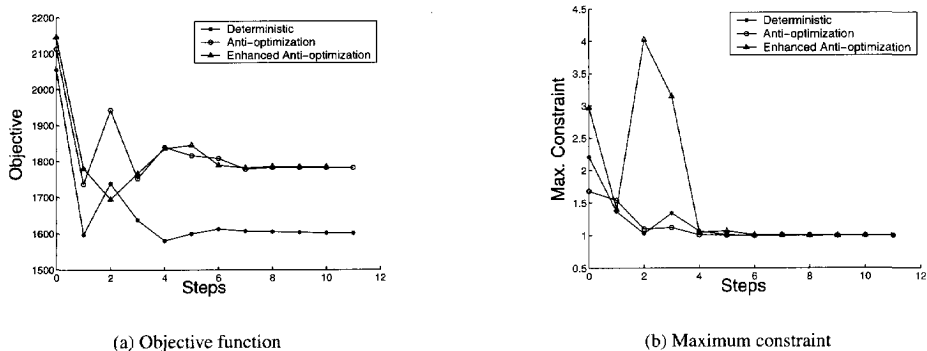


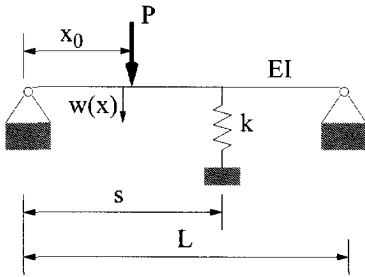
Figure 4.10: Optimization history for Ten-Bar-Truss example

Table 4.1: Comparison of deterministic and uncertainty-based optimization results for Ten-Bar-Truss problem: Here, g_{\max} represents the value for the maximum constraint violation.

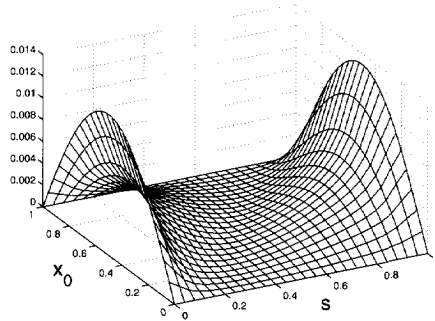
Type of optimization	f_0 lbs	g_{\max}	Num. of function evals	Rel. Num. of function evals
Deterministic	1600	1.00	137	1
Anti-opt	1782	1.00	51195	373
Enhanced Anti-opt	1784	1.00	10415	76

Results for the deterministic optimization, i.e. when the loads are at nominal values, match with those in Haftka *et al.* [38]. It is seen from the results obtained, that there is an increase in the objective function in case of uncertainty-based optimization as compared to the deterministic case, see Fig. 4.10 (a). Whereas convergence obtained for the constraints is very close as shown in Fig. 4.10 (b). In case of uncertainty-based optimization, results obtained using anti-optimization and enhanced anti-optimization are very close in terms of objective function and constraints. The number of steps required to obtain the convergence is comparable as well. However, there is a significant difference in the total number of response function evaluations required, see Table 4.1. Use of sensitivities in both the main- as well as anti-optimization together with the use of the database technique has reduced the total number of function evaluations by a factor of five.

4.3.2 Elastically supported beam



(a) Optimization problem formulation: Here $L = 1$ m, $P = 1000$ N, $k = 500000$ N/m, $EI = 1000$ N.m².



(b) Plot for the integrated displacement as a function of x_0 and s

Figure 4.11: Elastically Supported Beam example

An elastically supported beam, see Fig. 4.11, is used by Lombardi and Haftka [19] to test the anti-optimization technique in the presence of nonlinearities. One of the features of this problem is the strong dependence of the worst uncertainty on the design variable. As a consequence the present problem calls for the approach as studied here.

The problem consists of a beam loaded by a concentrated force and supported elastically to limit its vertical displacements, see Fig. 4.11 (a). The goal of the optimization here is to optimally place the elastic support so that the integral of the displacement function over the length of the beam is minimum. The location of the concentrated load represents the uncertainty variable. Assuming the nominal location of the concentrated load at the center of the beam ($\bar{x}_0 = 0.5L$), with $\epsilon = 0.5L$, the

lower and upper bounds on uncertainty (x_0) can be given as

$$\begin{aligned} x_0^l &= \bar{x}_0 - \varepsilon = 0, \\ x_0^u &= \bar{x}_0 + \varepsilon = L. \end{aligned} \tag{4.24}$$

Here, the objective of the anti-optimization is nonlinear. The displacement function $w(x, s, x_0)$ is analytically determined by integration of the fourth-order differential beam equation.

$$EI \frac{\partial^4 w}{\partial x^4} = P\delta(x - x_0) - kw(x)\delta(x - s). \tag{4.25}$$

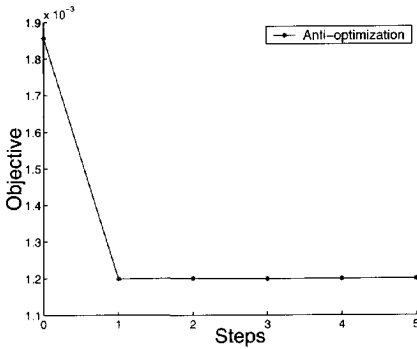
The main and anti-optimization problems are formulated as follows:

main optimization

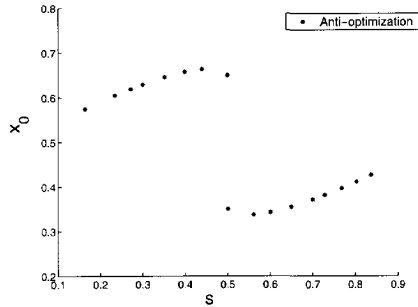
$$\min_s \int_0^L w(x, s, x_0) dx \quad \text{s.t.} \quad 0 \leq s \leq L, \tag{4.26}$$

anti-optimization

$$\max_{x_0} \int_0^L w(x, s, x_0) dx \quad \text{s.t.} \quad 0 \leq x_0 \leq L. \tag{4.27}$$



(a) Objective function for the uncertainty-based optimization is plotted vs steps

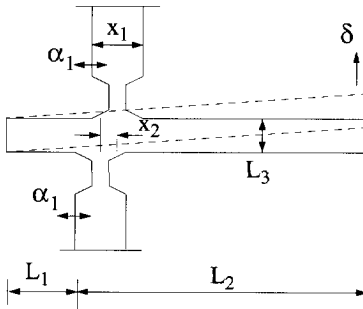


(b) Plot for the worst uncertainty (x_0) obtained during the uncertainty-based optimization for corresponding design variable (s).

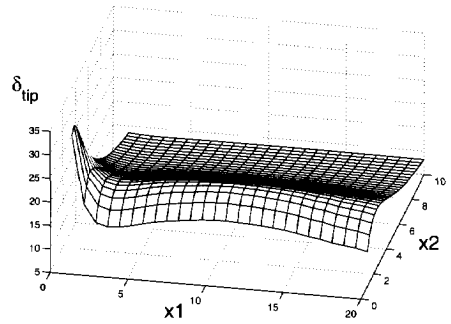
Figure 4.12: Optimization history for the elastically supported beam example

The actual integrated displacement is plotted in Fig. 4.11 (b). The result for the uncertainty-based optimization using anti-optimization technique is shown in Fig. 4.12 (a). As a result, the optimum location of the support is at 0.5 m, whereas the worst location of the concentrated load is at 0.35 m, which can be clearly seen from the actual plot of integrated displacement Fig. 4.11 (b). It can be seen from Fig. 4.12 (b), that the worst uncertainties obtained corresponding to the designs during anti-optimization, fluctuate significantly. They even show discontinuity depending upon the location of the load (x_0) with respect to the support (s). The present technique can handle such large fluctuating uncertainties and even discontinuities.

4.3.3 Embedded measurement MEMS structure



(a) Optimization problem formulation: Here, x_1 and x_2 are design variables, whereas α_1 is an uncertainty. $L_1 = 20\mu\text{m}$; $L_2 = 450\mu\text{m}$; $L_3 = 20\mu\text{m}$.



(b) The actual tip deflection of the embedded measurement structure example computed for various combinations of the design variables x_1 and x_2 is plotted here.

Figure 4.13: Embedded Measurement Structure example

The anti-optimization technique is applied to an embedded measurement MEMS structure, see Fig. 4.13 (a), as discussed in van Drieënhuizen *et al.* [35] and Goosen *et al.* [36]. The purpose of this microstructure is to obtain information on the strain state of certain layers in a MEMS device. This information is used to obtain an estimate for the internal stresses. In the development of MEMS, information on the internal stresses that arise due to processing steps is often crucial to the designer. The embedded measurement structure converts a contraction or expansion due to internal stresses into a rotation and displacement δ , see Fig. 4.13 (a), which can be determined by inspection using an optical microscope.

Here, the deterministic optimization consist of a maximization problem, in which the tip displacement (δ) is maximized without considering the variation in it as an effect of uncertainties. In case of uncertainty-based optimization the effect of uncertainties on the variation of tip deflection is considered. Actually this variation in the tip displacement is restricted by means of a constraint (3% variation is allowed). Uncertainties here, are mainly due to variation in the etching times and results in either contraction or expansion of the structure changing its dimensions. In the present problem uncertainty in only one direction, α_1 , is considered. The uncertainty α_1 , is specified here as a tolerance on the dimensions, see Fig. 4.13 (a). Notice, that the uncertainty α_1 actually influences the design variable x_1 .

The maximum displacement at the tip (δ) is the objective $f_0(\mathbf{x})$ of the main optimization as given by Eq. (4.19). In the present problem, constraint $f_1(\mathbf{x}, \alpha_1)$ used in the main-optimization limits the relative change in the tip deflection, due to the uncertainty (α_1), to a specified value (3%) as

$$\left\| \frac{f_0(\mathbf{x}) - f_0(\mathbf{x}, \alpha_1)}{f_0(\mathbf{x})} \right\| \leq 3\%. \quad (4.28)$$

Objective of the anti-optimization is to maximize the constraint $f_1(\mathbf{x}, \alpha_1)$ with respect to uncertainty α_1 subjected to bound $B_1(\alpha_1)$. Here, the bound B_1 is specified in the form of upper and lower bounds on the uncertainty α_1 as $[-0.2, 0.2] \mu\text{m}$, with the dimension of uncertainty $\varepsilon = 0.2 \mu\text{m}$. A parameterized FEM model of the MEMS structure is used as a simulation model in the optimization. Two-dimensional triangular plane-stress elements are used for modelling.

The actual tip deflection computed for various combinations of the design variables is plotted in Fig. 4.13 (b). It can be seen that there exists multiple local optima. Therefore the problem domain is split in two separate design problems, denoted Design-1 and Design-2. These two subproblems are studied separately and the results for them are compared.

Design-1

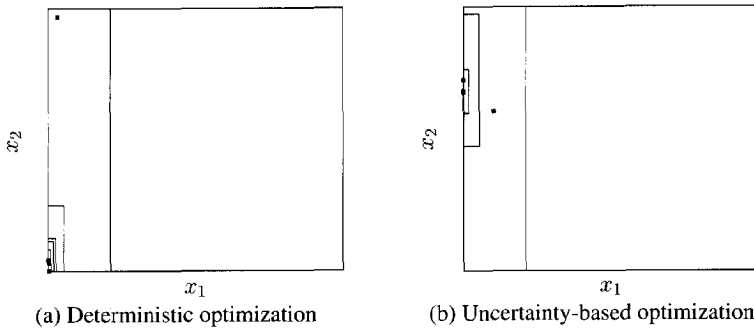


Figure 4.14: Optimization history in terms of move limits for embedded measurement structure example for Design-1. The design domain for this subproblem is $x_1 \in [1.0; 5.0] \mu\text{m}$ and $x_2 \in [1.0; 10.0] \mu\text{m}$.

The design domain for this part is given as $x_1 \in [1.0; 5.0] \mu\text{m}$ and $x_2 \in [1.0; 10.0] \mu\text{m}$. Whereas, the uncertainty domain is taken as $[-0.2; 0.2] \mu\text{m}$. The optimization history in terms of move limits is plotted in Fig. 4.14 (a) and Fig. 4.14 (b) for deterministic and uncertainty-based optimization respectively. In case of deterministic optimization, the tip deflection is maximized however it results in a variation of about 21%. Whereas, uncertainty-based optimization finds an optimum, which resulted in reduction of tip deflection but restricting the variation to 3%.

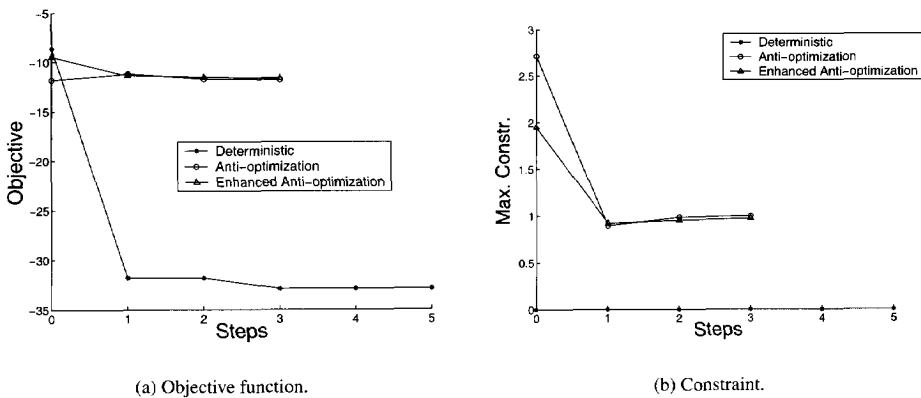


Figure 4.15: Optimization history for embedded measurement structure example for Design-1: The design domain for this subproblem is $x_1 \in [1.0; 5.0] \mu\text{m}$ and $x_2 \in [1.0; 10.0] \mu\text{m}$.

Table 4.2: Comparison of results for various optimization techniques applied to embedded measurement structure problem: Design-1

Type of optimization	x_1 μm	x_2 μm	f_0 μm	f_1	Num. of function evals	Rel. Num. of function evals
Deterministic	1.00	1.37	32.84	-	42	1
Anti-opt	1.00	7.08	11.80	0.99	1479	35
Enhanced Anti-opt	1.00	7.18	11.66	0.97	766	18

The results for the deterministic optimization and the uncertainty-based optimization using anti-optimization and enhanced anti-optimization are compared, for objective (δ) in Fig. 4.15 (a) and for the constraint (f_1) in Fig. 4.15 (b). It can be seen from Fig. 4.15 (a), that there is a significant reduction in the objective function in case of uncertainty-based optimization, in order to meet the requirement (3% variation). Comparison between results for anti-optimization and enhanced anti-optimization show similarity in terms of convergence and number of steps. Whereas number of response evaluations required differ significantly, see Table 4.2. The use of sensitivities and database technique has reduced substantially the total number of function evaluations required for anti-optimization, here the total function evaluations are halved.

Design-2

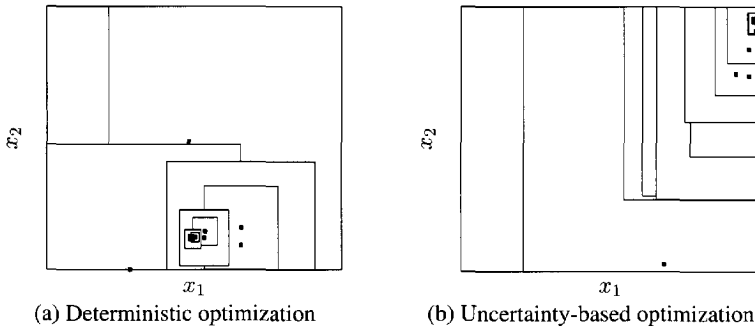


Figure 4.16: Optimization history in terms of move limits for embedded measurement structure example for Design-2. The design domain for this subproblem is as $x_1 \in [5.0; 20.0] \mu\text{m}$ and $x_2 \in [1.0; 10.0] \mu\text{m}$.

The design domain for this second subproblem is given as $x_1 \in [5.0; 20.0] \mu\text{m}$ and $x_2 \in [1.0; 10.0] \mu\text{m}$. Whereas, the uncertainty domain is taken as $[-0.2; 0.2] \mu\text{m}$. The optimization history in terms of move limits is plotted in Fig. 4.16 (a) and Fig. 4.16 (b) for deterministic and uncertainty-based optimization, respectively. A trend similar to Design-1 is seen, where uncertainty-based optimization finds an optimum with a reduced tip deflection as compared to the uncertainty-based optimization.

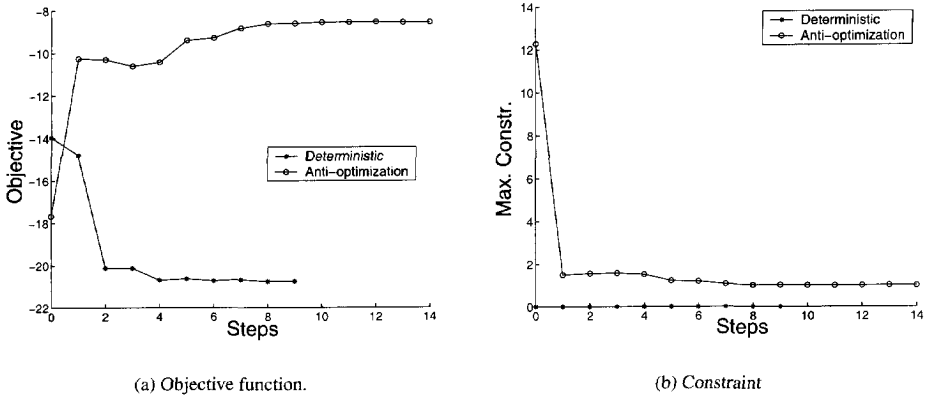


Figure 4.17: History of optimization for embedded measurement structure example for the constraint for Design-2. The design domain for this subproblem is as $x_1 \in [5.0; 20.0] \mu\text{m}$ and $x_2 \in [1.0; 10.0] \mu\text{m}$.

The results for the deterministic and uncertainty-based optimization are compared in Fig. 4.17 (a) and Fig. 4.17 (b). It can be seen that there is a significant reduction in the objective function in order to meet the requirement (3% variation).

Table 4.3: Comparison of results for the embedded measurement structure problem for sub-problem Design-1 and Design-2

	Type of optimization	x_1 μm	x_2 μm	f_0 μm	f_1	Num. of function evals
Design 1	Deterministic	1.00	1.37	32.84	-	42
	Anti-opt	1.00	7.08	11.80	0.99	1479
Design 2	Deterministic	10.30	2.08	20.76	-	70
	Anti-opt	19.81	9.55	8.55	0.99	5094

The results obtained for the two subproblems, are compared in Table 4.3. The design for subproblem Design-2 is quite similar to the baseline design in van Drieënhuizen *et al.* [35] and Goosen *et al.* [36]. The design for sub-problem Design-1 exhibits a larger tip deflection. It can be seen from the plot for the actual tip displacement, see Fig. 4.13 (b), that the local optima are quite close to those obtained by the optimization.

Table 4.4: Comparison of results for the embedded measurement structure problem for sub-problem Design-1: Comparison between parallel and sequential evaluation.

Type of Optimization	Computing Scheme	Wall-clock time Hour:Min:Sec
Deterministic	Sequential	1:01:00
	Parallel	0:13:6
Anti-opt	Sequential	41:32:50
	Parallel	5:56:55

Finally, wall-clock time required for the deterministic as well as uncertainty-based optimization using sequential and parallel computing is compared, see Table 4.4. Here, 10 processors are utilized for parallel computing. A substantial reduction in computing time is achieved. In case of deterministic optimization nearly 78 %, whereas in case of uncertainty-based optimization nearly 85 % reduction in the corresponding required wall clock time is achieved. It should be noted, that the evaluation of the sub-optimum at the end of every cycle increases the overall idle time. In case of anti-optimization, evaluation of sub-optimum involves an optimization. This can increase the overall idle time significantly. This idle time increases substantially with the increase in number of uncertainties. However, for the present problem, due to the small number of uncertainties, the efficiency achieved is higher as compared to that of deterministic optimization.

4.4 Discussion/Conclusion

The anti-optimization technique is modified here to make use of the design sensitivities, database technique, and parallel computing. This enhanced anti-optimization technique has increased the computational efficiency of the basic technique significantly, making its use practical for large scale applications.

It is seen from the numerical results obtained for the examples studied here, that there is a significant change in objective function in case of uncertainty-based optimization as compared to that of deterministic optimization. In case of uncertainty-based optimization, results obtained using different methods are quite close in terms of objective function value and number of steps required to converge. However, there is a significant difference in the total number of response function evaluations required. Use of sensitivities and database technique in the enhanced anti-optimization technique has shown significant reduction in the number of function evaluations as compared to that of anti-optimization. Use of parallel computing reduces the total time required for optimization substantially. Consequently, the anti-optimization technique developed here, can be applied efficiently to general problems for which uncertainties can be non convex or even discontinuous.

To summarize, uncertainties in design problems described by bounds can be handled safely and efficiently using the enhanced anti-optimization technique.

4.5 Acknowledgment

This research is supported by the Technology Foundation STW, applied science division of NWO and the technology program of the Ministry of Economic Affairs, The Netherlands.

Chapter 5

Cycle-based Alternating Anti-optimization

In this chapter uncertainty-based design optimization of a micro energy reclamation device is presented. The goal is to optimally design a Microelectromechanical Systems based device to extract maximum power from externally introduced vibrations. This microstructure consists of an array of piezoelectric composite cantilever beams connected to a free standing mass. Each cantilever beam undergoes deformation when subjected to external base vibrations. This deformation induces a mechanical strain in the beam resulting in the conversion to electric voltage due to the piezoelectric effect. In case of microstructures, uncertainties in geometry as well as material properties are large and therefore may have significant effects on the mechanical behavior. In the present chapter uncertainties in geometry and material properties are considered. A description of uncertainties via bounds on the uncertainty variables is adopted. Uncertainty-based design optimization is carried out using the anti-optimization technique.

5.1 Introduction

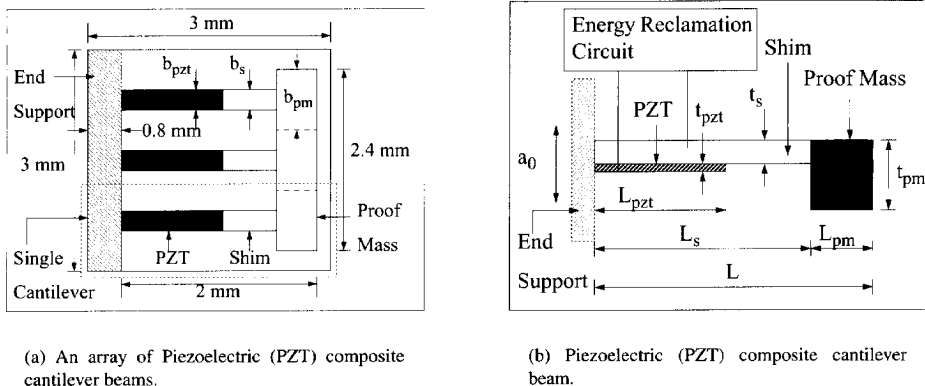


Figure 5.1: An energy reclamation device.

In the present study, design optimization of an energy reclamation device is considered. The detailed description of the electro-mechanical model is given in [39,40]. The overall purpose of the device is to extract maximum power from external base vibrations. An energy reclamation device consists of

an array of piezoelectric (PZT) composite cantilever beams arranged as shown in Fig. 5.1(a). Each cantilever beam consists of a perfectly bonded PZT patch [41] and a proof mass attached at the end, see Fig. 5.1(b). In a real application, the device is attached at the support to a vibrating surface, which implies that the whole structure is in an accelerating frame of reference. The proof mass at the tip translates the input acceleration into an effective force that deflects the beam. This effective force induces mechanical strain in the beam, which is converted into voltage (V) using the piezoelectric effect [41, 42]. The output voltage of the PZT can be reclaimed into usable power with the help of an energy reclamation circuit.

When dealing with Microelectromechanical Systems (MEMS), because of their small dimensions, tolerances on shapes are *relatively high* (1%-10%) [30, 31]. These variations in dimensions of MEMS structures can have a significant effect on their mechanical behavior. Furthermore, MEMS exhibit a large variation in their material properties (1%-15%) [43–46]. As a result, while designing MEMS, various types of uncertainties should be considered.

One way to deal with uncertainties, is to use probabilistic methods [8]. However, probabilistic methods require an abundance of experimental data [9]. Furthermore, even small inaccuracies in the statistical data can lead to large errors in the computed probability of failure to meet structural requirements [9]. Many times, for example in preliminary design phases, some experimental data is available but, it is not enough to construct reliable probability distributions. However, the available data can be used, particularly in combination with engineering experience, to set tolerances or bounds on uncertainties. Consequently, uncertainties will be identified as belonging to some closed sets, i.e. to be of Bounded-But-Unknown (BBU) nature [11, 12].

To tackle such BBU uncertainties, a technique based on *anti-optimization* (a term dubbed by Elishakoff [26]) is proposed in [7]. In this technique, uncertainty-based optimization is basically split in two parts, namely, main- and anti-optimization. The main optimization is treated as a standard minimization problem which searches for the best design in the design domain. The design domain is typically specified by upper- and lower bounds on design variables. The anti-optimization consist of performing numerical searches for the combination of uncertainties which yields the worst response for a given design and a particular response function. In the worst case scenario, an anti-optimization for every constraint is required. Within these anti-optimizations, the uncertainties are set as “design variables”, whereas the “design domain” is specified by the bounds on the uncertainties. Thus, anti-optimizations are nested within the main optimization, making it a two-level optimization problem, which can be very computationally intensive.

The anti-optimization technique is further developed and applied in [13, 34]. The technique is modified in [47] for using design sensitivity information, database technique and parallel computing in order to make the technique computationally efficient. In order to reduce the computational efforts, a different approach based on BBU uncertainties is proposed by Lombardi and Haftka [19]. Here, instead of nesting anti-optimization within the main optimization, anti- and main optimization are carried out alternately. Inspired by Lombardi and Haftka technique, a slightly modified technique, referred subsequently as *cycle-based alternating anti-optimization*, was studied in [20]. In this technique, anti-optimization is nested within the main optimization but carried out only at the sub-optimal point, i.e. the point obtained at the end of each optimization cycle. Because of its computational efficiency, this technique will be applied to the present problem of PZT composite beam optimization.

In case of the present problem, uncertainties involved in geometry as well as material properties are identified as belonging to some closed sets, i.e. to be of BBU nature. As mentioned, the uncertainty-based design optimization is carried out using the cycle-based alternating anti-optimization technique. The anti-optimization technique is embedded in a structural optimization setting using the Multipoint Approximation Method (MAM) [1–5].

Uncertainty-based design optimization technique using BBU uncertainties and the problem formulation for the optimization of a PZT composite beam are given in Section 5.2. In Section 5.4, results for the uncertainty-based optimization including uncertainties are compared with those for

the deterministic optimization. Moreover, optimal designs obtained are compared with the baseline design. Final discussion and conclusion are the subject of Section 5.5.

5.2 Design Optimization

5.2.1 Deterministic optimization

In the present chapter the Multipoint Approximation Method (MAM) is used for optimization. The interested reader is referred to the studies in [1–4]. The MAM is described in detail in [5]. The optimization problem using MAM can be formulated mathematically as follows:

$$\begin{aligned} \min_{\mathbf{x}} \quad & f_0(\mathbf{x}) \\ \text{s.t.} \quad & f_i(\mathbf{x}) \leq 1, \quad i = 1, \dots, n. \end{aligned} \quad (5.1)$$

Here, f_0 is the objective function and f_i are constraints, whereas \mathbf{x} is a set of design variables.

The basic idea is, that in a sub-domain of the search domain approximate response surfaces are constructed as functions of the design variables. The response surfaces are used as approximations of the actual, expensive-to-evaluate, response functions. For this, within a sub-domain of the design space a plan of experiments is generated using a space filling technique. The construction of the response surfaces is carried out using a weighted least-squares fit. The weights reflect the relative importance of the data to the optimization process. The minimization problem for the approximated response functions is solved to get a sub-optimal solution in the corresponding sub-domain. Based on the quality of sub-optimal solution of the current sub-domain the location and size of a new search sub-domain is defined. This process is repeated until convergence has occurred.

5.2.2 Uncertainty-based optimization

Bounded-But-Unknown Uncertainty

If the problem at hand is non-deterministic, i.e. there are uncertainties that play a non-negligible role, the response functions also depend on the uncertainty variables. The set of uncertainty variables will be denoted α , with

$$\alpha = (\alpha_1, \dots, \alpha_u). \quad (5.2)$$

Consequently, the response functions depend on both design variables and uncertainty variables, hence $f(\mathbf{x}, \alpha)$.

Even though insufficient information is available in order to perform a probabilistic analysis, it may be possible to determine or specify reasonable bounds on the uncertainties. In general, several bounds are introduced, each providing a bound for a group of uncertainty variables or all uncertainty variables simultaneously. At the same time we may want to measure the amount of uncertainty. Thus, measures for the dimensions of the subspace containing all possible selections of uncertainty variables are desired. For the application studied in the present chapter, uncertainties through simple box bounds are adopted. In general, the problem with uncertainties can be cast into a mathematical framework as follows. Assuming a set with b bounds, then a possible or *feasible* selection of α satisfies [13],

$$B_i(\alpha, \varepsilon) \leq 0, \quad \text{for } i = 1, \dots, b, \quad (5.3)$$

otherwise the selection of the uncertainty variables α is *infeasible*. The components of ε are used to specify the dimensions of the subspace of feasible uncertainty variables. We will therefore refer to these components as the *levels of uncertainty*. As we use these levels of uncertainty to describe the dimensions of a subspace, each of the components will be non-negative, i.e.

$$\varepsilon_j \geq 0, \quad \text{for } j = 1, \dots, r. \quad (5.4)$$

Note that the number of components of ε is not necessarily equal to the number of bounds being introduced.

It seems natural to assume that if the dimensions of the space of uncertainties have become zero, the uncertainty variables become deterministic. In other words, if $\varepsilon = \mathbf{0}$ then there is only a single solution $\alpha = \bar{\alpha}$ such that

$$B_i(\bar{\alpha}, \mathbf{0}) \leq 0, \quad \text{for } i = 1, \dots, b. \tag{5.5}$$

Moreover, for $\alpha = \bar{\alpha}$ the equal sign holds true.

Anti-optimization

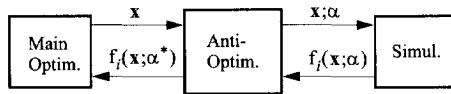


Figure 5.2: Anti-optimization Technique: Anti-optimization is carried out at every design (\mathbf{x}) for each constraint (f_i) to obtain corresponding worst set of uncertainties (α^*).

The optimization problem using BBU uncertainties can be formulated mathematically as:

$$\begin{aligned} \min_{\mathbf{x}} \quad & f_o(\mathbf{x}) \\ \text{s.t.} \quad & f_i(\mathbf{x}; \alpha_i^*) \leq 1, \quad i = 1, \dots, n, \end{aligned} \tag{5.6}$$

where α_i^* is the maximizer of

$$\begin{aligned} \max_{\alpha_i} \quad & f_i^*(\mathbf{x}; \alpha_i) \\ \text{s.t.} \quad & B_j(\alpha_i, \varepsilon) \leq 0, \quad j = 1, \dots, b. \end{aligned} \tag{5.7}$$

The minimization as defined in Eq. (5.6) will from here on be referred to as the main optimization. Notice that, in general, the evaluation of the constraints involves, for each set of design variables, anti-optimization of the individual constraints. This anti-optimization is reflected by Eq. (5.7). The anti-optimization technique as defined in Eq. (5.6) and Eq. (5.7), is depicted by Fig. 5.2.

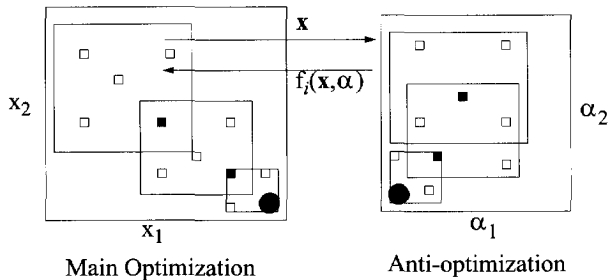


Figure 5.3: Anti-optimization technique in the MAM setting for a problem of two design variables (x_1 and x_2) and two uncertainties (α_1 and α_2). The big boxes indicate the search (sub-) domains. The small open boxes indicate sets of design variables (left) or uncertainty variables (right) for which function evaluations are carried out. The small solid boxes indicate solutions of the approximate optimization problems.

The anti-optimization technique is depicted in Fig. 5.3 in the MAM setting. It consists of an anti-optimization for every design point in the main optimization and for every constraint. The main optimization, Eq. (5.6), is treated as a standard minimization problem, which searches for the best design in the design domain. The design domain is specified by upper- and lower bounds on the design variables. The anti-optimizations, Eq. (5.7), consist of performing numerical searches for the worst sets of uncertainty variables while keeping all design variables constant. Thus, the anti-optimizations are maximization problems searching for the worst combinations of uncertainty variables for a given set of design variables. These searches are restricted by the bounds on the uncertainty variables.

The anti-optimization technique, as sketched above, can handle large uncertainties safely. Moreover, it can account for discontinuities if any exist. The price paid for this flexibility is the large amount of computing efforts required for anti-optimization processes. Significant computational costs can be saved if the anti-optimization problem is convex. In that case, the worst set of uncertainty variables will be located at the bound. Often the anti-optimization can be reduced to a systematic search along the vertices of the domain of feasible uncertainty variables [7].

Cycle-based alternating anti-optimization

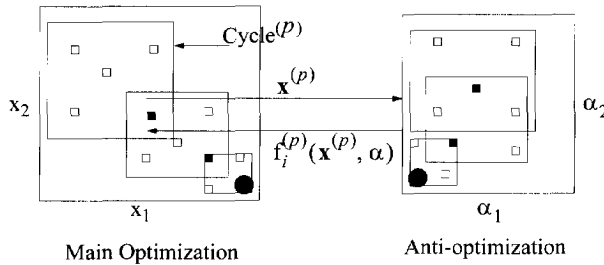


Figure 5.4: Cycle-based alternating anti-optimization technique: Anti-optimization is carried out at the end of every cycle of main optimization for every constraint.

In order to avoid nested anti-optimization, an alternative approach is described in [19]. In this approach, instead of using nested anti-optimization, which is very expensive, a technique is used alternating between main optimization and anti-optimization. A variation of such alternating anti-optimization technique, referred to as *Cycle-based* alternating anti-optimization technique, is proposed in [20]. In this method, anti-optimization is carried out not for every design but only for the sub-optimal design obtained at every cycle of the main optimization, see Fig. 5.4. The idea is to solve

$$\begin{aligned} \min_{\mathbf{x}} \quad & f_o^{(p)}(\mathbf{x}) \\ \text{s.t.} \quad & f_i^{(p)}(\mathbf{x}; \boldsymbol{\alpha}_i^{(p)}) \leq 1, \quad i = 1, \dots, n, \end{aligned} \tag{5.8}$$

for given $\boldsymbol{\alpha}_i^{(p)}$. This set of uncertainties are the maximizers of

$$\begin{aligned} \max_{\boldsymbol{\alpha}_i} \quad & f_i^{(p)}(\mathbf{x}^{(p)}; \boldsymbol{\alpha}_i) \\ \text{s.t.} \quad & B_j(\boldsymbol{\alpha}_i, \boldsymbol{\varepsilon}) \leq 0, \quad j = 1, \dots, b. \end{aligned} \tag{5.9}$$

Here, anti-optimization Eq. (5.9) is nested within main optimization Eq. (5.8). However, anti-optimization is carried out only at the sub-optimum $x^{(p)}$ obtained at the end of each cycle (p) of the main optimization. The sets of uncertainties ($\boldsymbol{\alpha}_i^{(p)}$) obtained by anti-optimization are used for the

next cycle of the main optimization. For the initial step, anti-optimization can be carried out for the initial design in order to get the worst set of uncertainties. Another choice would be to choose uncertainties arbitrarily or as $\alpha^{(p)} = \bar{\alpha}$, see Eq. (5.5). The latter choice is more suitable for the present optimization setting. In the present chapter, the cycle-based alternating anti-optimization technique is applied to the uncertainty-based optimization of the PZT composite cantilever beam.

5.3 PZT Energy Reclamation Device Optimization Problem Formulation

5.3.1 Objective function

The objective function for the current optimization problem is expressed as follows:

$$f_0(\mathbf{x}) = P_{\text{out}}. \quad (5.10)$$

where P_{out} is the electrical output power extracted from the device. The composite cantilever beam is subjected to external acceleration (a_0) as shown in Fig. 5.1(b). This external acceleration is specified in terms of external excitation frequency f_{ext} . Whereas f_n is the fundamental natural frequency of the cantilever beam. For the present problem support acceleration and excitation frequency is assumed as $a_0 = 1g$, where $g = 9.8 \text{ m/s}^2$ and $f_{\text{ext}} = 125 \text{ Hz}$.

When the fundamental natural frequency of the cantilever beam (f_n) matches the external excitation frequency (f_{ext}), i.e. at the resonance, the beam undergoes maximum deflection and therefore a maximum power is obtained. However, the objective function or power has an exponential increase near the resonance. Here, use of very high order polynomials (typically 7th order) is essential to get a good approximation for the power function. This can be computationally intensive and can become impractical when the number of design variables increases. To overcome this problem, log of the power function, which flattens it significantly, is used as the objective function. This allows the use of lower order polynomial (3rd order) to get an adequate approximation for the log of power function. Notice, since the problem needs to be formulated as a minimization problem, $-\log(P_{\text{out}})$ will be minimized.

5.3.2 Mechanical Constraints

Small deflection constraint: The Euler-beam theory for small deflections [48] is used to predict the deformations. Therefore, the tip deflection of the cantilever beam is restricted by

$$\frac{2.5 y_{\text{tip}}}{L} \leq 1, \quad (5.11)$$

where y_{tip} is the tip deflection and L is the overall length of the cantilever beam.

Stress constraint: At the resonance condition the cantilever beam may undergo large deflections and may crack. In order to avoid the damage due to fatigue and to stay within the linear elastic limit, the allowable bending stress is taken as 10 % of the maximum allowable bending stress (σ_{bm}). The constraint on bending stress in the cantilever beam is expressed as

$$\frac{\sigma_b}{0.1\sigma_{\text{bm}}} \leq 1, \quad (5.12)$$

where σ_b is the bending stress in the cantilever beam. Here, σ_{bm} is taken as 7 GPa [49].

Constraint on L/b ratio: It was found from preliminary results that the optimal design tends to move toward a design for which the length-to-width ratio for shim or PZT becomes very small. This can violate the Euler-beam theory assumption used in the electro-mechanical analysis. Therefore, the L/b ratio for shim and PZT is restricted by

$$\frac{3b_s}{L_s} \leq 1. \quad (5.13)$$

In the present chapter, effects of including this constraint on the optimization will be compared with those of excluding it.

5.3.3 Electrical Constraints

An electrical constraint is imposed on the minimum output voltage required to trigger the energy reclamation circuit as

$$\left(\frac{V_{\min}}{V_{\text{Th}}} \right) \leq 1; \quad V_{\min} = 2 \text{ Volts}, \quad (5.14)$$

where V_{Th} is the Thevenin voltage and V_{\min} is the minimum required output voltage for the device.

5.3.4 Design Variables

Based on a preliminary study, move limits on design variables \mathbf{x} are chosen to avoid practically impossible designs. The move limits on design variables used in the present optimization problem are

$$\begin{aligned} 100 &\leq x_1 \leq 2000 \text{ } (\mu\text{m}), \\ 0.05 &\leq x_2 \leq 0.95, \\ 50 &\leq x_3 \leq 800 \text{ } (\mu\text{m}), \\ 0.1 &\leq x_4 \leq 0.8, \\ 10 &\leq x_5 \leq 500 \text{ } (\mu\text{m}), \\ 3 &\leq x_6 \leq 100 \text{ } (\mu\text{m}), \end{aligned}$$

where x_1 is the overall length of cantilever beam (L), x_3 is the width of proof mass (b_{pm}), x_5 is the thickness of proof mass (t_{pm}), and x_6 is the thickness of shim (t_s), see Fig. 5.1. Other geometric parameters such as length of shim and PZT are taken as a fraction of total length (i.e. L) and the width of shim and PZT are taken as a fraction of width of proof mass (i.e. b_{pm}). These fractions are represented by the design variables x_2 and x_4 . Here, due to the fabrication limitations, t_{pzt} is kept fixed at the upper bound and an additional constraint ($b_{pzt} = b_s$) is imposed on the width of shim and PZT. Preliminary results have shown that the length of PZT remains almost equal to that of shim. This equality ($L_{pzt} = L_s$) is used here in order to reduce the total number of design variables. Remaining geometric parameters are obtained using

$$\begin{aligned} L_s &= x_1 \cdot x_2, \\ L_{pzt} &= L_s, \\ L_{pm} &= x_1 - L_s, \\ b_s &= x_3 \cdot x_4, \\ b_{pzt} &= b_s, \\ t_{pzt} &= 0.5 \text{ } (\mu\text{m}), \\ t_{pm} &= 500 \text{ } (\mu\text{m}), \end{aligned}$$

5.3.5 Uncertainties

For the present problem, the objective (P_{out}) is a function of design variables as well as uncertainties. Here, the effect of uncertainties on objective function can also be taken into account. One way to deal with this problem is, to carry out anti-optimization for the objective function together with constraints in order to get the worst cases. Secondly, at the end of the optimization, an anti-optimization and an optimization for fixed design variables can be carried out to set a bound on the objective function. In the present setting of uncertainty-based optimization, dependency of objective on the uncertainties is not considered. For the present problem, 5% uncertainty will be assumed in the design variables x such that the bounds on uncertainties can be given as $[0.95x_i; 1.05x_i]$. [43,44]. Whereas, higher variation can be expected in material properties of PZT [46, 50, 51]. Here, uncertainty in material properties of PZT such as, Young's Modulus (E_{pzt}), Density (ρ_{pzt}) and Piezoelectric Coefficient (d_{31}), will be taken as 15 %. It should be noted here, that because of the coupling between the material properties of PZT mentioned above, same uncertainty is used for these material properties of PZT. Uncertainties used in the present optimization are listed in Table 5.1.

Table 5.1: Uncertainties considered for the PZT composite cantilever beam

Thickness of shim (t_s)	$\pm 5\%$
Thickness of proof mass (t_{pm})	$\pm 5\%$
Material properties of PZT ($E_{pzt}, \rho_{pzt}, d_{31}$)	$\pm 15\%$

5.3.6 Material properties

Material properties used in the current electro-mechanical model for the calculation of the power are listed in Table 5.2.

Table 5.2: Material properties properties used in the electro-mechanical analysis of the PZT composite cantilever beam

Young's Modulus of Silicon (E_s)	169 GPa
Density of Silicon (ρ_s)	2330 kg/m ³
Young's Modulus of PZT (E_{pzt})	60 GPa
Density of PZT (ρ_{pzt})	7500 kg/m ³
Piezoelectric Coefficient (d_{31})	$-100 \cdot 10^{-12}$ mV
Relative permittivity (ϵ_r)	1000
Damping ratio (ζ)	0.01
$\tan \delta$	0.02

5.4 Optimization Results

Results for the design optimization of the PZT composite cantilever beam using the Multipoint Approximation Method are presented here. This includes results from deterministic as well as uncertainty-based optimization. Optimization is carried out in two different ways, first including the constraint on the L/b ratio of shim and PZT and secondly excluding this constraint. Results for deterministic and uncertainty-based optimization are compared with the baseline design. The baseline design was the first design proposed in [39, 40]. Details of the baseline design are included in Table 5.4.

5.4.1 Optimization including L/b constraint

In the present subsection the case with the constraint on the L/b ratio is studied. Optimization history against number of steps (cycles), see Fig. 5.5 and Fig. 5.6, is shown here in order to compare the convergence and number of steps for the deterministic and uncertainty-based optimization. The convergence and number of steps for deterministic and uncertainty-based optimization are comparable. In case of small deflection and stress constraint, worst sets of uncertainties obtained at the end of every cycle remain the same. Moreover, for these constraints worst set of uncertainties are found to be at the vertices of the uncertainty domain. Typical values of worst uncertainties for these constraints are given in Table 5.3. Due to this, the convergence for the small deflection constraint (Fig. 5.5(b)) and stress constraint (Fig. 5.6(a)) after few steps is smoothed. The constraint on L/b ratio of shim and PZT is independent of uncertainties that are considered presently. However, if uncertainties in width and length of shim and PZT are considered, it may influence this constraint. For the voltage constraint, worst set of uncertainties fluctuates, however this constraint is not violated throughout the optimization. In the early phase of the optimization small deflection constraint and stress constraint remain active. Whereas, the constraint on (L/b) ratio for shim (Fig. 5.6(b)) and small deflection constraint become active in the later stage. A comparison between results for deterministic and uncertainty-based optimization shows that there is a significant reduction (19 %) in the objective function value in order to account for uncertainties, see Table 5.4. Actual dimensions and the output power for the PZT composite beam corresponding to the optimal design are compared with those for the baseline design in Table 5.4.

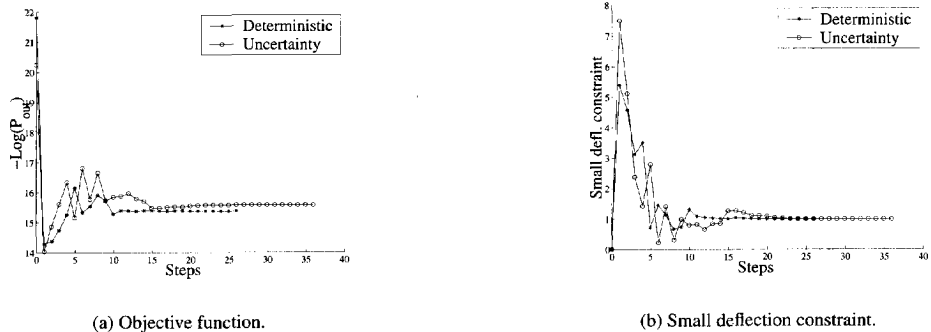


Figure 5.5: Optimization history with constraint on L/B ratio of Shim and PZT included in the optimization.

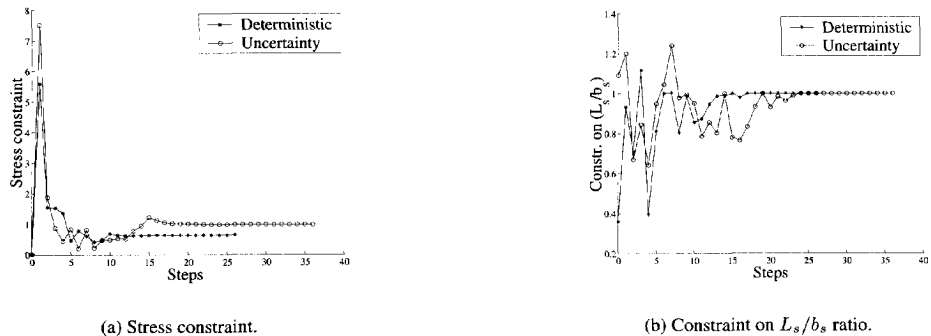


Figure 5.6: Optimization history with constraint on L/B ratio of Shim and PZT included in the optimization.

Table 5.3: Worst uncertainties obtained by anti-optimization for the small deflection and stress constraint

Thickness of shim (t_s)	-5 %
Thickness of proof mass (t_{pm})	+5 %
Material properties of PZT ($E_{pzt}, \rho_{pzt}, d_{31}$)	-15 %

5.4.2 Optimization excluding L/b constraint

The optimization here is exactly the same as the previous but the constraint on L/b ratio for shim and PZT is not included.

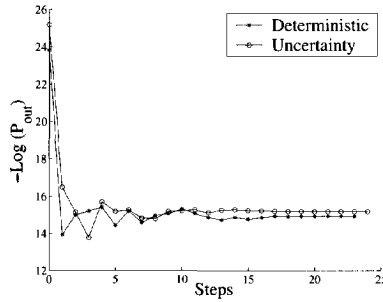
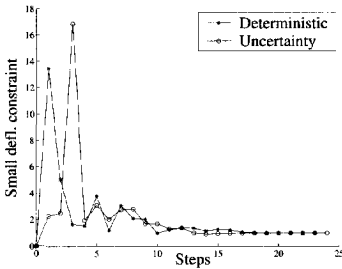
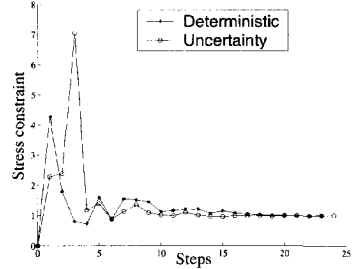


Figure 5.7: Optimization history for objective: Constraint on L/B ratio of Shim and PZT is not included in the optimization.



(a) Small deflection constraint.



(b) Stress constraint.

Figure 5.8: Optimization history for constraints: Constraint on L/B ratio of Shim and PZT is not included in the optimization.

Optimization history for the objective function and constraints shows similar trends, see Fig. 5.7 and Fig. 5.8, except that the constraint on (L/b) ratio for shim is not included. There is a significant increase (57 %) in the output power as compared to the previous optimization. Whereas the output power is almost doubled as compared to that for the baseline design, see Table 5.4. However, the design corresponding to this case resembles a plate like structure. Therefore this optimal design should be validated with the help of Finite Element Analysis. Moreover, it gives a direction in order to further improve the output power.

Table 5.4: Actual dimensions and the output power of the PZT composite cantilever beam for the optimal design is compared with those for baseline design: Case-I is including constraint on (L/b) ratio of shim and PZT whereas Case-II is without including this constraint. $a_0 = 1g$, $f_{ext} = 125\text{Hz}$.

Design			$L_s = L_{pzt}$ μm	L_{pm} μm	$b_s = b_{pzt}$ μm	b_{pm} μm	t_s μm	t_{pzt} μm	t_{pm} μm	P_{out} μW
Baseline			1000	1000	200	800	6	0.5	500	0.16
Optimal	Case-I	Deter.	705	1295	235	800	5.2	0.5	500	0.21
		Uncert.	439	1561	146	800	6.25	0.5	500	0.17
	Case-II	Deter.	217	1780	411	800	3.12	0.5	500	0.33
		Uncert.	242	1758	413	800	3.6	0.5	500	0.26

5.5 Discussion and Conclusions

Results for optimization show a good convergence. Use of the log of the power function as a objective function in the optimization has made it possible to use relatively lower order polynomial for adequate approximation of the objective function. This has substantially reduced the number of function evaluations required for the optimization.

In case of deterministic optimization a significant improvement is achieved in the output power as compared to that of the baseline design by nearly 30 % when the constraint on the length-to-width ratio (L/b) for shim and PZT is included. The power is almost doubled when the constraint on the L/b ratio is not included. The design corresponding to this case resembles a plate like structure. Therefore this optimal design should be validated with the help of Finite Element Analysis. It is further advantageous to use a plate model for optimization in order to remove the restriction on optimization due to the constraint on the L/b ratio.

In case of uncertainty-based optimization there is a significant reduction (nearly 20 %) in the output power as compared to that of deterministic optimization, in order to account for uncertainties. Uncertainties in MEMS structures can be accounted for quite efficiently with the help of the cycle-based alternating anti-optimization technique. In future research work, the effect of uncertainties on the objective function will also be studied in detail. Other uncertainties, such as uncertainties in width and length of shim and PZT will also be considered in future study.

5.6 Acknowledgment

This research is supported by the University of Florida, USA, and Delft University of Technology, Technology Foundation STW, applied science division of NWO and the technology program of the Ministry of Economic Affairs, The Netherlands. The research work in this chapter is carried out in collaboration with the Interdisciplinary Microsystems Group of the University of Florida.



Chapter 6

Cycle-based Alternating Anti-optimization combined with Nested Parallel Computing

In this chapter a new method for uncertainty-based design optimization based on an anti-optimization approach using Bounded-But-Unknown uncertainties is studied on the basis of a practical application. The basic anti-optimization technique looks at the worst case scenario by finding the worst settings of the uncertainties for each constraint evaluation separately. This *Rigorous* anti-optimization technique involves two-level optimization in which anti-optimization is nested within the main optimization, making it computationally exhaustive. In the alternative *Lombardi-Hafika* approach, anti- and main optimization are carried out alternately avoiding the nested approach, which is quite efficient. A new cycle-based alternating technique based on a similar idea is studied in this chapter. In this technique, anti-optimization is carried out at the end of every cycle of the main optimization. The above anti-optimization techniques are studied and compared on the basis of an illustrative Elastically Supported Beam example. Additionally, in the present chapter, a nested parallel computing strategy is developed in order to make the cycle-based alternating technique computationally efficient when a cluster of computers is available for function evaluation. This is particularly essential in case of practical problems involving expensive function evaluations, e.g., using Finite Element Analysis. The effectiveness of the cycle-based alternating technique combined with nested parallel computing is demonstrated by application to the uncertainty-based shape optimization of a Shape Memory Alloy Microgripper.

Key words: Bounded-But-Unknown Uncertainties, Optimization, Anti-optimization, Parallel Computing, Shape Memory Alloy, Microgripper

6.1 Introduction

Many practical design optimization tasks involve uncertainties. In case statistical data on uncertainties is available, it can be used to construct statistical distributions for uncertainties. If such distributions are sufficiently reliable, a reliability-based design can be obtained by using probabilistic methods, see textbook Elishakoff [8]. In general, probabilistic methods require an abundance of experimental data and even small inaccuracies in the statistical data can lead to large errors in the computed probability of failure, Elishakoff [9]. However, in case of practical applications, it often happens that there is not enough data available to construct reliable distributions. This can be particularly the case in early stages of a design process. In such situations, the computed reliability of a structure can exhibit large errors. This can be crucial in applications which are required to perform without failure or with very small probability of failure for the entire life span, for example, in case of space applications. On the other hand, the available data in combination with engineering experience can be used to set tolerances or bounds on uncertainties, within which the distribution is unknown,

thus identifying uncertainties as Bounded-But-Unknown (BBU) (Ben-Haim and Elishakoff [11] and Ben-Haim [12]).

The anti-optimization technique described in Elishakoff *et al.* [7] tackles the BBU uncertainties using the worst case approach. This technique involves vertex checking of the uncertainty domain in order to obtain the worst response of the structure. This technique is computationally very efficient for convex problems, however its application is limited to such problems. A more generalized approach, which can handle non-convexities, is adopted in Van Keulen *et al.* [13] and Gurav *et al.* [34]. Here this generalized or *Rigorous* anti-optimization is applied to the uncertainty-based design optimization of a car deck floor of a ferry. However, this technique suffers from the required large number of expensive function evaluations due to the underlying two-level nested optimization. The *Enhanced* anti-optimization technique that uses sensitivities, a database and parallel computing to make it computationally efficient is studied in Gurav *et al.* [47] on the basis of a practical application related to Microelectromechanical Systems. The technique still becomes computationally expensive for an increasing number of design variables and uncertainties.

This has motivated the search for alternative approaches, which avoid such two-level nested optimization. In one such approach, proposed by Lombardi and Haftka [19], anti- and main optimization are carried out alternately, thereby avoiding the nested approach. This approach can converge very fast in case of problems involving convexities and is quite efficient in terms of the number of required function evaluations. However, in case of non-convex problems, for which the worst case can fluctuate from design to design, it may require large number of optimization cycles to converge. Inspired by the Lombardi-Haftka technique, a slightly modified approach is adopted in the present chapter. Here, in the proposed cycle-based alternating technique, anti-optimization is carried out at the end of each cycle of the main optimization to obtain the worst sets of uncertainties. These obtained worst sets of uncertainties are used during the next cycle of the main optimization. For the initial cycle of the main optimization, nominal values of uncertainties are used. This technique also suffers from slow convergence in case of uncertainties fluctuating with respect to changes in the design. Nevertheless it is quite efficient in terms of the number of function evaluations as compared to the Enhanced anti-optimization technique. In case of fluctuating uncertainties, the cycle-based alternating technique is efficient as compared to the Lombardi-Haftka technique due to the increase in number of iterations for such problems. Additionally, use of derivatives of responses with respect to uncertainties for estimation of worst uncertainties during the cycle, can improve the convergence of the cycle-based technique.

Many times the function evaluations involve computationally expensive finite element analysis (FEA). The number of such FEAs required in the uncertainty-based design optimization can be quite high depending on the problem at hand. For such problems, it is necessary to perform function evaluations in parallel using a cluster of fast computers. In the present chapter, a nested parallel computing approach is used in combination with the cycle-based technique, in order to optimize a Shape Memory Alloy (SMA) Microgripper involving computationally expensive FEA. The parallel computing framework used here is developed in PYTHON, Lutz [24].

The techniques for uncertainty-based optimization discussed above are embedded in a structural optimization setting using the Multipoint Approximation Method (MAM) [1–3]. The different techniques will be studied and compared on the basis of an Elastically Supported Beam problem, see Lombardi and Haftka [19]. To demonstrate the ability of the proposed cycle-based alternating technique to solve practical problems involving expensive FEA, the uncertainty-based shape optimization of an SMA Microgripper is considered in the current chapter. In this study, uncertainties affect relevant environmental operating conditions as well as parameters in the SMA material model.

The basic optimization problem formulation together with a short description on the MAM is given in Section 6.2. The BBU description of uncertainties is the subject of Section 6.3. Various uncertainty-based design optimization techniques using BBU uncertainties are described in Section 6.4. In Section 6.5, the anti-optimization techniques are studied on the basis of various examples. The results for the uncertainty-based optimization are compared for the Elastically Supported

Beam problem in Section 6.5.1. The uncertainty-based design optimization of the SMA Microgripper is studied in Section 6.6. Final discussion and conclusion are the subject of Section 6.7. The information on SMA material model is given in Appendix, Section 6.8.1.

6.2 Multipoint Approximation Method

6.2.1 Introduction

In the present chapter the MAM is used as a basis for optimization. Often practical applications involve numerical evaluation of response functions. From an optimization point of view, these types of problems can either suffer from numerical noise or the large computational time involved. The MAM, which is based on the sequential application of Response Surface Methodology, see Khuri and Cornell [22] and Myers and Montgomery [23], can be applied to such problems. The interested reader is referred to the studies by Toropov *et al.* [1, 2] and Van Keulen and Toropov [3, 4]. The MAM uses sequential approximations to the responses in order to reduce the number of expensive numerical response evaluations. However, it should be noted here, that it suffers from the so-called curse of dimensionality, i.e. it becomes inefficient with the increase in dimensions (number of design variables). A MAM-based framework for the optimization of structures is fully described in Jacobs *et al.* [5].

6.2.2 Optimization problem formulation

Designing a structure implies that a design concept has to be selected, which subsequently has to be optimized. The latter involves the selection of design variables, which determine, among other features, the dimensions, shapes and materials to be used. This set of n design variables is denoted as \mathbf{x} , with

$$\mathbf{x} = (x_1 \dots x_n). \quad (6.1)$$

Throughout the present chapter, it is assumed that all design variables are continuous.

The behavior of the structure is described by the response functions, which are functions of the design variables. These response functions are denoted as \mathbf{f} with

$$\mathbf{f} = (f_0 \dots f_m), \quad (6.2)$$

which may reflect, for example, weight, cost, buckling loads, maximum equivalent stress, or strain levels.

The optimization problem can be formulated mathematically as

$$\begin{aligned} \min_{\mathbf{x}} \quad & f_0(\mathbf{x}) \\ \text{s.t.} \quad & f_i(\mathbf{x}) \leq 1, \quad i = 1, \dots, m, \\ & A_j \leq x_j \leq B_j, \quad j = 1, \dots, n. \end{aligned} \quad (6.3)$$

Here, f_0 is the objective function and f_i are constraints. The design space is represented by the upper and lower limits on x_j , A_j and B_j , respectively.

The MAM is based on a sequential replacement of the actual optimization problem, as described by Eq. (6.3), by a series of approximate optimization problems as depicted in Fig. 6.1. The approximate optimization problem (AOP) for a cycle p , can be formulated as

$$\begin{aligned} \min_{\mathbf{x}} \quad & \tilde{f}_0^{(p)}(\mathbf{x}) \\ \text{s.t.} \quad & \tilde{f}_i^{(p)}(\mathbf{x}) \leq 1, \quad i = 1, \dots, m, \\ & A_j^{(p)} \leq x_j \leq B_j^{(p)}, \quad j = 1, \dots, n, \\ & A_j^{(p)} \geq A_j, \quad B_j^{(p)} \leq B_j. \end{aligned} \quad (6.4)$$

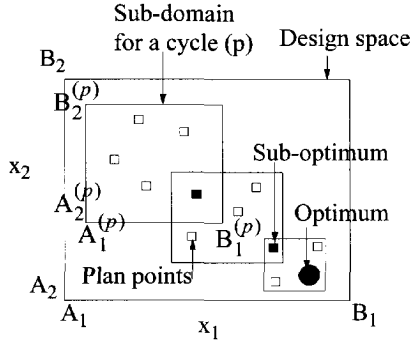


Figure 6.1: Optimization using the MAM for a problem of two design variables (x_1 and x_2).

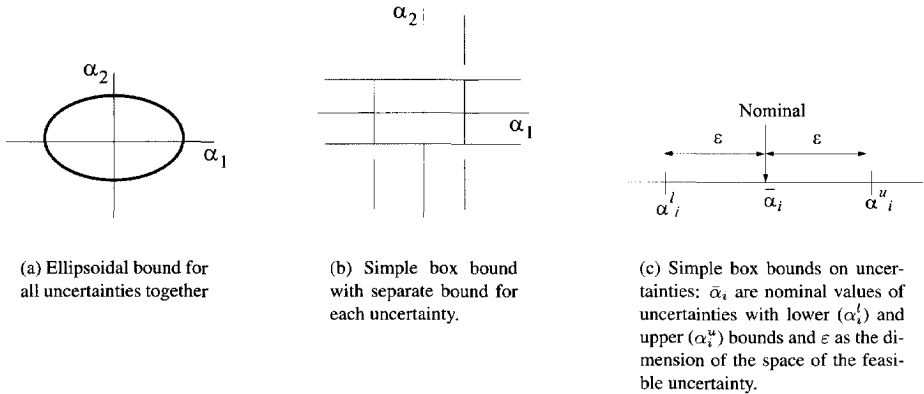
Here, the response functions are replaced with approximate functions over the sub-domain for a cycle. For the current AOP, $\hat{f}_i^{(p)}(\mathbf{x})$ are considered as adequate approximations of $f_i(\mathbf{x})$ over the sub-domain (p) represented by the move limits $A_j^{(p)}$ and $B_j^{(p)}$, see Fig. 6.1. It should be noted here that the move limits for the initial cycle ($A_j^{(0)}$ and $B_j^{(0)}$), can be chosen either arbitrarily or based on engineering experience. Many times this can significantly influence the convergence. For example, if the initial move limits include the optimum, then the optimization can converge quite rapidly.

6.3 Bounded-But-Unknown Uncertainty

If the problem at hand is non-deterministic, i.e. there are uncertainties that play a non-negligible role, the response functions also depend on the uncertainties. The set of uncertainty variables will be denoted α , with

$$\alpha = (\alpha_1 \dots \alpha_u). \tag{6.5}$$

Consequently, the response functions depend on both design variables and uncertainties, hence $f(\mathbf{x}, \alpha)$.



(a) Ellipsoidal bound for all uncertainties together

(b) Simple box bound with separate bound for each uncertainty.

(c) Simple box bounds on uncertainties: $\bar{\alpha}_i$ are nominal values of uncertainties with lower (α_i^l) and upper (α_i^u) bounds and ϵ as the dimension of the space of the feasible uncertainty.

Figure 6.2: Bounds on uncertainties.

In the present chapter, uncertainties are modelled using the BBU approach. In this, several bounds can be introduced, each providing a bound for a group of uncertainty variables or all uncertainty variables simultaneously, for example see Fig. 6.2. At the same time, we may want to measure the amount of uncertainty. Thus, measures for the dimensions of the subspace containing all possible selections of uncertainty variables are desired. This can be cast into a mathematical framework as follows. Assuming a set with b bounds, then a possible or *feasible* selection of α satisfies, see Van Keulen *et al.* [13];

$$B_i(\alpha, \varepsilon) \leq 0, \quad \text{for } i = 1, \dots, b. \quad (6.6)$$

Otherwise the selection of the uncertainty variables α is *infeasible*. Here, the components of ε are used to specify the dimensions of the space of feasible uncertainty variables. We will therefore refer to these components as the *levels of uncertainty*.

In the present chapter, simple box bounds, see Fig. 6.2(b & c), are used to specify uncertainties as

$$(\alpha_i - \bar{\alpha}_i)^2 - \varepsilon^2 \leq 0. \quad (6.7)$$

This type of bounds generally come from a tolerance specified on a nominal value, for example, due to the manufacturing induced inaccuracies. These bounds can be alternatively represented in terms of lower (α_i^l) and upper bounds (α_i^u) on uncertainties as

$$\begin{aligned} \alpha_i^l &= \bar{\alpha}_i - \varepsilon, \\ \alpha_i^u &= \bar{\alpha}_i + \varepsilon. \end{aligned} \quad (6.8)$$

Note that the bounds used in this study were chosen based on engineering intuition rather than a detailed analysis, since the purpose of the present examples is mainly to illustrate the proposed optimization technique. However, the same procedure can be applied with different bounds in practical situations where more detailed data is available.

6.4 Uncertainty-based optimization using Anti-optimization

6.4.1 Anti-optimization

The anti-optimization technique to tackle BBU uncertainties consists of two levels of optimization, the outer level consists of the main optimization and anti-optimization is nested within it at the inner level. The main optimization here is a standard minimization problem that searches for the best design in the design domain. Anti-optimization is performed for every constraint in order to obtain the worst values of constraints for each design within the main optimization. The anti-optimization problem using BBU uncertainties can be formulated mathematically as:

$$\begin{aligned} \min_{\mathbf{x}} \quad & f_o(\mathbf{x}) \\ \text{s.t.} \quad & f_i(\mathbf{x}; \alpha_i^*) \leq 1, \quad i = 1, \dots, m, \end{aligned} \quad (6.9)$$

where α_i^* is the maximizer of

$$\begin{aligned} \max_{\alpha_i} \quad & f_i^*(\mathbf{x}; \alpha_i) \\ \text{s.t.} \quad & B_j(\alpha_i, \varepsilon) \leq 0, \quad j = 1, \dots, b. \end{aligned} \quad (6.10)$$

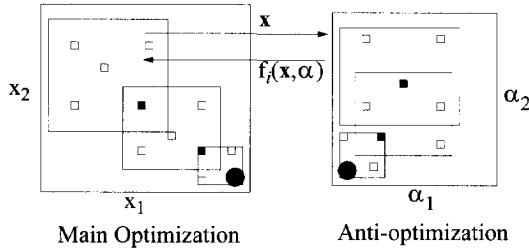


Figure 6.3: Anti-optimization technique in the MAM setting for a problem of two design variables (x_1 and x_2) and two uncertainties (α_1 and α_2). The big boxes indicate the search (sub-) domains. The small open boxes indicate sets of design variables (left) or uncertainty variables (right) for which function evaluations are carried out. The small solid boxes indicate solutions of the approximate optimization problems.

Here, $f_0(\mathbf{x})$ is the objective function and $f_i(\mathbf{x}; \alpha_i)$ are constraints, whereas $B_j(\alpha_i, \epsilon)$ are bounds on uncertainties. The minimization as defined in Eq. (6.9) will be referred to as the main optimization. Notice that, in general, the evaluation of the constraints involves, for each set of design variables, anti-optimization of the individual constraints. This anti-optimization is reflected by Eq. (6.10). The anti-optimization technique in the setting of the MAM is depicted in Fig. 6.3. For the applications studied in the present chapter, uncertainties through simple box bounds see Fig. 6.2(b & c) and Eq. (6.8) are adopted. Therefore, the constrained maximization problem, as defined by Eq. (6.10), reduces to an unconstrained maximization problem as

$$\begin{aligned} \max_{\alpha_i} \quad & f_i^*(\mathbf{x}; \alpha_i) \\ \text{s.t.} \quad & \alpha_i^l \leq \alpha_i \leq \alpha_i^u. \end{aligned} \quad (6.11)$$

The above *Rigorous* anti-optimization technique can handle large uncertainties safely. Moreover, it can account for discontinuities, if any. The price paid for this flexibility is the large computing effort required for the anti-optimization processes. In case of practical problems involving large numbers of design variables and uncertainties, anti-optimization can become very computationally expensive. In order to reduce the total number of expensive numerical response evaluations, the anti-optimization technique is modified in Gurav *et al.* [47] by making use of a database techniques and sensitivities.

In this *Enhanced* anti-optimization, derivative information, if available, is utilized to decrease the required total number of expensive function evaluations. In many cases of computational response analysis, gradient information can often be obtained at a fraction of the computing time as compared to the analysis itself, van Keulen *et al.* [14] and van Keulen and de Boer [15, 16]. This sensitivity information can be used in addition to the function values to construct Gradient Enhanced Response Surfaces (GERS), van Keulen and Vervenne [17, 18]. This incorporation of sensitivities can improve the quality of the response surfaces. Alternatively, fewer response evaluations may be required to construct the approximations. Thus, using derivative information may decrease the total number of expensive function evaluations and hence may speed up the numerical optimization process. Similarly, a database technique is used to modify the anti-optimization technique in order to reduce the number of expensive function evaluations required within each anti-optimization. For this purpose, the worst sets of uncertainties obtained by anti-optimizations are stored in a database. When there is enough data available in the database, it is used to create starting points for the anti-optimizations. Often this can speed up the anti-optimization processes significantly. Additionally, a parallel computing strategy is combined with anti-optimization in Gurav *et al.* [47] in order to speed up the whole procedure.

6.4.2 Lombardi-Haftka alternating anti-optimization

Although the *Enhanced* anti-optimization provides a quite efficient way of handling uncertainties, it becomes increasingly impractical with an increasing number of design variables and uncertainties. Therefore it is necessary to think of alternative approaches. In Lombardi-Haftka [19], nesting of anti-optimization within the main optimization is avoided. In this method, the main and anti-optimization is carried out alternately as follows:

Solve

$$\begin{aligned} \min_{\mathbf{x}} \quad & f_o(\mathbf{x}) \\ \text{s.t.} \quad & f_i(\mathbf{x}; \alpha_i^*) \leq 1, \quad i = 1, \dots, n. \end{aligned} \quad (6.12)$$

for given worst set of uncertainties α_i^* . These uncertainties are kept constant for each of the constraints until convergence of the main optimization, Eq. (6.12), has been obtained. Thereafter, new settings of the uncertainties α_i^* are determined through anti-optimizations for the optimum \mathbf{x}^* obtained by Eq. (6.12) as

$$\begin{aligned} \max_{\alpha_i} \quad & f_i(\mathbf{x}^*; \alpha_i) \\ \text{s.t.} \quad & \alpha_i^l \leq \alpha_i \leq \alpha_i^u. \end{aligned} \quad (6.13)$$

These cycles are repeated until convergence. For the initial iteration uncertainties are chosen arbitrarily or as $\alpha^* = \bar{\alpha}$, see Fig. 6.2(c). This process is converged if

$$\left\| \frac{f_0 - f_{0\text{prev}}}{f_0} \right\| \leq \text{tolerance, and} \quad (6.14)$$

$$\left\| \frac{\alpha_{ik}^* - \alpha_{ik\text{prev}}^*}{\alpha_{ik}^*} \right\| \leq \text{tolerance} \quad i = 1, \dots, n; \quad k = 1, \dots, u. \quad (6.15)$$

Thus, convergence is defined based on relative change in the objective function, Eq. (6.14), and the worst set of uncertainties corresponding to each constraint, Eq. (6.15).

6.4.3 Cycle-based alternating Anti-optimization

The Lombardi-Haftka technique can be quite efficient in terms of number of expensive function evaluations in case of problems involving convexities. However, it can suffer from a bad convergence in cases for which worst uncertainties fluctuate from design to design. Inspired by Lombardi and Haftka [19], in the present chapter a slightly modified approach is presented. The idea is to solve

$$\begin{aligned} \min_{\mathbf{x}} \quad & f_o^{(p)}(\mathbf{x}) \\ \text{s.t.} \quad & f_i^{(p)}(\mathbf{x}; \alpha_i^p) \leq 1, \quad i = 1, \dots, n, \end{aligned} \quad (6.16)$$

for given α_i^p . This set of uncertainties consists of the maximizers of

$$\begin{aligned} \max_{\alpha_i} \quad & f_i^{(p)}(\mathbf{x}^p; \alpha_i) \\ \text{s.t.} \quad & \alpha_i^l \leq \alpha_i \leq \alpha_i^u. \end{aligned} \quad (6.17)$$

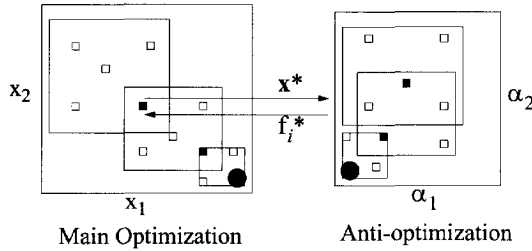


Figure 6.4: Cycle-based Alternating Anti-optimization technique in the MAM setting for a problem of two design variables (x_1 and x_2) and two uncertainties (α_1 and α_2). Here the anti-optimization is carried out only at the end of every cycle that is for the sub-optimal designs indicated by the solid boxes.

Here, Eq. (6.16) represents the main optimization for the p^{th} cycle which is solved first to obtain corresponding sub-optimum \mathbf{x}^p . For the initial cycle, the worst set of uncertainties α_i^p needed in Eq. (6.16) are chosen arbitrarily or as $\alpha^p = \bar{\alpha}$, see Fig. 6.2(c). Then, anti-optimization represented by Eq. (6.17) is carried out at the sub-optimum (\mathbf{x}^p) to obtain the worst set of uncertainties (α_i^p), which will be used in the next cycle of the main optimization. During every cycle of the main optimization depending on the optimization history, the size and direction of the subdomain keeps changing until the convergence as depicted in Fig. 6.4.

In the cycle-based alternating technique, during every cycle of main optimization, evaluation of constraints does not involve expensive anti-optimization, which makes it computationally less expensive. Eventhough in the technique suffers from slower convergence in case of fluctuating uncertainties, it shows better convergence as compared to the Lombardi-Haftka technique. Moreover, with the increase in number of iterations, Lombardi-Haftka technique becomes computationally very expensive in terms of total function evaluations as compared to the cycle-based alternating technique. Additionally, in some situations if additional information is available, such as approximate estimation of worst uncertainties through derivatives, it can be utilized during the cycle. This can significantly improve the convergence of the technique.

6.4.4 Combined Cycle-based alternating and Asymptotic method

The Asymptotic method uses derivatives of the response functions with respect to uncertainties to estimate worst set of uncertainties. In case of fluctuating uncertainties, when the Asymptotic method is combined with the cycle-based alternating technique, it tremendously improves the convergence of the cycle-based alternating technique. The Asymptotic method is fully described in Van Keulen *et al.* [13] and discussed here for the type of problems dealt within the present chapter.

Here, approximations for responses are constructed using Taylor series around $\alpha = \bar{\alpha}$ for a given design \mathbf{x} . These Taylor series read

$$\Delta f_i = \frac{\partial \bar{f}_i}{\partial \alpha_k} \Delta \alpha_k + \frac{1}{2} \frac{\partial^2 \bar{f}_i}{\partial \alpha_k \partial \alpha_l} \Delta \alpha_k \Delta \alpha_l + \dots, \quad (6.18)$$

with

$$\Delta f_i = f_i(\mathbf{x}, \alpha) - \bar{f}_i = f_i(\mathbf{x}, \alpha) - f_i(\mathbf{x}, \bar{\alpha}). \quad (6.19)$$

It is important to emphasize that it is not always possible to construct the above Taylor series. This is, for example, the case when a response function is continuous but its derivatives are discontinuous. If the above Taylor series can be created, then first-order approximations for the response functions

are obtained by dropping all higher-order terms, giving

$$\Delta f_i = \frac{\partial \bar{f}_i}{\partial \alpha_k} \Delta \alpha_k. \quad (6.20)$$

It is important to realize that the derivatives of the response functions with respect to the uncertain variables are relatively inexpensive to calculate, provided efficient algorithms for sensitivity analysis are available, van Keulen [14]. Using the approximations for the response functions given by Eq. (6.20), the maximization problem given by Eq. (6.17) in order to find the worst set of uncertainties for a given design \mathbf{x} is replaced by

$$\begin{aligned} \max_{\Delta \alpha_i} \quad & \mathbf{h}_i^T \Delta \alpha \\ \text{s.t.} \quad & \alpha_i^l \leq \alpha_i \leq \alpha_i^u, \end{aligned} \quad (6.21)$$

with

$$\mathbf{h}_i^T = \left(\frac{\partial \bar{f}_i}{\partial \alpha_1}, \dots, \frac{\partial \bar{f}_i}{\partial \alpha_n} \right). \quad (6.22)$$

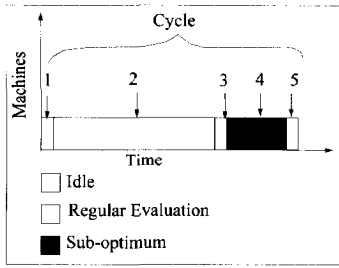
As discussed before, in case of the cycle-based alternating technique, during the cycle worst sets of uncertainties are kept constant while computing responses. These worst sets of uncertainties are updated at the end of the optimization cycle by anti-optimization carried out for the sub-optimum. In the present combined technique, during each cycle estimation of worst uncertainties by means of Asymptotic method Eq. (6.21) is used. However, the rigorous check by means of full anti-optimization Eq. (6.17) at the end of cycle to update the worst set of uncertainties is still kept. Additionally, this worst set of uncertainties obtained at the end of a cycle is used as a basis for the Taylor series approximation for the next cycle instead of nominal values of uncertainties, i.e. $\mathbf{h}_i^T|_{\alpha=\alpha^*}$. The Asymptotic evaluation of worst uncertainties during the cycle can be solved computationally inexpensively whereas it can improve the convergence significantly in case of fluctuating uncertainties. In the present chapter the cycle-based alternating technique combined together with the asymptotic method is studied using an Elastically Supported Beam example, Section 6.5.1.

6.4.5 Parallel Computing

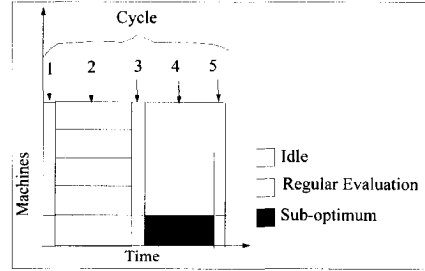
Optimization using Parallel Computing

In many practical problems, evaluation of response functions involves computationally expensive FEA. For such problems, design optimization requiring a large number of such expensive FEAs will easily become impractical. This number of FEAs can increase exponentially with the increase in the number of design variables and/or uncertainties. Here, to evaluate response using FEAs in parallel, clusters of multiple processors can be utilized to improve the efficiency of the method, see Van Keulen and Toropov [25].

Optimization using the MAM, involves various steps such planning of experiments, response evaluation, response surface approximation, nonlinear minimization problem and movelimit strategy, see Section 6.2. The computing times required for these steps of a typical optimization are represented approximately in Fig. 6.5 (a). It can be clearly seen here, that evaluation of the plan points is computationally the most expensive phase, whereas the nonlinear minimization programming (NMP) problem and move limit strategy are relatively computationally very cheap. When a cluster of several processors is available for computation, it can be used to evaluate the expensive response evaluations in parallel, see Fig. 6.5 (b).



(a) Plan points are evaluated sequentially



(b) Plan points are evaluated using parallel computing

Figure 6.5: A cycle in optimization using the MAM: Steps involved are 1. Planning, 2. Evaluation of plan points, 3. NMP, 4. Evaluation of sub-optimum, 5. Move limit strategy.

It should be noted here that an additional response evaluation is required at the end of the cycle to evaluate the sub-optimum of the AOP. In the present setting for response evaluation, splitting of the individual response evaluation is not possible, therefore every response can only be evaluated by a single processor. Because of this, during the evaluation of the sub-optimum only a single processor can be utilized, keeping the other processors idle. This increases the overall idle time significantly.

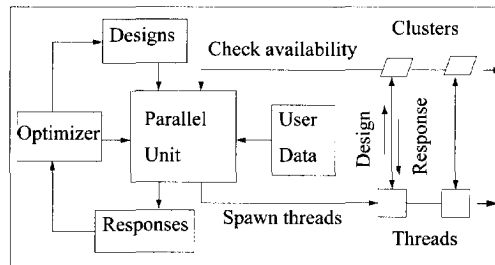


Figure 6.6: A framework for parallel computing using the Threading module of PYTHON.

The parallel computing framework used in the present research is developed in PYTHON, see the textbook Lutz [24]. To start multiple threads in parallel, the Threading module from PYTHON is used in the current framework. This framework is depicted in Fig. 6.6. Here, each job involves evaluation of response function using, for example FEA. The number of such jobs that can be started at a time in parallel, depends on the number of processors available for computation.

During the evaluation of an individual job, first the design parameters are sent to the remote processor, see Fig. 6.6. Then the actual evaluation of responses, for example by using FEA, is started on the remote processor by the associated thread. When the evaluations for the job are finished, corresponding responses are received back and are associated with the job. As soon as the processor finishes response evaluation and becomes available for computation, next job in the queue is submitted to it. The procedure is repeated until all the jobs are evaluated.

It should be mentioned here, that the communication between the master and slaves, is through files contained data, for example, flags indicating whether the submitted job is finished or not. The communication using files does increase the overhead time, however in practical cases this is negligible compared to the time required for an individual response evaluation.

Uncertainty-based Optimization using Nested Parallel Computing

In case of uncertainty-based design optimization using anti-optimization, the overall number of required FEAs is quite high compared to the deterministic optimization. Therefore, to have a practical technique that can tackle uncertainties in practical design optimization problems, it is necessary to use parallel computing. In Gurav *et al.* [47], parallel computing is combined with *Enhanced* anti-optimization to carry out uncertainty-based design optimization of a practical MEMS structure involving expensive FEA. However, the strategy used there for the parallel computing is rather simple, and does not lead to the best utilization of the available computing power. In the present chapter, an improved strategy for parallel computing is combined with the cycle-based alternating technique to carry out uncertainty-based design optimization efficiently.

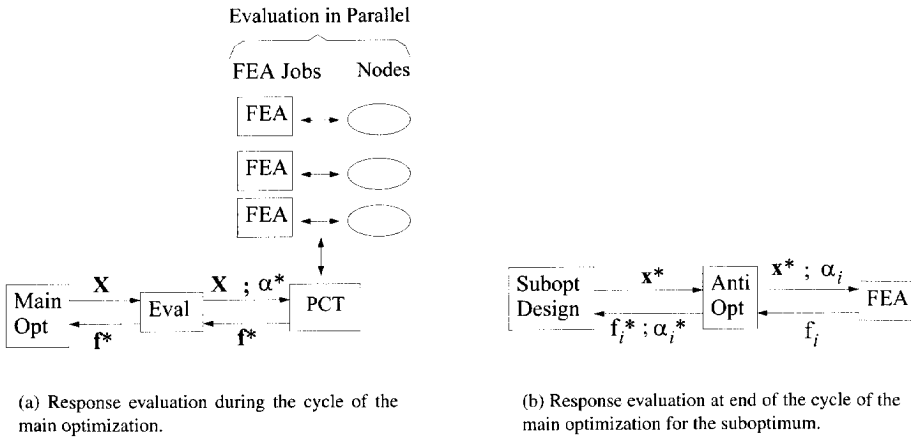


Figure 6.7: Response evaluation for the main optimization for the Cycle-based technique. Here worst uncertainties obtained from the previous cycle are used for the evaluation. Response evaluation involves FEA in parallel.

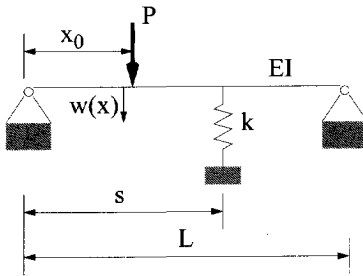
While combining the Parallel Computing together with the cycle-based alternating technique, various strategies were considered. The effectiveness of these strategies for Parallel Computing is discussed by means of a virtual problem involving four constraints, whereas the number of nodes available for carrying out computation are assumed to be three. It should be noted here, that these strategies differ only in the evaluation of the suboptimum at the end of the cycle of the main optimization, see Fig. 6.7(b). The evaluation of responses during the cycle of the main optimization involving expensive FEAs are carried out in parallel using available nodes as shown in Fig. 6.7(a) in the same way for all strategies.

In case of Strategy I, see Fig. 6.8(a), all anti-optimizations can be started in parallel, running one anti-optimization on one node. Each anti-optimization requires several cycles for convergence and each iteration involves evaluation of constraints by means of FEAs in series on the corresponding node. It can be easily seen here that for the current fictitious problem, the number of anti-optimizations mismatch the number of available nodes. For this problem three anti-optimizations corresponding to three constraints can be started in parallel on three nodes. However, during the evaluation of the fourth anti-optimization, only one node is utilized whereas all other nodes remain idle. The overall idle time can significantly increase with the increase in the difference between number of constraints and number of nodes. Furthermore, increase in the computational time for a single FEA can add up to this idle time for such problems. However this strategy can give good efficiency when the number of constraints matches the number of nodes.

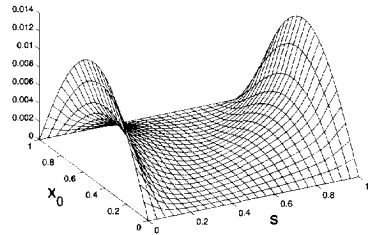
These designs actually involve expensive FEAs. All designs collected by the Scheduler are then evaluated in parallel, as shown in Fig. 6.9. It can be clearly seen that this nested Parallel Computing involves two levels. In the outer level, anti-optimizations are started in parallel, whereas in the inner level, the actual evaluation of designs within anti-optimizations is carried out in parallel. Here efficiency does not get affected even if the number of anti-optimizations and nodes does not match. Moreover, making a common list of all FEAs and then evaluating them in parallel utilizes the available nodes more efficiently. The complexity involved in the implementation is quite clear. On the other hand, the computational power is utilized quite efficiently with this strategy.

6.5 Applications

6.5.1 Elastically supported beam



(a) Optimization problem formulation: Here $L = 1 \text{ m}$, $P = 1000 \text{ N}$, $k = 500000 \text{ N/m}$, $EI = 1000 \text{ N.m}^2$.



(b) Plot of the integrated displacement as a function of x_0 and s

Figure 6.10: Elastically Supported Beam example

An elastically supported beam, see Fig. 6.10, is used by Lombardi and Haftka [19] to test the anti-optimization technique in the presence of nonlinearities. One of the features of this problem is the strong dependence of the worst uncertainty on the design variable. In the present chapter, different anti-optimization techniques as discussed before are studied on the basis of this example. For comparative study, for this test example similar notation as in Lombardi and Haftka [19] is used.

In this problem, a beam loaded by a concentrated force is supported elastically to limit its vertical displacements, see Fig. 6.10 (a). The goal of the optimization here is to optimally place the elastic support, in order to minimize the integral of the displacement over the length of the beam. The location of the concentrated force P is uncertain. Assuming the nominal location of the concentrated force at the center of the beam ($\bar{x}_0 = 0.5L$), with $\varepsilon = 0.5L$, the lower and upper bounds on uncertainty (x_0) can be given as

$$\begin{aligned} x_0^l &= \bar{x}_0 - \varepsilon = 0, \\ x_0^u &= \bar{x}_0 + \varepsilon = L. \end{aligned} \tag{6.23}$$

Here, the nonlinear displacement function $w(x, s, x_0)$ is the objective of the anti-optimization and is analytically determined by integration of the fourth-order differential equation of the beam,

$$EI \frac{\partial^4 w}{\partial x^4} = P\delta(x - x_0) - kw(x)\delta(x - s). \tag{6.24}$$

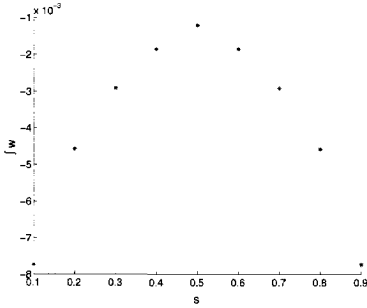
The main and anti-optimization problems are formulated as follows:

Solve the main optimization to obtain minimizers s for given x_0

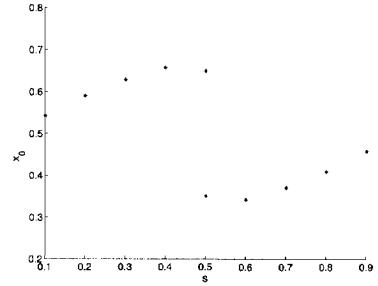
$$\min_s \int_0^L w(x, s, x_0) dx \quad \text{s.t.} \quad 0 \leq s \leq L, \quad (6.25)$$

and solve the anti-optimization to obtain maximizers x_0 for given s as

$$\max_{x_0} \int_0^L w(x, s, x_0) dx \quad \text{s.t.} \quad 0 \leq x_0 \leq L. \quad (6.26)$$



(a) Plot for the worst response ($\int w$) obtained by anti-optimization corresponding to each design variable (s) value.



(b) Plot for the worst uncertainty (x_0) obtained by anti-optimization corresponding to each design variable (s) value.

Figure 6.11: Anti-optimization results for fixed set of designs for the elastically supported beam example

The actual integrated displacement is plotted in Fig. 6.10 (b). It can be clearly seen here, that the displacement function is highly nonlinear, and displays a saddle-shape response formed due to the discontinuity depending upon the location of the load (x_0) with respect to the location of the support (s). As a result, the worst location of the load (x_0) strongly depends on the location of the elastic support (s) and can fluctuate from point to point. In the first study, for selected designs (s) at regular intervals, anti-optimization is carried out to find the worst location of uncertainty (x_0) and the corresponding worst response ($\int w$), see Fig. 6.11. It can be clearly seen here, that the worst uncertainty (x_0) varies with respect to the design (s) and additionally it shows a discontinuity at $s = 0.5L$. Here, the optimum location of the support is at 0.5m, whereas the worst location of the load is either at 0.35m or at 0.65m depending on the location of the load with respect to the support.

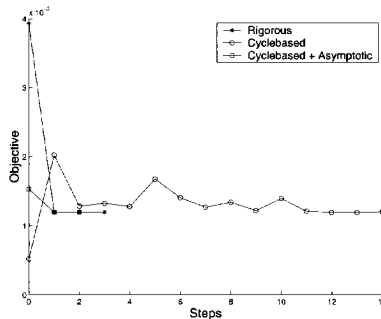
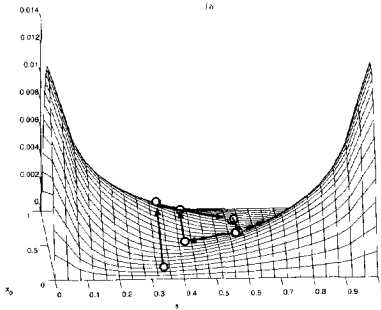
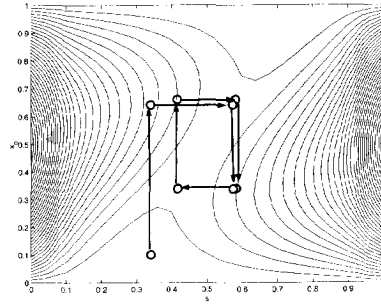


Figure 6.12: Optimization history for the elastically supported beam problem: comparison of uncertainty-based optimization using different techniques.



(a) Plot of the integrated displacement function together with the optimization history for the Lombardi-Haftka Method.



(b) Contour plot for the integrated displacement function together with the optimization history for the Lombardi-Haftka Method.

Figure 6.13: Optimization history using Lombardi-Haftka method for the elastically supported beam example

Table 6.1: Comparison between uncertainty-based optimization results using different methods for ESB problem

	s	$\int w$	Number of function evaluations
Rigorous	0.4987	1.1993e-03	720
Cyclebased	0.4985	1.2048e-03	676
Cyclebased+Asymptotic	0.4997	1.1997e-03	100

The uncertainty-based optimization problem as described by Eq. (6.25) and Eq. (6.26) is carried out here using different techniques. The results are compared here for the efficiency in terms of convergence and total number of function evaluations. The optimization history of the different techniques is compared for convergence in Fig. 6.12, whereas the total number of function evaluations are compared in Table 6.1. It can be clearly seen here, that in case of alternating techniques the convergence, in terms of number of steps, deteriorates as compared to the Rigorous technique, see Fig. 6.12 and Fig. 6.13. As mentioned before, in case of the Lombardi-Haftka technique due to the fluctuating uncertainties, the process did not converge, see Fig. 6.13. In case of Rigorous technique the convergence is very good, i.e. very few steps required for the convergence, however the number of total function evaluations is relatively quite high, see Table 6.1. The total number of function evaluations here can increase rapidly with the increase in design variables, uncertainties and number of optimization cycles. It can be clearly seen here that inspite of having a large number of steps required in case of the cycle-based technique, the total function evaluations required are significantly less. Moreover, if the number of steps required for the convergence can be reduced, the gain in function evaluations can be substantial. In case of the combined cycle-based and asymptotic technique, convergence improves significantly due to the incorporation of derivative information for predicting the worst uncertainties during each cycle, see Fig. 6.12. It should be noticed here that the derivative are obtained analytically for this problem. The number of total function evaluations required for combined cycle-based technique, are substantially smaller than that for other techniques, see Table 6.1.

6.6 Shape Memory Alloy Microgripper Optimization Under Uncertainty

6.6.1 Introduction

The problem considered in this section is the shape optimization of a shape memory alloy microgripper. Shape memory alloys (SMA's) are materials in which a solid-state phase transformation can occur under the influence of a change in temperature or stress state. Internally, the lattice structure of the alloy changes from one configuration to another. The transformation is accompanied by a transformation strain, that can be used for actuation. Compared to other actuator materials, SMA's are capable of generating relatively large strains and stresses. This makes these materials very interesting for many applications. For further information about SMA's, see e.g. Otsuka and Wayman [52] or Duerig *et al.* [53]. The focus of the present study is on the so-called R-phase transformation in nickel-rich NiTi alloys. The thermomechanical behavior of this material has been studied experimentally by Tobushi *et al.* [54], and stress-strain curves at various temperatures are shown in Fig. 6.14. Unlike most SMA's, this R-phase transformation is characterized by a small hysteresis and a relatively narrow thermal operating range. These properties are attractive for actuator applications Kohl *et al.* [55]. The fact that in this case relatively small temperature changes can still induce significant SMA effects, makes that also *in vivo* medical applications might be possible using this alloy. The present microgripper design study is situated in that context.

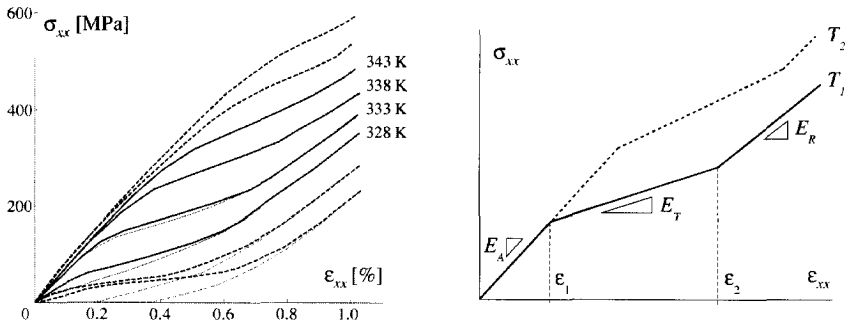


Figure 6.14: Experimental stress-strain data at different temperatures for a NiTi alloy, Tobushi *et al.* [54]. Thick and thin lines represent loading and unloading curves, respectively (left). The right diagram shows a schematic stress-strain diagram illustrating the piecewise linear approximation used in the SMA model.

The constitutive model used to describe this SMA behavior focuses on the temperature range of 328–343 K, where the hysteresis is sufficiently small to be neglected. A piecewise linear approximation is fitted to the stress-strain curves, as schematically illustrated in Fig. 6.14, Langelaar and Van Keulen [56]. The associated expressions and parameter values are given in the Appendix, Section 6.8.1, as well as the generalization of the model to a three-dimensional setting. A detailed treatment of this model is outside the scope of the present chapter, and can be found in other publications, Langelaar *et al.* [57, 58]. Note that the selected temperature range is not directly suited for *in vivo* applications, but because the transformation temperatures can be influenced by heat treatments and alloy composition, Sawada *et al.* [59], lowering this range to acceptable temperatures is possible.

6.6.2 Microgripper model

Before discussing the formulation of the optimization problem, the microgripper design concept is presented here. The conceptual design of this gripper is shown in Fig. 6.15. It consists of an identical top and bottom arm made of folded Ni-Ti plates. An initial deformation is applied in order to generate internal stresses in the material, which are required to make use of the shape memory effect. Starting from the undeformed configuration in Fig. 6.15, the ends of the outer plates are pinched toward the inner plates. In this situation, the equilibrium configuration of each arm can be changed by changing the temperature of either the inner or outer plates. Resistive heating is used for this purpose, and to guide the electrical current through individual plates a slit is present along the length of each plate. Heating the inner plates will cause the tip ends to move apart, opening the gripper. Similarly, heating the outer plates will make them move toward each other, closing the gripper. In the closing configuration, clamping forces of 100 mN are applied in z-direction at the tips of the gripper, acting against the closing forces. A related microgripper design problem has been studied before by Langelaar and Van Keulen [60]. However, in that case, uncertainties were not considered in the shape optimization. In the present problem, uncertainties in both the operating conditions and the SMA material properties are taken into account.

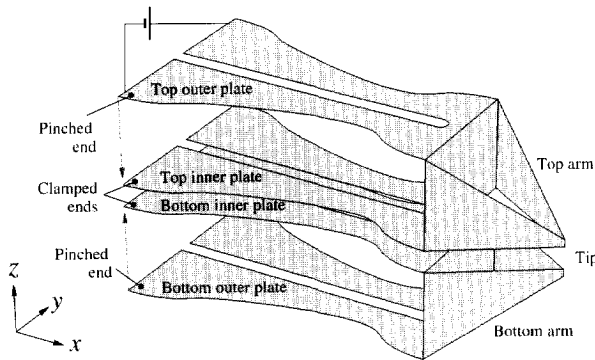


Figure 6.15: Conceptual gripper geometry in the undeformed configuration.

Because of symmetry, only a quarter of the gripper needs to be modeled: in this case half the top arm is used. This part together with the parameterization of the geometry is shown in Fig. 6.16. The design variables chosen for this design problem are the plate thickness T , the undeformed arm height H , the actuation plate end width W_1 , and the shape of the actuation plate. This shape is described by a quadratic B-spline, Farin [61], and the y -coordinates of the two middle control points are used as design variables: Y_1 and Y_2 . Previous design studies have shown that the plate end width W_0 always remains at its upper bound, therefore it is excluded from the present design problem and set to 15 mm, based on previous studies. Further geometrical details of the miniature gripper are listed in Table 6.7 in the Appendix, Section 6.8.2.

The gripper is simulated by finite element analysis of the parameterized design shown in Fig. 6.16. For both the opened and closed case, a quasi-static electrical, thermal and mechanical analysis is performed, to simulate the SMA behavior under the influence of Joule heating. Dissipated heat from the electrical analysis is used as a heat source in the thermal analysis, and the resulting temperature distribution is used in the mechanical analysis. Physical constants used in the simulations are collected in Table 6.8 in the Appendix. Particularly the mechanical analysis is computationally intensive, because of the nonlinear SMA material model as well as the consideration of geometrical nonlinearities. An adaptive incremental-iterative scheme is used to ensure robust convergence. A

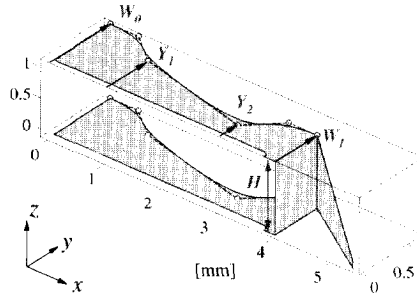


Figure 6.16: Design parameterization of the gripper. Because of symmetry, only a quarter is considered.

triangular shell element is used for the mechanical analysis, Van Keulen and Booiij [62].

6.6.3 Optimization problem formulation

The objective chosen for this design study is to maximize the range of motion of the gripper tips, i.e. the stroke of the gripper. Therefore, the difference between the z-coordinates of the gripper tip displacement u_z^{tip} in open and closed configurations is taken as the objective function:

$$\max_{\mathbf{x}} u_z^{\text{tip, open}}(\mathbf{x}) - u_z^{\text{tip, closed}}(\mathbf{x}) \quad (6.27)$$

Here (\mathbf{x}) represents the vector of design variables. The design variables for the current problem, see Fig. 6.16, are represented in Table 6.2.

Table 6.2: Design variables (\mathbf{x}) for the design optimization of the SMA gripper.

Design variable	Symbol	Lower bound	Upper bound	Unit
Plate thickness	T	0.05	0.3	mm
Gripper arm height	H	0.3	2	mm
Plate shape control point 1	Y_1	0.01	1.5	mm
Plate shape control point 2	Y_2	0.01	1.5	mm
Plate front width	W_1	0.1	1.5	mm
Applied voltage	V	0.001	0.5	V

The considered gripper optimization problem also involves a number of constraints. The validity of the material model is limited to a certain strain range, therefore a constraint on the effective strain ε_e is added in both the open and closed configuration. In addition, motivated by the possibility to use this SMA material for *in vivo* active devices, the thermal operating range is limited to 10 K. This means that per element in the finite element mesh, the following constraints are added to the optimization problem:

$$g_\varepsilon^{(i)} = \frac{\varepsilon_e^{(i)}}{\varepsilon_e^{(max)}} \leq 1 \quad (6.28)$$

$$g_T^{(i)} = \frac{T^{(i)} - T_{min}}{T_{max} - T_{min}} \leq 1 \quad (6.29)$$

The maximum effective strain $\varepsilon_e^{(max)}$ is set to 1%, and the minimum and maximum temperature values used are 328 and 338 K, respectively. A minimum value is included in the formulation in order to scale the temperature constraint properly.

To reduce the number of individual constraints and to make the anti-optimization approach feasible, a Kreisselmeier-Steinhauser [63] constraint aggregation function is used. This aggregation function in its standard form is given by:

$$KS(g) = \frac{1}{\rho} \ln \left(\sum_{i=1}^N e^{\rho g_i} \right) \quad (6.30)$$

where N is the number of individual constraints g_i (e.g. the number of elements) and ρ is a parameter that determines the bias of the aggregation. A higher value of ρ puts larger weightage on higher constraint values more, tending toward a maximum-operator, whereas a lower weight on lower constraint values, tending towards average. In this study, in order to reduce the contribution of local violations, a modified Kreisselmeier-Steinhauser function is used. Here, in order to reduce the contribution of local violations, the individual element constraint values are weighted by the associated element area A_i as

$$KS_A(g) = \frac{1}{\rho} \ln \left(\frac{1}{\sum_{i=1}^N A_i} \cdot \sum_{i=1}^N A_i e^{\rho g_i} \right) \quad (6.31)$$

Note that the use of this Kreisselmeier-Steinhauser function can not prevent a small number of isolated individual violations of the aggregated constraints. However, for a suitable choice of the parameter ρ the violations remain very small and limited in number. $\rho = 40$ has been used here, as this turned out to give a satisfactory behavior.

The resulting optimization problem is now given by:

$$\begin{aligned} & \max_{\mathbf{x}} \left(u_z^{\text{tip, open}}(\mathbf{x}) - u_z^{\text{tip, closed}}(\mathbf{x}) \right)^{(p)} \\ & \text{Subject to:} \\ & KS_A^{(p)}(g_\varepsilon^{\text{open}}(\mathbf{x}; \boldsymbol{\alpha}_1^{(p)})) \leq 1 \\ & KS_A^{(p)}(g_\varepsilon^{\text{closed}}(\mathbf{x}; \boldsymbol{\alpha}_2^{(p)})) \leq 1 \\ & KS_A^{(p)}(g_T^{\text{open}}(\mathbf{x}; \boldsymbol{\alpha}_3^{(p)})) \leq 1 \\ & KS_A^{(p)}(g_T^{\text{closed}}(\mathbf{x}; \boldsymbol{\alpha}_4^{(p)})) \leq 1 \\ & \mathbf{x}^l \leq \mathbf{x} \leq \mathbf{x}^u \end{aligned} \quad (6.32)$$

The lower and upper bounds of the design variables are represented by \mathbf{x}^l and \mathbf{x}^u , respectively, and $\boldsymbol{\alpha}_i^{(p)}$ denotes the worst settings for the uncertainties corresponding to each of the constraints in optimization cycle p , obtained as the maximizers of the following anti-optimization problems:

$$\begin{aligned} & \max_{\boldsymbol{\alpha}_1} KS_A^{(p)}(g_\varepsilon^{\text{open}}(\mathbf{x}^{(p)}; \boldsymbol{\alpha}_1)) \quad \text{s.t.} \quad \boldsymbol{\alpha}^l \leq \boldsymbol{\alpha}_1 \leq \boldsymbol{\alpha}^u \\ & \max_{\boldsymbol{\alpha}_2} KS_A^{(p)}(g_\varepsilon^{\text{closed}}(\mathbf{x}^{(p)}; \boldsymbol{\alpha}_2)) \quad \text{s.t.} \quad \boldsymbol{\alpha}^l \leq \boldsymbol{\alpha}_2 \leq \boldsymbol{\alpha}^u \\ & \max_{\boldsymbol{\alpha}_3} KS_A^{(p)}(g_T^{\text{open}}(\mathbf{x}^{(p)}; \boldsymbol{\alpha}_3)) \quad \text{s.t.} \quad \boldsymbol{\alpha}^l \leq \boldsymbol{\alpha}_3 \leq \boldsymbol{\alpha}^u \\ & \max_{\boldsymbol{\alpha}_4} KS_A^{(p)}(g_T^{\text{closed}}(\mathbf{x}^{(p)}; \boldsymbol{\alpha}_4)) \quad \text{s.t.} \quad \boldsymbol{\alpha}^l \leq \boldsymbol{\alpha}_4 \leq \boldsymbol{\alpha}^u \end{aligned} \quad (6.33)$$

Here $\mathbf{x}^{(p)}$ represents the suboptimal design obtained in the main optimization problem Eq. (6.32) and anti-optimizations are carried out for this design for each constraint, as specified in Eq. (6.33). For evaluation of the objective, a complete electro-thermo-mechanical analysis is required for both the opened and closed configuration. However, for the constraint values, which are the objectives in the anti-optimization problems, no full gripper simulation is required. For instance, for $KS_A(g_\varepsilon^{\text{open}})$, only an electro-thermo-mechanical analysis is required for the opened configuration. And for $KS_A(g_T^{\text{open}})$,

an electro-thermal analysis for the opened configuration is sufficient. In relation to the computational effort required for the nonlinear mechanical analysis involving an incremental-iterative solution process, the computational effort required for this electro-thermal analysis is virtually zero. Therefore, significant computational savings were possible by exploiting these observations in the practical implementation, leading in this case to a reduction of the computational effort by approximately a factor 4.

Table 6.3: Uncertainty variables α for the gripper problem, their deterministic or nominal values together with their upper and lower bounds.

Uncertainty variable	Symbol	Nominal value	Lower bound	Upper bound	Unit
Face convection coefficient	h	2.0	1.8	2.2	$\text{kWm}^{-2}\text{K}^{-1}$
Ambient temperature	T_a	328	327.6	328.4	K
Austenite Young's modulus	E_A	68.939	63.0	75.0	GPa
R-phase apparent Young's modulus	E_R	45.612	43	48	GPa
Initial apparent transition Young's modulus	E_0	20.006	19.5	20.5	GPa
Poisson ratio	ν	0.3333	0.3	0.36	-

The uncertainty variables contained in the set α that are selected for the present design problem are listed in Table 6.3, together with their nominal values and their bounds. The ambient temperature is considered uncertain because it is hard to control. The convection coefficient is difficult to determine unless the environmental conditions are well known and stable, which is not likely to be the case. The other uncertainty variables are parameters of the SMA constitutive model, and these account for any inaccuracy that might be present in the measurements, as well as unknown aspects of the SMA behavior that have not been included in the modeling. One could think of, for instance, the minor hysteresis that has been neglected in the formulation of the SMA model. The range for these parameters has been chosen such, that it covers a substantial deviation of the modeled material behavior. This is illustrated by the stress-strain diagram shown in Fig. 6.17, which visualizes the effect of the uncertainties in E_A , E_R and E_0 and T_a on the one-dimensional material model. The variation of the ambient temperature is assumed to directly affect the temperature of the SMA material, which is the worst case situation.

In order to visualize the effect of the uncertainties on the material model in the plane stress setting used in the gripper model itself, and to include the effect of the uncertainty in the Poisson ratio ν , two new quantities are defined. A first measure to illustrate the effect is the difference between the largest and smallest Von Mises stress value $\Delta\sigma_{VM}$ at a certain strain state, for any combination of uncertainty values in the defined ranges:

$$\Delta\sigma_{VM}(\varepsilon_1, \varepsilon_2) = \max_{\alpha} \sigma_{VM}(\varepsilon_1, \varepsilon_2; \alpha) - \min_{\alpha} \sigma_{VM}(\varepsilon_1, \varepsilon_2; \alpha) \quad (6.34)$$

where ε_1 and ε_2 are the principal strains, and σ_{VM} is the Von Mises stress. In order to be able to judge the relative magnitude of this difference, also a quantity Ψ is introduced where $\Delta\sigma_{VM}$ is normalized by the nominal value of the Von Mises stress at the considered strain state:

$$\Psi(\varepsilon_1, \varepsilon_2) = \frac{\Delta\sigma_{VM}(\varepsilon_1, \varepsilon_2)}{\sigma_{VM}(\varepsilon_1, \varepsilon_2)} \quad (6.35)$$

These two quantities are visualized in Fig. 6.18 and Fig. 6.19, respectively, for various values of the nominal temperature. Again the variation of the ambient temperature is assumed to directly

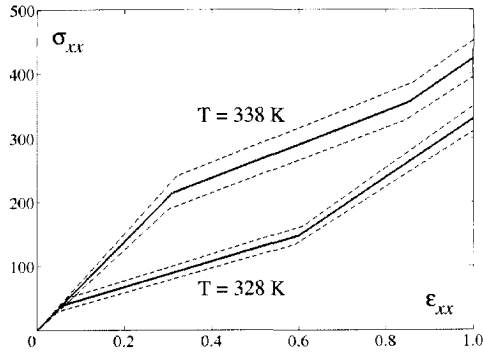


Figure 6.17: One-dimensional stress-strain curves according to the deterministic model (thick lines) and the range covered by the uncertain material parameters (gray), at different temperatures.

affect the temperature of the material. Note that the relative effect of the uncertainties is quite large, roughly 20–25% on average, and that the uncertainties affect different strain states differently. Because of this, the equilibrium configuration of the gripper will therefore most likely be affected by the uncertainties. Hence it is hard to make a statement about which combination of uncertainty variables will result in the worst value for strain constraints.

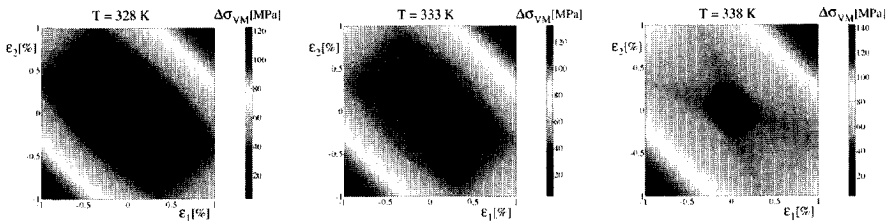


Figure 6.18: Maximum difference in Von Mises stress at different strain states due to the effect of the uncertainties, at different nominal temperatures.

In contrast to the strain constraint, the temperature constraint is affected only by the uncertainties in the ambient temperature and the convection coefficient. In fact, on physical grounds it is clear that the largest value for the temperature constraint is obtained when the ambient temperature uncertainty is at its upper bound and the convection coefficient is at its lower bound. But in this study, no use is made of this knowledge, and the temperature constraints are treated in the most general way.

6.6.4 Results

Using the cycle-based alternating anti-optimization technique proposed in this chapter, design optimization of the SMA microgripper has been performed. The even more efficient combined cycle-based alternating and asymptotic method could not be employed because sensitivity information was not available. Linear approximations have been used for response surfaces, both in main and anti-optimization. The PYTHON-based nested parallel computing framework reduced the total time of the optimization process, and a cluster of 14 CPUs (1 GHz Pentium) was used. Both the deterministic and uncertainty-based optimization converged after ca. 20 iterations, and the evolution of the

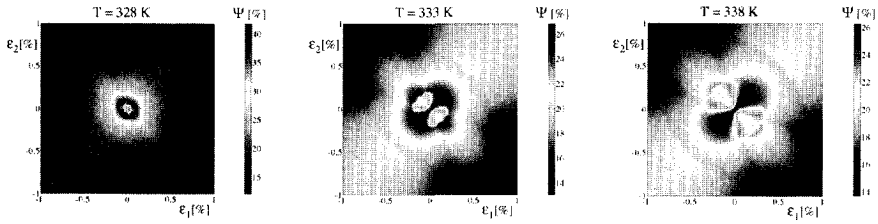


Figure 6.19: Maximum difference in Von Mises stress relative to the nominal value at different strain states due to the effect of the uncertainties, at different nominal temperatures.

objective and constraint values are depicted in Fig. 6.20 and Fig. 6.21, respectively.

The objective history of the deterministic case shows a sharp spike at the fourth step, where the stroke of the gripper even becomes negative. This is clearly undesirable, and possibly is caused by the inability of that design to generate the required clamping force. However, the optimizer recovers in the subsequent step. The activity of the constraints shown in Fig. 6.21 shows that all constraints are relevant to the design problem. This is confirmed by the fact that the final constraint values shown in Table 6.4 are all very close to 1.

The design variable values and the responses of the final designs are also listed in Table 6.4. The stroke in case of the uncertainty-based design is ca. 15% less than that of the deterministic design. Accounting for uncertainties essentially requires the design to move further away from the deterministic constraints, resulting in a reduction of the objective. Note that in the present study, effect of uncertainties only on constraint functions is considered due to the present setting of the optimizer. However, effect of uncertainties on objective function is considered separately at the end of both optimizations. In this, a separate anti-optimization for the optimal design is carried out in order to anticipate influence of uncertainties on objective function. This anti-optimization is carried out for the optimal design corresponding to both deterministic as well as uncertainty-based design optimization separately. In case of deterministic optimization the stroke reduces from 0.4341 mm (Table 6.4) to 0.3259 mm, whereas in case of uncertainty-based optimization it reduces from 0.3684 mm (Table 6.4) to 0.2728 mm. However, present technique can be extended to include influence of uncertainties on objective in a similar way as that for constraints.

The total number of FEAs and wall clock time required for both deterministic and uncertainty-based optimization are compared in Table 6.4. In case of uncertainty-based optimization the required FEAs are 30 times that of deterministic optimization, which clearly shows the need of smart techniques such as Nested Parallel Computing in order to make the uncertainty-based optimization practical. The efficient use of available computational power by means of Nested Parallel Computing has brought down the relative wall clock time for uncertainty-based optimization to 7.5 times that of deterministic optimization.

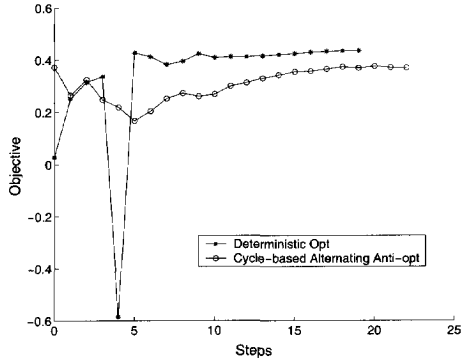
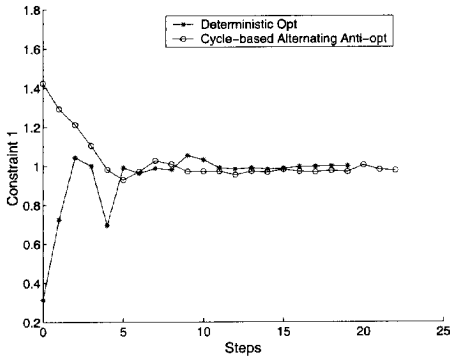
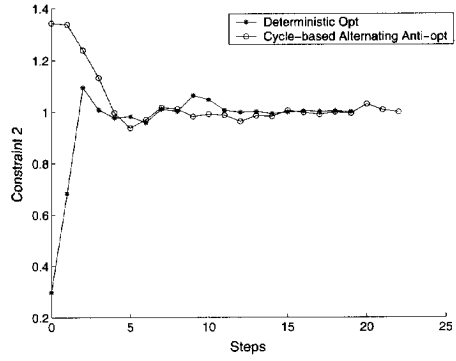


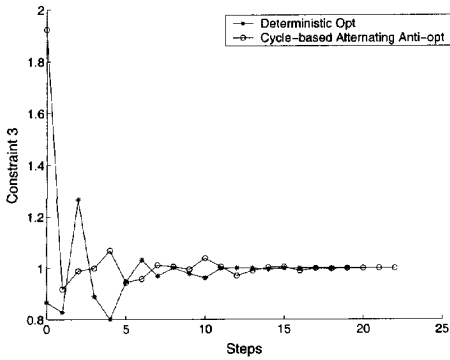
Figure 6.20: Optimization history: objective function



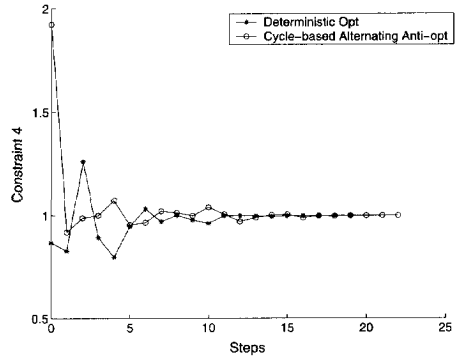
(a) Evolution of $KS_A(g_\epsilon^{open})$.



(b) Evolution of $KS_A(g_\epsilon^{closed})$.



(c) Evolution of $KS_A(g_T^{open})$.



(d) Evolution of $KS_A(g_T^{closed})$.

Figure 6.21: Optimization history: constraints.

Table 6.4: Comparison between deterministic and uncertainty-based optimization results using cycle-based alternating anti-optimization for the SMA microgripper problem.

	Deterministic	Uncertainty-based
Optimal Response		
f [mm]	0.4341	0.3684
$KS_A(g_\varepsilon^{\text{open}})$	0.9992	0.9776
$KS_A(g_\varepsilon^{\text{closed}})$	0.9999	0.9983
$KS_A(g_T^{\text{open}})$	0.9999	0.9998
$KS_A(g_T^{\text{closed}})$	0.9979	0.9982
Optimal Design		
T [mm]	0.0974	0.1022
H [mm]	1.1703	1.0463
Y_1 [mm]	1.2485	1.3047
Y_2 [mm]	1.1125	1.0208
W_1 [mm]	1.4001	1.2703
V [V]	0.0603	0.0553
Total No. of FEA	221	6645
Relative No. of FEA	1	30
Wall clock time [hours:min]	8:17	62:12
Relative Wall clock time	1	7.5

The geometries of the SMA gripper corresponding to the optimal designs obtained in the deterministic and uncertainty-based optimization are depicted in Fig. 6.22. From the top and side views, it can clearly be seen that the deterministic design is wider at the front and also higher. A geometrical difference that cannot be seen in Fig. 6.22 is that the plates are 5% thicker in the uncertainty-based design. The operation of the gripper is demonstrated in Fig. 6.23, which shows a side view of the optimal uncertainty-based gripper in the open and closed configuration.

Table 6.5: Worst set of uncertainties obtained for the uncertainty-based optimum for each constraint for the SMA microgripper problem.

	$KS_A(g_\varepsilon^{\text{open}})$	$KS_A(g_\varepsilon^{\text{closed}})$	$KS_A(g_T^{\text{open}})$	$KS_A(g_T^{\text{closed}})$
Worst Uncertainties				
h/\bar{h}	1.08485	0.9	0.9	0.9
T_a/\bar{T}_a	1.00122	1.00122	1.00122	1.00122
E_A/\bar{E}_A	1.08792	1.08792	-	-
E_R/\bar{E}_R	0.94273	0.94273	-	-
E_0/\bar{E}_0	0.97470	0.97470	-	-
$\nu/\bar{\nu}$	1.08	1.08	-	-

In the case of uncertainty-based optimization, the values of the uncertainty variables that yield the worst (i.e. largest) constraint values for the final design are listed in Table 6.5 for all four constraints. For the temperature constraints, only the uncertainties in the thermal quantities are meaningful, and it turns out that indeed their worst case values are as predicted earlier. Inspection shows that all of the uncertainty variables are at either their lower or upper bound for the final design, except the face convection coefficient h at the strain constraint for the opened case $KS_A(g_\varepsilon^{\text{open}})$. Evaluation of this constraint with h at its lower and upper bound confirmed that indeed the worst value is obtained for h at an interior value. When considering the evolution of this uncertainty variable h

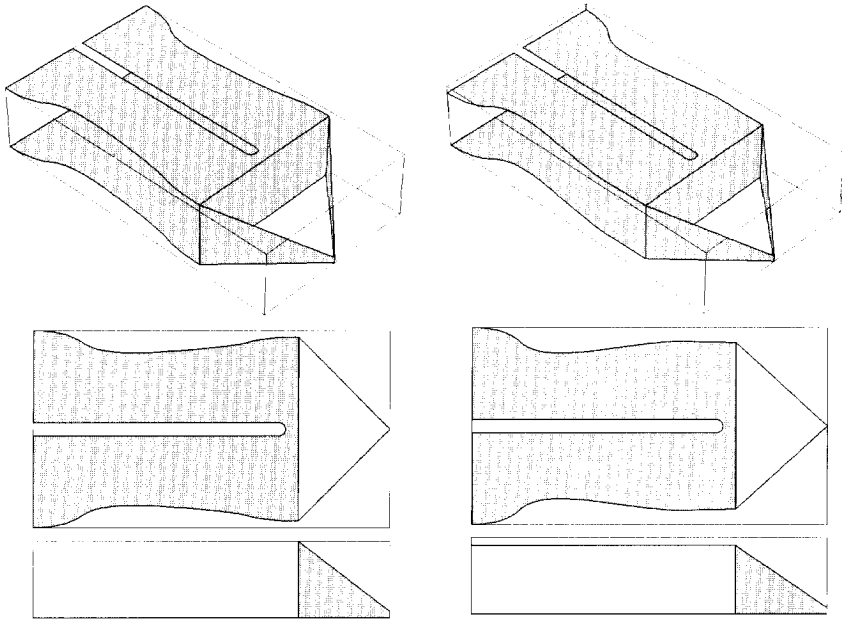


Figure 6.22: Undeformed geometries of the optimal designs obtained by deterministic optimization (left) and optimization considering bounded-but-unknown uncertainties (right).

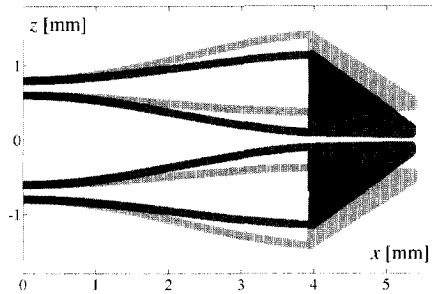
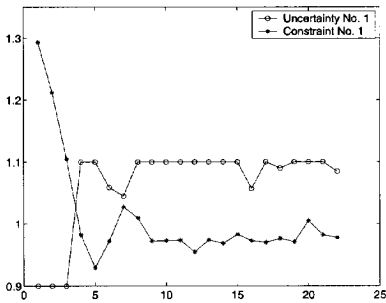
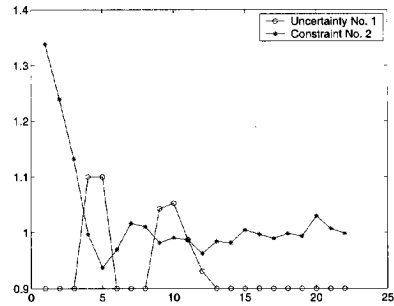


Figure 6.23: Side view of the optimized gripper in opened (light gray) and closed (dark gray) configuration.

during the optimization process, as depicted in Fig. 6.24, it turns out that in many other steps also interior worst-case values are found, in both strain constraints. Also, for the strain constraint in the opened case $KS_A(g_e^{open})$, the uncertainty variable h initially stays at the lower bound, but changes to values equal or close to the upper bound. From this observation, it can be concluded that the present uncertainty-based SMA gripper optimization problem also exhibits fluctuating uncertainties. The worst case for uncertainty variable h clearly is design-dependent, and also takes interior values. The complexity and nonlinearity of the model results leads to non-convexity in the uncertainty-based design optimization. In general, for complex models, it is hard to predict which combination of uncertainties will result in the worst constraint values, and whether even interior worst cases are possible. Therefore the proposed anti-optimization technique is the best choice for such problems, even though it is computationally more involved than approaches that rely on, e.g., vertex checking.



(a) Plot for the normalized worst value of the uncertainty in face convection coefficient h/\bar{h} and the worst value of constraint $KS_A(g_e^{open})$ obtained by anti-optimization corresponding to suboptimal design at each step.



(b) Plot for the normalized worst value of the uncertainty in face convection coefficient h/\bar{h} and the worst value of constraint $KS_A(g_e^{closed})$ obtained by anti-optimization corresponding to suboptimal design at each step.

Figure 6.24: Anti-optimization results in terms of worst set of uncertainties and constraint corresponding to suboptimal design at each step for the Shape Memory Alloy Microgripper problem.

6.7 Discussion/Conclusion

The cycle-based alternating anti-optimization technique combined with Nested Parallel Computing is successfully applied to the design optimization of an SMA Microgripper involving bounded-but-unknown uncertainties. This allows for practical optimization-based design of SMA devices in situations where e.g. the material properties and operating conditions are not exactly known, but where bounds on their values can be specified. The worst set of uncertainties turned out to be design-dependent, and the cycle-based alternating technique proved to be able to handle this situation effectively.

The optimization problem involving bounded-but-unknown uncertainties is solved using an anti-optimization technique. To demonstrate and compare various anti-optimization approaches, the elastically supported beam problem from literature is used here. For this test problem, the worst set of uncertainties is also strongly dependent on the design, and fluctuates considerably from design to design. This situation is the most challenging case for efficient anti-optimization, however many problems of realistic complexity, such as the SMA Microgripper problem, share this characteristic. For such problems exhibiting fluctuating worst uncertainties, it is shown that the Cycle-based alternating technique is more efficient than the existing Lombardi-Hafika alternating technique in terms of convergence. Rigorous anti-optimization proves to be better than the Cycle-based technique in

terms of good convergence. However, since the number of function evaluations required for the rigorous approach can quickly become prohibitive as the problem size increases, in terms of the number of design variables, uncertainties and constraints, the rigorous approach quickly becomes impractical for problems involving computationally expensive function evaluations.

Further improvement of the effectiveness of the Cycle-based technique is possible with the use of derivative information. It is demonstrated by means of the elastically supported beam problem that combining the Cycle-based technique with the Asymptotic method, which uses derivative information for prediction of worst cases, is significantly more efficient than all other examined techniques, in terms of both the convergence and number of function evaluations. In the present study however, this combined Cycle-based and Asymptotic method is not applied in the SMA Microgripper optimization, because of the lack of the required derivative information.

For the problems involving computationally expensive response evaluations, use of Parallel Computing is essential to make the above optimization techniques computationally feasible. For the SMA Microgripper problem, which involves computationally expensive finite element simulations, the Cycle-based technique combined with Nested Parallel Computing enabled the practical application of anti-optimization. For this problem, the total number of FEAs required for uncertainty-based optimization is 30 times that of the deterministic optimization. In case of sequential evaluation for this problem, total wall clock time required for uncertainty-based optimization would also be 30 times that of deterministic optimization. However, the use of Nested Parallel Computing has brought down this overall duration of uncertainty-based optimization to merely 7.5 times that of deterministic optimization, which illustrates the effectiveness of the parallel computing strategy.

To summarize, uncertainties in design problems described by bounds can be handled safely and efficiently using the cycle-based alternating anti-optimization technique. In case of practical optimization problems involving computationally expensive function evaluations, the Cycle-based technique combined with the Nested Parallel computing provides a general and efficient approach to tackle uncertainties.

6.8 Appendix

6.8.1 Material Model for Shape Memory Alloy

This appendix summarizes the SMA constitutive model for the R-phase transformation. The one-dimensional stress-strain curves at a certain temperature T , shown in Fig. 6.14, are approximated by a piecewise linear function consisting of three parts:

$$\sigma_{xx} = \begin{cases} \varepsilon_{xx} \leq \varepsilon_1 & : \sigma_0 = E_A \varepsilon_{xx} \\ \varepsilon_1 < \varepsilon_{xx} \leq \varepsilon_2 & : \sigma_1 = E_T (\varepsilon_{xx} - \varepsilon_1) + \sigma_0(\varepsilon_1) \\ \varepsilon_{xx} > \varepsilon_2 & : \sigma_2 = E_R (\varepsilon_{xx} - \varepsilon_2) + \sigma_1(\varepsilon_2) \end{cases} \quad (6.36)$$

where $\varepsilon_1, \varepsilon_2$ and E_T are linear functions of temperature:

$$\begin{aligned} \varepsilon_1(T) &= K_\varepsilon(T - T_0) + \varepsilon_0 \\ \varepsilon_2(T) &= \varepsilon_1(T) + \Delta \\ E_T(T) &= K_E(T - T_0) + E_0 \end{aligned} \quad (6.37)$$

and E_A and E_R are constant parameters. ε_1 and ε_2 are the transition strains at which the R-phase transformation starts and finishes. E_T is the apparent Young's modulus $d\sigma_{xx}/d\varepsilon_{xx}$ during the phase transition. By curve fitting, the parameters defining the material behavior can be determined. Values for the parameters can be found in Table 6.6.

The three-dimensional stress-strain relation is given by:

$$\boldsymbol{\sigma} = (KK + 2GG)\boldsymbol{\varepsilon} \quad (6.38)$$

Here σ is the second Piola-Kirchhoff stress in vector notation, K is the bulk ratio and G is the effective shear ratio. The matrices \mathbf{G} and \mathbf{K} in the preceding equations are constant and given by:

$$\mathbf{G} = \frac{1}{3} \begin{bmatrix} 2 & -1 & -1 & 0 & 0 & 0 \\ -1 & 2 & -1 & 0 & 0 & 0 \\ -1 & -1 & 2 & 0 & 0 & 0 \\ 0 & 0 & 0 & 3 & 0 & 0 \\ 0 & 0 & 0 & 0 & 3 & 0 \\ 0 & 0 & 0 & 0 & 0 & 3 \end{bmatrix}, \quad \mathbf{K} = \begin{bmatrix} 1 & 1 & 1 & 0 & 0 & 0 \\ 1 & 1 & 1 & 0 & 0 & 0 \\ 1 & 1 & 1 & 0 & 0 & 0 \\ 0 & 0 & 0 & 0 & 0 & 0 \\ 0 & 0 & 0 & 0 & 0 & 0 \\ 0 & 0 & 0 & 0 & 0 & 0 \end{bmatrix} \quad (6.39)$$

For a given value of the shear ratio G , this stress-strain relation corresponds to the well-known Hooke's Law for linear elasticity. To account for the isochoric R-phase transformation strain, the value of G becomes dependent on the effective strain ε_e , which is defined by:

$$\varepsilon_e^2 = \frac{2}{3} \varepsilon^T \mathbf{G} \varepsilon \quad (6.40)$$

At a given temperature T , the one-dimensional model gives a linear relationship between the uniaxial stress and strain component: its general form is $\sigma_{xx} = A\varepsilon_{xx} + B$, for each segment of the piecewise linear model given in Eq. (6.36). From this, the relation between G and ε_e can be obtained:

$$G = \frac{3K}{9K - A} \left(A + \frac{B}{\varepsilon_e} \right) \quad (6.41)$$

The tangent operator of this material model in the three-dimensional setting is obtained by differentiation of the stress-strain relation in Eq. (6.38), which yields:

$$\frac{d\sigma}{d\varepsilon} = K\mathbf{K} + 2G\mathbf{G} + \frac{4}{3\varepsilon_e} \frac{dG}{d\varepsilon_e} \mathbf{G} \varepsilon \varepsilon^T \mathbf{G} \quad (6.42)$$

Table 6.6: Parameter values for the SMA model.

K_ε	$2.55 \times 10^{-4} \text{ K}^{-1}$	K_E	619 MPa K^{-1}
ε_0	5.71×10^{-4}	Δ	54.2×10^{-4}
E_0	20.0 GPa	T_0	328 K
E_A	68.9 GPa	E_R	45.6 GPa

6.8.2 Additional tables

Table 6.7: Significant coordinates of B-spline control points and other points defining the geometry of the miniature gripper.

Point	x [mm]	y [mm]	Point	x [mm]	y [mm]
Control point 1	0	15	Control point 2	0.5	15
Control point 3	1	Y_1	Control point 4	3	Y_2
Control point 5	3.5	W_1	Control point 6	4	W_1
Tip	5.377	0	Slit end	3.8	0

Table 6.8: Physical constants used in the finite element modeling.

Quantity	Value	Quantity	Value
Electrical conductivity	$1.25 \cdot 10^6 \text{ Sm}^{-1}$	Thermal conductivity	$21 \text{ Wm}^{-1}\text{K}^{-1}$
Thermal convection coefficient	$2.0 \cdot 10^3 \text{ Wm}^{-2}\text{K}^{-1}$	Ambient temperature	328 K

6.9 Acknowledgment

Part of this research is supported by the Technology Foundation STW, applied sciencedivision of NWO and the technology program of the Ministry of Economic Affairs, The Netherlands.

Chapter 7

Anti-optimization using Combined Response Surface

In this chapter a new approach for uncertainty-based design optimization using anti-optimization is proposed, which uses a combined response for design variables and uncertainties. The anti-optimization technique used here involves a two-level nested optimization. In the outer level, the main optimization is carried out, which searches for the best design. In the inner level, anti-optimization is carried out to find the worst sets of uncertainties, which provide the worst possible values for the constraints. The basic optimization technique used for both the main and anti optimization relies on sequential response surface approximations. The proposed approach is based on a combined response surface (CRS). Thus, a common design of experiment is carried out for the combined space of design variables and uncertainties. The response evaluations for this combined design of experiment are then used to construct a CRS, which is a function of both the design variables and the uncertainties. The present technique involves an iterative process, in which two separate optimization problems, namely the main and anti-optimization, are solved alternately. In the main optimization, the objective function is minimized subjected to a set of constraints for a given or fixed sets of uncertainties. For the optimal design resulted from the main optimization, anti-optimization is carried out for each of the constraints in order to obtain worst values for these constraints. The worst sets of uncertainties corresponding to each of the constraints are used in the main optimization during the next iteration. This iterative procedure continues until convergence is obtained. This technique is very flexible in terms of dealing with different types of problems. The method is applicable to both convex as well as non-convex problems. In the latter situation, nonlinear approximations are more advantageous. Like most other response surface based techniques, the method suffers from the 'curse of dimensionality'. The CRS technique is applied in the present chapter to a practical application from MEMS, which is a Piezoelectric energy reclamation device. This MEMS device has uncertainties in its dimensions and material properties.

Key words: Anti-optimization, Bounded-But-Unknown Uncertainties, Combined Response Surface, MEMS

7.1 Introduction

Many practical design optimization tasks involve uncertainties. When enough data on uncertainties is available, it can be used to construct statistical distributions for uncertainties. However, it often happens that there is not enough data available to construct reliable distributions. This can be particularly the case in early stages of a design process. In such situations, the available data in combination with engineering experience can be used to set tolerances or bounds on uncertainties, within which the exact distribution is unknown, thus identifying uncertainties as Bounded-But-Unknown (BBU) as in Ben-Haim and Elishakoff [11] and Ben-Haim [12]. The anti-optimization technique described in Elishakoff *et al.* [7] checks the vertices of the uncertainty domain in order to obtain the worst response of the structure. This technique is computationally very efficient for problems with convexities, however its application is limited to convex problems.

A more generalized or *Rigorous* anti-optimization, which can handle non-convexities, is adopted in Van Keulen *et al.* [13] and Gurav *et al.* [34]. However, this technique suffers from the required large number of expensive function evaluations due to the underlying two-level nested optimization. In order to make it computationally efficient, the *Enhanced* anti-optimization technique that uses sensitivities, a database technique and parallel computing to make it computationally efficient is studied in Gurav *et al.* [47]. The technique still becomes computationally expensive for an increasing number of design variables and uncertainties, which stimulates search for alternative approaches. In an alternative approach, proposed by Lombardi and Haftka [19], anti- and main optimization are carried out alternately, thereby avoiding the nested approach. This approach can converge very fast in case of problems involving convexities and is quite efficient in terms of the number of required function evaluations. However, it may expose bad convergence if the worst case fluctuates from design to design. Based on a similar principle, a *Cycle-based* alternating anti-optimization approach is studied in Gurav *et al.* [64]. This approach partially overcomes the convergence problems in case of non-convexities and is computationally quite efficient.

In this chapter, an alternative approach based on combined response surfaces (CRS) for design variables and uncertainties is studied. In this technique, both the main and the anti optimization operate on the same response surface. These CRSs are generated using a design of experiments including both design variables and uncertainties. The main optimization here finds the best design for fixed sets of uncertainties. For the sub-optimal design obtained by the main optimization, an anti-optimization is carried out for every constraint to determine the associated worst set of uncertainties. The worst set of uncertainties corresponding to each of the constraints is kept fixed during next iteration of the main optimization. This iterative process continues until the convergence has been obtained.

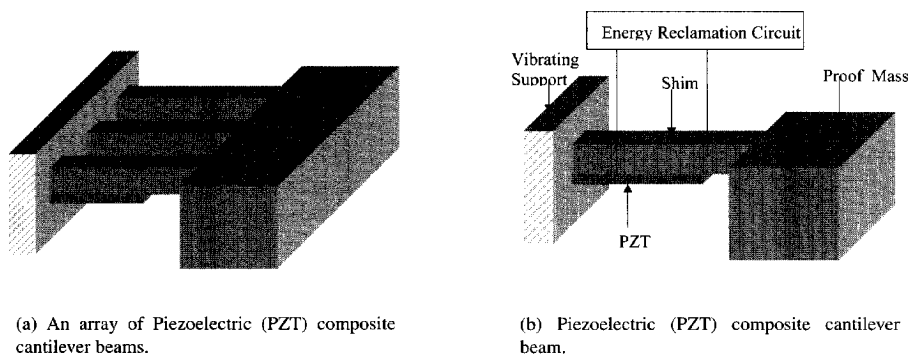


Figure 7.1: An energy reclamation device.

The proposed CRS technique is used to optimally design a Piezoelectric energy reclamation device. The detailed description of the electro-mechanical model for this problem is given in [39, 40]. The overall purpose of the device is to extract maximum power from external base vibrations. The energy reclamation device at hand consists of an array of piezoelectric (PZT) composite cantilever beams arranged as shown in Fig. 7.1(a). Each cantilever beam consists of a perfectly bonded PZT patch [41] and a proof mass attached at the end, see Fig. 7.1(b). In a real application, the device is attached at the support to a vibrating surface. The proof mass at the tip translates the input acceleration into an effective force that deflects the beam. This effective force induces mechanical strain in the beam, which is converted into a voltage (V) using the piezoelectric effect [41, 42]. The output voltage of the PZT can be reclaimed into usable power with the help of an energy reclamation circuit. When dealing with Microelectromechanical Systems (MEMS), because of their small dimensions, tolerances on shapes are *relatively* high (1%-10%) [30, 31]. These variations in dimen-

sions of MEMS structures can have a significant effect on their mechanical behavior. Furthermore, MEMS exhibit a large variation in their material properties (1%-15%) [43–46]. As a result, while designing MEMS, various types of uncertainties should be considered.

7.2 Multipoint Approximation Method

In the present chapter the MAM, see Toropov *et al.* [1,2] and Van Keulen and Toropov [3,4], is used as a basis for optimization. Many times practical applications involve numerical evaluation of response functions. From an optimization point of view, these types of problems can either suffer from numerical noise or the large computational time involved. The MAM, which is based on sequential use of Response Surface Methodology can be applied to such problems. The MAM uses approximations for the responses in order to reduce the number of expensive numerical response evaluations. However, it should be noted here, that it suffers from the so-called curse of dimensionality, i.e. it becomes inefficient with the increase in dimensions (number of design variables).

The optimization problem can now be formulated mathematically as

$$\begin{aligned} \min_{\mathbf{x}} \quad & f_0(\mathbf{x}) \\ \text{s.t.} \quad & f_i(\mathbf{x}) \leq 1, \quad i = 1, \dots, m, \\ & A_j \leq x_j \leq B_j, \quad j = 1, \dots, n. \end{aligned} \tag{7.1}$$

Here, f_0 is the objective function and f_i are constraints, whereas \mathbf{x} is a set of design variables. The design space is represented by the upper and lower limits on x_j , A_j and B_j , respectively.

The MAM is based on a replacement of the actual optimization problem, as described by Eq. (7.1), by a series of approximate optimization problems as depicted in Fig. 7.2. The approximate optimization problem (AOP) for a cycle p , can be formulated as

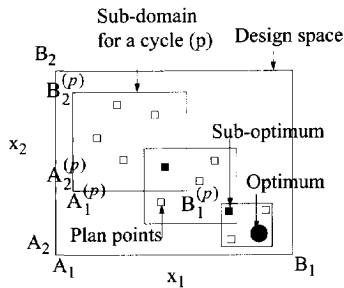


Figure 7.2: Optimization using the MAM for a problem of two design variables (x_1 and x_2).

$$\begin{aligned} \min_{\mathbf{x}} \quad & \tilde{f}_0^{(p)}(\mathbf{x}) \\ \text{s.t.} \quad & \tilde{f}_i^{(p)}(\mathbf{x}) \leq 1, \quad i = 1, \dots, m, \\ & A_j^{(p)} \leq x_j \leq B_j^{(p)}, \quad j = 1, \dots, n, \\ & A_j^{(p)} \geq A_j, \quad B_j^{(p)} \leq B_j. \end{aligned} \tag{7.2}$$

Here, the response functions are replaced with approximate functions over the subdomain for a cycle. For the current AOP, $\tilde{f}_i^{(p)}(\mathbf{x})$ are considered as adequate approximations of $f_i(\mathbf{x})$ over the subdomain (p) represented by the move limits $A_j^{(p)}$ and $B_j^{(p)}$, see Fig. 7.2. It should be noted here that the move limits for the initial cycle ($A_j^{(0)}$ and $B_j^{(0)}$), can be chosen either arbitrarily or based on engineering experience. Many times this can significantly influence the convergence.

7.3 Bounded-But-Unknown Uncertainty

If the problem at hand is non-deterministic, i.e. there are uncertainties that play a non-negligible role, the response functions also depend on the uncertainties. The set of uncertainty variables will be denoted α , with

$$\alpha = (\alpha_1 \dots \alpha_u). \tag{7.3}$$

Consequently, the response functions depend on both design variables and uncertainties, hence $f(\mathbf{x}, \alpha)$.

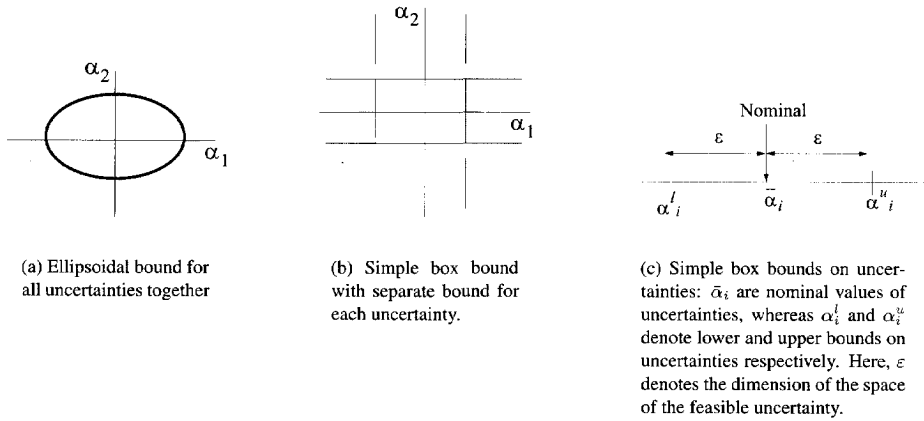


Figure 7.3: Bounds on uncertainties.

In the present chapter, uncertainties are modelled using the BBU approach. In this, several bounds can be introduced, each providing a bound for a group of uncertainty variables or all uncertainty variables simultaneously, for example see Fig. 7.3. At the same time, we may want to measure the amount of uncertainty. Thus, measures for the dimensions of the subspace containing all possible selections of uncertainty variables are desired. This can be cast into a mathematical framework as follows. Assuming a set with b bounds, then a possible or *feasible* selection of α satisfies, see Van Keulen *et al.* [13]:

$$B_i(\alpha, \epsilon) \leq 0, \quad \text{for } i = 1, \dots, b. \tag{7.4}$$

Otherwise the selection of the uncertainty variables α is *infeasible*. Here, the components of ϵ are used to specify the dimensions of the space of feasible uncertainty variables. We will therefore refer to these components as the *levels of uncertainty*.

In the present chapter, simple box bounds, see Fig. 7.3(b & c), are used to specify uncertainties as

$$(\alpha_i - \bar{\alpha}_i)^2 - \epsilon^2 \leq 0. \tag{7.5}$$

These type of bounds generally come from a tolerance specified on a nominal value, for example, due to the manufacturing induced inaccuracies. In case of applications, where a very high performance is required against failure, such sharp bounds become practical. These bounds can be alternatively represented in terms of lower (α_i^l) and upper bounds (α_i^u) on uncertainties as

$$\begin{aligned} \alpha_i^l &= \bar{\alpha}_i - \epsilon, \\ \alpha_i^u &= \bar{\alpha}_i + \epsilon. \end{aligned} \tag{7.6}$$

7.4 Uncertainty-based optimization using Anti-optimization

7.4.1 Anti-optimization using Combined Response Surface

The basic technique used here is anti-optimization that actually tries to incorporate worst possible responses, as a function of uncertainties, in the optimization procedure. Here, the optimization problem involves several cycles before convergence. Each cycle of this optimization process, involves an iterative process which iterates between two separate optimization problems before converging to a suboptimal solution. In the present technique, CRS is used as a basis for both the main as well as with anti-optimization. In order to construct a CRS, a design of experiment is planned for the combined design space of design variables and uncertainties at the beginning of each cycle. Based

on the FEAs obtained for this combined design of experiment, CRSs are fitted for all responses as a function of design variables as well as uncertainties. These CRSs are used in the iterative process of every cycle as follows:

$$\begin{aligned} \min_{\mathbf{x}} \quad & \tilde{f}_0(\mathbf{x}, \boldsymbol{\alpha}) \\ \text{s.t.} \quad & \tilde{f}_i(\mathbf{x}; \boldsymbol{\alpha}_i^*) \leq 1, \quad i = 1, \dots, m, \end{aligned} \tag{7.7}$$

where $\boldsymbol{\alpha}_i^*$ is the maximizer of

$$\begin{aligned} \max_{\boldsymbol{\alpha}_i} \quad & \tilde{f}_i^*(\mathbf{x}^*; \boldsymbol{\alpha}_i) \\ \text{s.t.} \quad & B_j(\boldsymbol{\alpha}_i, \varepsilon) \leq 0, \quad j = 1, \dots, b. \end{aligned} \tag{7.8}$$

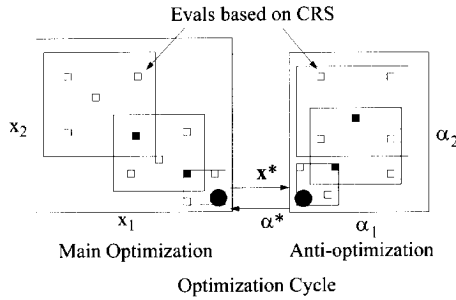


Figure 7.4: Anti-optimization technique in the MAM setting for a problem of two design variables (x_1 and x_2) and two uncertainties (α_1 and α_2). The big boxes indicate the search (sub-) domains. The small open boxes indicate sets of design variables (left) or uncertainty variables (right) for which function evaluations are carried out using CRSs. The small solid boxes indicate solutions of the sub-problems.

Here, $\tilde{f}_0(\mathbf{x})$ is the CRS for the objective function and $\tilde{f}_i(\mathbf{x}, \boldsymbol{\alpha}_i)$ are CRSs for constraints, whereas $B_j(\boldsymbol{\alpha}_i, \varepsilon)$ are bounds on uncertainties. The main optimization as defined in Eq. (7.7) is a standard minimization, where objective function is minimized subjected to a set of constraints. For the evaluation of constraint values in Eq. (7.7), the worst set of uncertainties ($\boldsymbol{\alpha}_i^*$) are kept fixed during a cycle of the main optimization. It is assumed, that the objective is not affected by the uncertainties. However, in practice when such effect is significant it can be tackled in the same way as that for the constraints where it is considered in all situations. The anti-optimization as reflected by Eq. (7.8) solves a maximization problem in order to obtain the worst possible values for the constraints with respect to uncertainties. It should be noticed here that such anti-optimizations are carried out for the optimal design (\mathbf{x}^*) obtained from the main optimization and for every constraint. The worst sets of uncertainties ($\boldsymbol{\alpha}_i^*$) obtained by anti-optimizations Eq. (7.8) are kept fixed during the main optimization Eq. (7.7) of next iteration. For the initial iteration uncertainties are chosen arbitrarily or as $\boldsymbol{\alpha}^* = \bar{\boldsymbol{\alpha}}$, see Fig. 7.3(c). These main and anti-optimizations are carried out alternately until convergence is obtained. This iterative process is converged if

$$\left\| \frac{\tilde{f}_0 - \tilde{f}_{0\text{prev}}}{\tilde{f}_0} \right\| \leq \text{tolerance}, \quad \text{and} \tag{7.9}$$

$$\left\| \frac{\alpha_{ik}^* - \alpha_{ik\text{prev}}^*}{\alpha_{ik}^*} \right\| \leq \text{tolerance} \quad i = 1, \dots, n; \quad k = 1, \dots, u. \tag{7.10}$$

where P_{out} is the electrical output power extracted from the device. The composite cantilever beam is subjected to external acceleration (a_0) as shown in Fig. 7.5(b). This external acceleration is specified in terms of external excitation frequency f_{ext} . Whereas f_n is the fundamental natural frequency of the cantilever beam. For the present problem support acceleration and excitation frequency is assumed as $a_0 = 1g$, where $g = 9.8 \text{ m/s}^2$ and $f_{ext} = 125 \text{ Hz}$.

When the fundamental natural frequency of the cantilever beam (f_n) matches the external excitation frequency (f_{ext}), i.e. at the resonance, the beam undergoes maximum deflection and therefore a maximum power is obtained. However, the objective function or power has an exponential increase near the resonance. Here, use of very high order polynomials (typically 7th order) is essential to get a good approximation for the power function. This can be computationally intensive and can become impractical when the number of design variables increases. To overcome this problem, log of the power function, which flattens it significantly, is used as the objective function. This allows the use of lower order polynomial (3rd order) to get an adequate approximation for the log of power function. Notice, since the problem needs to be formulated as a minimization problem, $-\log(P_{out})$ will be minimized.

7.5.3 Mechanical Constraints

Small deflection constraint: The Euler-beam theory for small deflections [48] is used to predict the deformations. Therefore, the tip deflection of the cantilever beam is restricted by

$$\frac{2.5 y_{tip}}{L} \leq 1, \quad (7.13)$$

where y_{tip} is the tip deflection and L is the overall length of the cantilever beam.

Stress constraint: At the resonance condition the cantilever beam may undergo large deflections and may crack. In order to avoid the damage due to fatigue and to stay within the linear elastic limit, the allowable bending stress is taken as 10 % of the maximum allowable bending stress (σ_{bm}). The constraint on bending stress in the cantilever beam is expressed as

$$\frac{\sigma_b}{0.1\sigma_{bm}} \leq 1, \quad (7.14)$$

where σ_b is the bending stress in the cantilever beam. Here, σ_{bm} is taken as 7 GPa [49].

7.5.4 Electrical Constraints

An electrical constraint is imposed on the minimum output voltage required to trigger the energy reclamation circuit as

$$\left(\frac{V_{min}}{V_{Th}} \right) \leq 1; \quad V_{min} = 2 \text{ Volts}, \quad (7.15)$$

where V_{Th} is the Thevenin voltage and V_{min} is the minimum required output voltage for the device.

7.5.5 Design Variables

Based on a preliminary study, move limits on design variables x are chosen to avoid practically impossible designs. The move limits on design variables used in the present optimization problem

are

$$\begin{aligned}
 100 &\leq x_1 \leq 2000 \text{ } (\mu\text{m}), \\
 0.05 &\leq x_2 \leq 0.95, \\
 50 &\leq x_3 \leq 800 \text{ } (\mu\text{m}), \\
 0.1 &\leq x_4 \leq 0.8, \\
 10 &\leq x_5 \leq 500 \text{ } (\mu\text{m}), \\
 3 &\leq x_6 \leq 100 \text{ } (\mu\text{m}),
 \end{aligned}$$

where x_1 is the overall length of cantilever beam (L), x_3 is the width of proof mass (b_{pm}), x_5 is the thickness of proof mass (t_{pm}), and x_6 is the thickness of shim (t_s), see Fig. 7.5. Other geometric parameters such as length of shim and PZT are taken as a fraction of total length (i.e. L) and the width of shim and PZT are taken as a fraction of width of proof mass (i.e. b_{pm}). These fractions are represented by the design variables x_2 and x_4 . Here, due to the fabrication limitations, t_{pzt} is kept fixed at the upper bound and an additional constraint ($b_{pzt} = b_s$) is imposed on the width of shim and PZT. Preliminary results have shown that the length of PZT remains almost equal to that of shim. This equality ($L_{pzt} = L_s$) is used here in order to reduce the total number of design variables. Remaining geometric parameters are obtained using

$$\begin{aligned}
 L_s &= x_1 \cdot x_2, \\
 L_{pzt} &= L_s, \\
 L_{pm} &= x_1 - L_s, \\
 b_s &= x_3 \cdot x_4, \\
 b_{pzt} &= b_s, \\
 t_{pzt} &= 0.5 \text{ } (\mu\text{m}), \\
 t_{pm} &= 500 \text{ } (\mu\text{m}),
 \end{aligned}$$

7.5.6 Uncertainties

For the present problem, the objective (P_{out}) is a function of design variables as well as uncertainties. Here, the effect of uncertainties on objective function can also be taken into account. One way to deal with this problem is, to carry out anti-optimization for the objective function together with constraints in order to get the worst cases. Secondly, at the end of the optimization, an anti-optimization and an optimization for fixed design variables can be carried out to set a bound on the objective function. In the present setting of uncertainty-based optimization, dependency of objective on the uncertainties is not considered. For the present problem, 5% uncertainty will be assumed in the design variables \mathbf{x} such that the bounds on uncertainties can be given as $[0.95x_i; 1.05x_i]$. [43,44]. Whereas, higher variation can be expected in material properties of PZT [46, 50, 51]. Here, uncertainty in material properties of PZT such as, Young's Modulus (E_{pzt}), Density (ρ_{pzt}) and Piezoelectric Coefficient (d_{31}), will be taken as 15 %. It should be noted here, that because of the coupling between the material properties of PZT mentioned above, same uncertainty is used for these material properties of PZT. Uncertainties used in the present optimization are listed in Table 7.1.

Table 7.1: Uncertainties considered for the PZT composite cantilever beam

Thickness of shim (t_s)	$\pm 5 \%$
Thickness of proof mass (t_{pm})	$\pm 5 \%$
Material properties of PZT ($E_{pzt}, \rho_{pzt}, d_{31}$)	$\pm 15 \%$

7.5.7 Material properties

Material properties used in the current electro-mechanical model for the calculation of the power are listed in Table 7.2.

Table 7.2: Material properties used in the electro-mechanical analysis of the PZT composite cantilever beam

Young's Modulus of Silicon (E_s)	169 GPa
Density of Silicon (ρ_s)	2330 kg/m ³
Young's Modulus of PZT (E_{pzt})	60 GPa
Density of PZT (ρ_{pzt})	7500 kg/m ³
Piezoelectric Coefficient (d_{31})	$-100 \cdot 10^{-12}$ mV
Relative permittivity (ϵ_r)	1000
Damping ratio (ζ)	0.01
$\tan \delta$	0.02

7.6 Optimization Results

Results for the design optimization of the PZT composite cantilever beam using the anti-optimization based on CRS are presented here. This includes results from deterministic as well as uncertainty-based optimization. Results for deterministic and uncertainty-based optimization are compared with the baseline design. The baseline design was the first design proposed in [39, 40]. Details of the baseline design are included in Table 7.3.

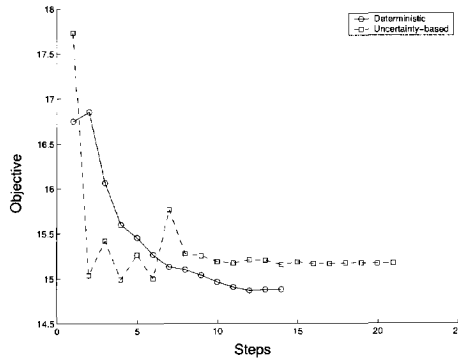


Figure 7.6: Optimization history for objective.

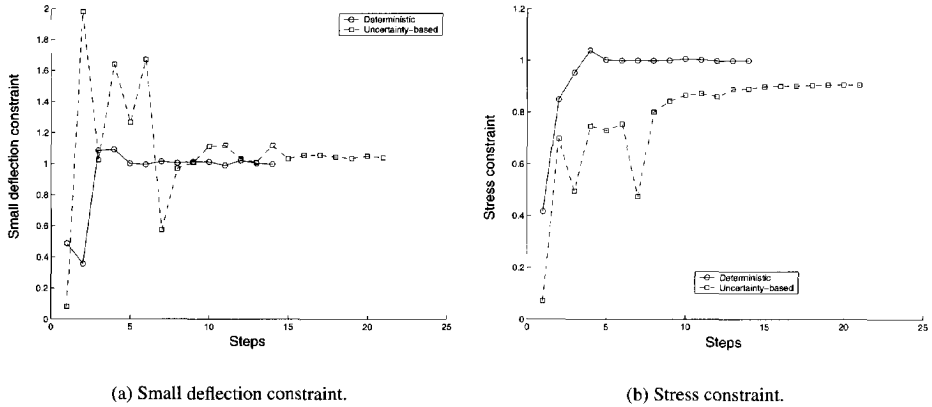


Figure 7.7: Optimization history for constraints.

Table 7.3: Actual dimensions and the output power of the PZT composite cantilever beam for the optimal design is compared with those for baseline design: Case-I is including constraint on (L/b) ratio of shim and PZT whereas Case-II is without including this constraint. $a_0 = 1g$, $f_{ext} = 125\text{Hz}$.

Design		$L_s = L_{pzt}$ μm	L_{pm} μm	$b_s = b_{pzt}$ μm	b_{pm} μm	t_s μm	t_{pzt} μm	t_{pm} μm	P_{out} μW
Baseline		1000	1000	200	800	6	0.5	500	0.16
Optimal	Deter.	208	1792	447	800	3	0.5	500	0.34
	Uncert.	237	1727	569	750	3	0.5	476	0.25

Table 7.4: Worst uncertainties obtained by anti-optimization for the small deflection and stress constraint

Thickness of shim (t_s)	-5 %
Thickness of proof mass (t_{pm})	+5 %
Material properties of PZT (E_{pzt} , ρ_{pzt} , d_{31})	-15 %

The optimization results for deterministic and uncertainty-based optimization using CRS are compared for convergence and number of steps in Fig. 7.6 and Fig. 7.7. Actual dimensions and the output power for the PZT composite beam corresponding to the optimal design are compared with those for the baseline design in Table 7.3. There is a substantial increase in the output power as a result of design optimization as compared to that of the baseline design. The increase in output power is 56 % for the uncertainty-based optimization, whereas it is almost doubled in case of deterministic optimization.

The optimization history as a function of the number of steps (cycles), for the objective function is provided in Fig. 7.6. A comparison between results for deterministic and uncertainty-based optimization shows that there is a significant reduction (26 %) in the objective function value in order to account for uncertainties, see Table 7.3. The optimization history for active constraints is compared for the deterministic and uncertainty-based optimization in Fig. 7.7. In the early phase of the optimization both small deflection constraint (Fig. 7.7(a)) and stress constraint (Fig. 7.7(b)) remain

active, whereas at later stage only small deflection constraint remains active. The convergence and number of steps are quite comparable for both constraints.

In case of small deflection and stress constraint, worst sets of uncertainties obtained at the end of every cycle remain the same. Moreover, for these constraints worst set of uncertainties are found to be at the vertices of the uncertainty domain. Typical values of worst uncertainties for these constraints are given in Table 7.4. For the voltage constraint, worst set of uncertainties fluctuates, however this constraint is not violated throughout the optimization.

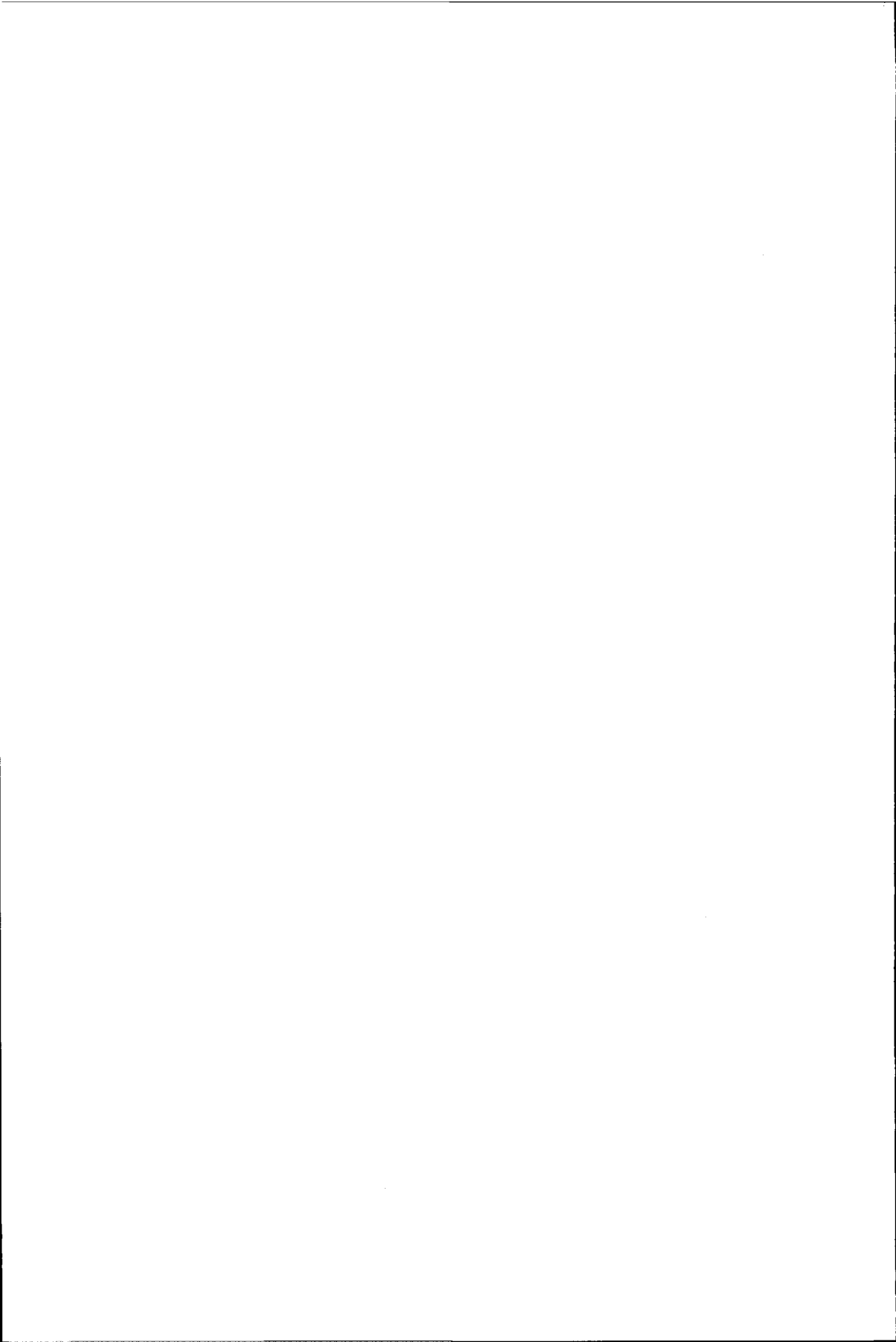
7.7 Discussion and Conclusions

In the present thesis, uncertainties of BBU nature are successfully incorporated in the design optimization process by using CRS for design variables and uncertainties. Use of CRS makes the anti-optimization technique quite flexible in terms of tackling various type of problems. In case of convex uncertainties with limited influence, use of linear approximations for CRS brings the technique close to the asymptotic estimation of uncertainties, which is computationally quite efficient and accurate enough for these problems. In case of non-convexities or largely fluctuating uncertainties, the problem can be solved using higher order approximations. It should be noticed here however, that using higher order CRS can become disadvantageous for problems with many design variables and uncertainties. Finally, its easy implementation makes it a very attractive technique to deal with BBU uncertainties.

In the present thesis, uncertainty-based design optimization of a Piezoelectric Energy reclamation device is carried out using CRS technique. In case of uncertainty-based optimization there is a significant reduction (nearly 20 %) in the output power as compared to that of deterministic optimization, in order to account for uncertainties.

7.8 Acknowledgment

This research is supported by the University of Florida, USA, and Delft University of Technology, Technology Foundation STW, applied science division of NWO and the technology program of the Ministry of Economic Affairs, The Netherlands. We acknowledge here Anurag Kasyap and Dr. Sheplak for providing us with the application problem and the analysis model of Piezoelectric Energy Reclamation Device for this study.



Chapter 8

Conclusions and Recommendations

8.1 Conclusions

In the present thesis, optimization techniques to tackle optimization tasks with Bounded-But-Unknown (BBU) uncertainties are studied. BBU uncertainties are described in terms of bounds or tolerances without having any statistical data. In this thesis, the anti-optimization technique to tackle BBU uncertainties is modified to make it more efficient. As mentioned in the Introduction, first the basic or *Rigorous* anti-optimization technique is modified in order to reduce the number of computationally expensive FEAs. In addition, various alternative approaches are studied in the present thesis. This includes a Cycle-based alternating anti-optimization and a Combined Response Surface (CRS) technique.

8.1.1 Enhanced Anti-optimization

The *Rigorous* anti-optimization technique offers a method to deal with BBU uncertainties, without information on statistical distributions. Moreover, it can be applied to both convex as well as non-convex uncertainties. The price paid for this flexibility is a reduction in computational efficiency due to the required large number of expensive function evaluations. The *Enhanced* anti-optimization uses derivative information and a database technique to reduce the number of expensive function evaluations, resulting in substantial improvement in computational efficiency. This technique is first studied on the basis of test examples and applied to practical problems, such as a car deck floor of a ferry (Chapter 3) and an embedded measurement structure (Chapter 4) for MEMS. For the deck optimization problem, the total number of response evaluations (FEAs) has come down from 5417 to 481 (almost 11 times less) by the use of derivatives and the database technique. For the embedded measurement structure, the total number of response evaluations are halved by the use of derivatives and the database technique. It should be made clear that for this problem the number of design variables and uncertainties involved are relatively small as compared to the deck problem and therefore the reduction that can be achieved is less. Additionally, for the embedded measurement structure, Parallel Computing is used to carry out function evaluations in parallel, in order to reduce computing time. For this problem, Parallel Computing has reduced the wall clock time by nearly 85 %.

Use of sensitivities

Use of derivative information to construct Gradient Enhanced Response Surface (GERS) is advantageous in two ways. First, it improves the quality of the response surface, resulting in better convergence. Second, it requires fewer FEAs to construct the response surfaces, thus reducing the overall number of FEAs. In the present *Enhanced* anti-optimization, derivatives are used in both the main and anti-optimization. This has reduced substantially the overall number of FEAs, making the

technique computationally more efficient. It is concluded here, that the *Enhanced* method can deal with BBU uncertainties quite efficiently, provided gradient information is available at relatively low computational costs.

Use of database technique

Use of the database technique is successful to speed up the anti-optimizations. Here, the history of anti-optimizations for each design is stored in a database. When there is enough data available in the database, it is used to generate good starting points for the anti-optimizations. Use of the database technique has significantly improved the overall computational efficiency of the technique by reducing the number of iterations necessary for convergence.

Parallel Computing

Use of Parallel Computing to carry out expensive function evaluations has significantly improved the computational efficiency of the technique. Here, a cluster of many computers is utilized for evaluating expensive FEAs in parallel. The Parallel Computing framework embedded within the anti-optimization technique is applied successfully to the embedded measurement structure for MEMS. For the embedded measurement structure, use of the Parallel Computing has reduced the wall clock time required for the anti-optimization by nearly 85 % and for the deterministic optimization by 78 %. Finally, it is concluded that if sufficient computing power is available together with derivative information, the *Enhanced* anti-optimization technique can deal with uncertainties robustly and efficiently.

8.1.2 Alternating Anti-optimization

Cycle-based alternating technique

Often, the available computing power is quite limited. This is particularly relevant when many design and/or uncertainty variables are available. Moreover, due to the complexities involved in the simulation model, obtaining derivatives can either be difficult or computationally expensive. For such problems, the *Enhanced* anti-optimization technique can still become impractical. In the present thesis, alternative approaches that avoid two-level optimization, as in case of *Rigorous* and *Enhanced* anti-optimization, have been studied. The Cycle-based alternating anti-optimization technique studied in the present thesis is very efficient as compared to the *Enhanced* anti-optimization. Additionally, it overcomes the slow convergence as observed in the Lombardi-Haftka approach when the worst uncertainties fluctuate w.r.t. change in design. The Cycle-based technique is studied on the basis of a test problem having nonlinear and largely fluctuating uncertainties and is applied to practical applications such as a piezoelectric energy reclamation device (Chapter 5). In case of the piezoelectric energy reclamation device, optimizations are carried out first, by including a constraint on length to width ratio of the shim (Design-I) and second, by excluding this constraint (Design-II). For Design-I, the output power obtained by the uncertainty-based optimization is slightly higher as compared to that of the baseline design. For Design-II, there is almost 60 % increase in the output power obtained by the uncertainty-based optimization as compared to that of the baseline design.

Nested Parallel Computing

While using Parallel Computing in optimization, the additional function evaluation required at the end of an optimization cycle keeps one processor busy and all others idle. With the increase in number of cycles in optimization the overall idle time increases, and, consequently, reduces the overall efficiency of the Parallel Computing scheme. For the *Enhanced* anti-optimization technique every individual function evaluation involves anti-optimization for every constraint. Moreover, each

individual anti-optimization involves several cycles. Thus, the overall idle time associated to the additional response evaluations can grow exponentially. In case of the Cycle-based anti-optimization technique, anti-optimization is carried out only at the suboptimal design for every constraint. Use of the simple Parallel Computing scheme (as discussed in Chapter 4) here, could become quite inefficient. The Nested Parallel Computing Scheme (as discussed in Chapter 6), overcomes this problem. In this scheme, all the anti-optimizations for the suboptimal design are evaluated in parallel. Moreover, for each anti-optimization the actual response evaluations are also carried out in parallel. This scheme is quite efficient in keeping all the processors busy during the optimization, thus, reducing the overall idle time significantly.

The proposed scheme is applied successfully to a SMA microgripper problem, see Chapter 6. For this microgripper problem, the total number of FEAs required for the uncertainty-based optimization is nearly 30 times that of a deterministic optimization. Consequently, in case of sequential evaluation of responses, the total wall clock time required for the uncertainty-based optimization should also be 30 times that of the deterministic optimization. Use of the Nested Parallel Computing scheme, with a cluster of 14 CPUs, has brought down this wall clock time for the uncertainty-based optimization to merely 7.5 times that of the deterministic optimization.

It is concluded here that the Cycle-based technique provides a very efficient way to tackle uncertainties while designing. Particularly for the problems involving computationally expensive FEAs, the Cycle-based technique combined with the Nested Parallel Computing is quite efficient and provides a very practical approach.

8.1.3 Combined Response Surface-based anti-optimization

In an alternative approach considered in this thesis, use of a Combined Response Surface (CRS) for design variables as well as uncertainties is exploited. The ease of implementation and flexibility in tackling problems with different types of uncertainties are attractive features of this technique. The method is applicable to both convex as well as non-convex problems. In the latter situation, nonlinear approximations are more advantageous. Like most other response surface based techniques, the method suffers from the 'curse of dimensionality'. In the present thesis, this technique is applied successfully to a piezoelectric energy reclamation MEMS device. For the piezoelectric energy reclamation device, optimization is carried out without including the constraint on length to width ratio of the shim. Here, the deterministically optimized output power is almost double as compared to that of the baseline design. A significant reduction (nearly 20 %) is seen in the output power for the uncertainty-based optimization as compared to that of deterministic optimization. Still, the output power obtained by the uncertainty-based optimization is nearly 60 % higher than that of the baseline design. Although, the present approach is quite elegant from an implementation point of view, it is concluded here that this approach is only suited for small scale problems, i.e. involving a small number of design variables and/or uncertainties.

8.2 Recommendations

For practical problems, for which information on uncertainties is available only in the form of bounds without any knowledge on statistical distributions, the anti-optimization techniques studied in the present thesis are recommended here. It should be noted however, that the present methodology relies heavily on response surface approximations that are constructed using a limited number of FEAs. Quite often such response surface-based models suffer from high numerical noise. Moreover, the required number of response evaluations can grow exponentially with the increase in design variables and/or uncertainties, thus limiting its applicability. Nevertheless, it provides a very general way to tackle convex as well as non-convex uncertainties.

For applications with a very small probability of failure, for example, in aerospace applications, the methods in the present thesis are very suited. However, these methods are not limited to such

cases only, but are quite general and can be applied to a variety of practical problems. They are particularly useful when the information on uncertainties is available in the form of tolerances or bounds. For practical applications involving FEAs, a combination of the efficient Parallel Computing scheme and the uncertainty-based techniques developed in the present thesis is strongly recommended.

8.2.1 Enhanced Anti-optimization

In case of problems with highly nonlinear and largely fluctuating uncertainties, most other techniques suffer from slow convergence. For such problems, if sensitivities are available inexpensively, use of the *Enhanced* anti-optimization is recommended here. For the problems involving computationally expensive FEAs, this technique is not recommended unless enough computational power is available. This depends, among others, on the number of design variables and/or uncertainties.

8.2.2 Cycle-based Alternating Anti-optimization

This technique is more efficient in terms of overall number of response evaluations as compared to other techniques studied in the present thesis and is therefore recommended in general. In case of non-convexities, however, it may suffer from slower convergence. Combining the asymptotic method, which uses derivatives, with the Cycle-based technique can partially overcome this problem. This technique is particularly recommended when very limited computing power is available with respect to the problem size and if the response evaluation involves expensive FEA.

8.2.3 Combined Response Surface-based anti-optimization

Use of CRS for design variables and uncertainties makes implementation very easy and flexible. However, a higher order response surface may be required if the response as a function of the design variables and/or the uncertainties is highly nonlinear. This may limit its use to small scale problems. Alternatively, it may become inefficient for problems with a large number of design variables and/or uncertainties, due to the so called 'dimensionality curse'. For most problems with a small number of design variables and/or uncertainties, this technique is highly recommended.

8.3 Future work

Further study will be carried out with the Cycle-based and the CRS-based anti-optimization technique. The Cycle-based technique combined with the asymptotic method can be studied further on the basis of a practical problem involving FEA, for which sensitivities are easily and cheaply available. The CRS technique can be exploited further to include sensitivities, a database technique and Parallel Computing. It could be studied further on the basis of practical applications. The applications studied in the present thesis, such as piezoelectric device, microgripper and embedded measurement structure, can be further investigated by adding more design variables, uncertainties and constraints, which were otherwise excluded based on preliminary studies and owing to the practical limitations, such as, limited computing power and unavailability of derivatives.

Additionally, some practical tools such as, a mechanism to check convexity or nonconvexity w.r.t. uncertainties, could be implemented in the current framework. This early stage information could help to choose the best optimization technique. For example, for convex uncertainties vertex checking would be sufficient. Techniques studied in the present thesis can be extended further to include additional information such as distributions based on limited data or data at intermediate intervals within the bounds.

References

- [1] V. V. Toropov, A. A. Filatov, and A. A. Polynkine. Multiparameter structural optimization using fem and multipoint explicit approximations. *Structural Optimization*, 6:7–14, 1993.
- [2] V. V. Toropov, F. van Keulen, V. L. Markine, and L. F. Alvarez. Multipoint approximations based on response surface fitting: a summary of recent results. In *In: V.V. Toropov (ed.) Engineering Design Optimization, Proceedings of 1st, ASMO UK /ISSMO conference, 8-9 July, pages 371–380, Bradford, UK, 1999.* University Press.
- [3] F. van Keulen and V. V. Toropov. Multipoint approximations for structural optimization problems with noisy response functions. In *ISSMO/NASA/AIAA First Internet Conference on Approximations and Fast Reanalysis in Engineering Optimization, 14-27 June, 1998.* CD-ROM.
- [4] F. van Keulen and V. V. Toropov. New developments in structural optimization using adaptive mesh refinement and multipoint approximations. *Engineering Optimization*, 29:217–234, 1997.
- [5] J. H. Jacobs, L. F. P. Etman, F. van Keulen, and J. E. Rooda. Framework for sequential approximate optimization. *Struct. Multidisc. Optim.*, 27(5):384–400, 2004.
- [6] W. L. Oberkampf, J. C. Helton, and K. Sentz. Mathematical representation of uncertainty. In *Proceedings of the 42nd AIAA/ASME/ASCE/AHS/ASC Structures, Structural Dynamics, and Materials Conference and Exhibit, Seattle, WA, U.S.A., Paper 1242, 16-19 April, 2001.* CD-ROM.
- [7] I. Elishakoff, R. T. Haftka, and J. J. Fang. Structural design under bounded uncertainty-optimization and anti-optimization. *International Journal of Computers & Structures*, 53:1401–1405, 1994.
- [8] I. Elishakoff. *Probabilistic methods in the theory of structures.* John Wiley and Sons, 1983.
- [9] I. Elishakoff. *Whys and hows in uncertainty modelling: Chap. 5 - Are probabilistic and anti-optimization approaches compatible?* SpringerWienNewYork, 1999.
- [10] H.-R. Bae, R. V. Grandhi, and R. A. Canfield. Epistemic uncertainty quantification techniques including evidence theory for large scale structures. *Computers & Structures*, 82:1101–1112, 2004.
- [11] Y. Ben-Haim and I. Elishakoff. *Convex models of uncertainty in applied mechanics.* Elsevier, 1990.
- [12] Y. Ben-Haim. *Robust reliability in the mechanical sciences.* Springer, 1996.
- [13] F. van Keulen, H. J. Damveld, I. Elishakoff, and V. V. Toropov. Bounded-but-unknown uncertainties in design optimization. In *Proceedings of the 42nd AIAA/ASME/ASCE/AHS/ASC Structures, Structural Dynamics, and Materials Conference and Exhibit, Seattle, WA, U.S.A., Paper 1242, 16-19 April, 2001.* CD-ROM.
- [14] F. van Keulen, R. T. Haftka, and N. H. Kim. Review of options for structural design sensitivity analysis. part 1: Linear systems, in press. *Computer Methods in Applied Mechanics and Engineering*, 2005.

- [15] F. van Keulen and H. de Boer. Rigorous improvement of semi-analytical design sensitivities by exact differentiation of rigid body motions. *Int. J. Numerical Methods in Engineering*, 42:71–91, 1998.
- [16] H. de Boer and F. van Keulen. Refined semi-analytical design sensitivities. *Int. J. Solids and Structures*, 37(46-47):6961–6980, 2000.
- [17] F. van Keulen and K. Vervenne. Gradient-enhanced response surface building. *Struct. Multi-disc. Optim.*, 27(5):337–351, 2004.
- [18] K. Vervenne and F. van Keulen. An alternative approach to response surface building using gradient information. In *Proceedings of the 43rd AIAA/ASME/ASCE/AHS/ASC Structures, Structural Dynamics, and Materials Conference and Exhibit, Denver, CO, USA, Paper 1584, 22-25 April, 2002*. CD-ROM.
- [19] M. Lombardi and R. T. Haftka. Anti-optimization technique for structural design under load uncertainties. *Computer Methods in Applied Mechanics and Engineering*, 157:19–31, 1998.
- [20] S. P. Gurav, M. Langelaar, J. F. L. Goosen, and F. van Keulen. Different approaches to deal with bounded-but-unknown uncertainties: Application to mems. In *Proceedings of the 5th World Conference on Structural and Multidisciplinary Optimization, Venice, Italy., 19-23 May, 2003*.
- [21] X. Qu, S. Venkataraman, and R. T. Haftka. Response surface options for reliability-based optimization of composite laminate. In *Proceedings of the 8th ASCE Specialty Conference on Probabilistic Mechanics and Structural Reliability, PMC2000-131, 2000*.
- [22] A. I. Khuri and J. A. Cornell. *Response Surfaces, Design and Analyses, Second Edition, Revised and Expanded*. Marcel Dekker, Inc., New York, 1996.
- [23] R. H. Myers and D. C. Montgomery. *Response Surface Methodology; Process and Product Optimization using Designed Experiments*. John Wiley & Sons Inc., New York, 1995.
- [24] M. Lutz. *Programming Python*. O'Reilly, 2001.
- [25] F. van Keulen and V. V. Toropov. The multipoint approximation method in a parallel computing environment. *ZAMM*, 79(S1):S67–S70, 1999.
- [26] I. Elishakoff. An idea of uncertainty triangle. *The Shock & Vibration Digest*, 22, 1990.
- [27] F. van Keulen, B. Liu, and R. T. Haftka. Noise and discontinuity issues in response surfaces based on functions and derivatives. In *Proceedings of the 41st AIAA/ASME/ASCE/AHS/ASC Structures, Structural Dynamics, and Materials Conference and Exhibit, Atlanta, GA, 3-6 April 2000, Paper AIAA-00-1363, 2000*. CD-ROM.
- [28] S. R. Lauridsen, S. R. Vitali, F. van Keulen, R. T. Haftka, and J. I. Madsen. Response surface approximations using gradient information. In *World Congress of Structural and Multidisciplinary Optimization, Dalian, China, June 4-8, 2001*.
- [29] F. van Keulen and J. Booi. Refined consistent formulation of a curved triangular finite rotation shell element. *Int. J. Numerical Methods in Engineering*, 39:2803–2830, 1996.
- [30] J. V. Clark, D. Garmire, M. last, J. Demmel, and S. Govindjee. Practical techniques for measuring mems properties. In *Proc. of the NanoTech 2004, Boston, MA, USA, 7-11 March, 2004*.
- [31] K. Pister. Introduction to mems design and fabrication. In *EECS 245 Reader University of California, Berkeley, CA, pp. 9-45, 2001*.

- [32] A. R. de Faria. Buckling optimization and antioptimization of composite plates: uncertain loading combinations. *Int. J. Numerical Methods in Engineering*, 53:719–732, 2002.
- [33] S. Adali, F. Lene, G. Duvaut, and V. Chiaruttini. Optimization of laminated composites subject to uncertain buckling loads. *Composite Structures*, 62:261–269, 2003.
- [34] S. P. Gurav, K. Vervenne, H. J. Damveld, and F. van Keulen. Bounded-but-unknown uncertainties in design optimization by combining the multipoint approximation method and design sensitivities. In *Proceedings of the 43rd AIAA/ASME/ASCE/AHS/ASC Structures, Structural Dynamics, and Materials Conference and Exhibit, Denver, CO, U.S.A., Paper 1759, 22-25 April, 2002*.
- [35] B. P. van Drieënhuizen, J. F. L. Goosen, P. J. French, and R. F. Wolffenbaffel. Comparison of techniques for measuring both compressive and tensile stress in thin films. *Sensors and Actuators*, 37-38:756–765, 1993.
- [36] J. F. L. Goosen, B. P. van Drieënhuizen, P. J. French, and R. F. Wolffenbuttel. Stress measurements structures for micromachined sensors. In *Proc. Transducers '93, pp. 783-786, 1993*.
- [37] S. P. Gurav, A. Kasyap, M. Sheplak, L. Cattafesta, R. T. Haftka, J. F. L. Goosen, and F. van Keulen. Uncertainty-based design optimization of a micro piezoelectric composite energy reclamation device. In *Proceedings of the 10th AIAA/ISSMO Multidisciplinary Analysis and Optimization Conference, Aug. 31 - Sept. 1, 2004*.
- [38] R. T. Haftka and Z. Gürdal. *Elements of structural optimization*. Kluwer Academic Publishers, second revised edition edition, 1990.
- [39] A. Kasyap. A theoretical and experimental study of piezoelectric composite cantilever beams for energy reclamation. Master's thesis, University of Florida, 2002.
- [40] A. Kasyap, J. Lim, K. Ngo, A. Kurdila, T. Nishida, M. Sheplak, and L. Cattafesta. Energy reclamation from a vibrating piezoceramic composite beam. In *Proc. of the 9th Int. Congress on Sound and Vibration, Orlando, FL, USA, 8-10 July, 2002*.
- [41] E. F. Crawley and J. D. de Luis. Use of piezoelectric actuators as elements of intelligent structures. *AIAA*, 25:1373–1385, 1987.
- [42] L. N. Cattafesta, S. Garg, and A. E. Washburn. Piezoelectric actuators for fluid-flow control. In *Proc. of the SPIE, 3044:147-157, 1997*.
- [43] B. D. Jensen, M. P. de Boer, N. D. Masters, F. Bitsie, and D. A. La Van. Interferometry of actuated microcantilevers to determine material properties and test structure nonidealities in mems. *Journal of Microelectromechanical Systems*, 10(3):336–346, 2001.
- [44] P. M. Osterberg and S. D. Senturia. M-test: A test chip for mems material property measurement using electrostatically actuated test structures. *Journal of Microelectromechanical Systems*, 6(2):107–118, 1997.
- [45] W. N. Sharpe, K. T. Turner, and R. L. Edwards. Tensile testing of polysilicon. *Experimental Mechanics*, 39(3):162–170, 1999.
- [46] S. Nakamura, H. Numasato, K. Sato, M. Kobayashi, and I. Naniwa. A push-pull multi-layered piggyback pzt actuator. *Microsystem Technologies*, 8:149–154, 2002.
- [47] S. P. Gurav, J. F. L. Goosen, and F. van Keulen. Uncertainty-based design optimization of structures using bounded-but-unknown uncertainties, design sensitivities and parallel computing: Application to MEMS. *Computers & Structures*, 83/14:1134–1149, 2005.

- [48] W. T. Thomson. *Theory of Vibration with Applications*. Prentice Hall, 4th edition, 1993.
- [49] K. E. Peterson. Silicon as a mechanical material. In *Proc. of IEEE*, 70, pp. 420-457, 1982.
- [50] D. Halliday and R. Resnick. *Fundamentals of physics*, p.808. John Wiley & Sons, third edition.
- [51] P. A. Tipler and G. Mosca. *Fundamentals of physics: Extended edition*, Ch.36, p.1211. Freeman & Co., third extended edition.
- [52] K. Otsuka and C.M. Wayman, editors. *Shape Memory Materials*. Cambridge University Press, 1998.
- [53] T.W. Duerig, K.N. Melton, D. Stöckel, and C.M. Wayman, editors. *Engineering Aspects of Shape Memory Alloys*. Butterworth-Heinemann, London, 1990.
- [54] H. Tobushi, K. Tanaka, K. Kimura, T. Hori, and T. Sawada. Stress-strain-temperature relationship associated with the R-phase transformation in Ti-Ni shape memory alloy. *JSME International Journal Series I - Solid Mechanics Strength of Materials*, 35(3):278-284, July 1992.
- [55] M. Kohl, D. Brugger, M. Ohtsuka, and T. Takagi. A novel actuation mechanism on the basis of ferromagnetic SMA thin films. 114(2-3):445-450, September 2004. Selected papers from Transducers 03.
- [56] M. Langelaar and F. van Keulen. A simple R-phase transformation model for engineering purposes. *Materials Science and Engineering: A - Structural Materials: Properties, Microstructure and Processing*, 378(1-2):507-512, July 2004.
- [57] M. Langelaar and F. van Keulen. Modeling of a shape memory alloy active catheter. In *12th AIAA/ASME/AHS Adaptive Structures Conference, Palm Springs, CA*, 2004. AIAA paper 2004-1653.
- [58] M. Langelaar, G.H. Yoon, Y.Y. Kim, and F. van Keulen. Topology optimization of shape memory alloy thermal actuators using element connectivity parameterization. In preparation.
- [59] T. Sawada, H. Tobushi, K. Kimura, T. Hattori, K. Tanaka, and P.H. Lin. Stress-strain-temperature relationship associated with the R-phase transformation in TiNi shape memory alloy (influence of shape memory processing temperature). *JSME International Journal Series A: Mechanics and Material Engineering*, 36(1):395-401, 1993.
- [60] M. Langelaar and F. van Keulen. Design optimization of shape memory alloy structures. In *10th AIAA/ISSMO Multidisciplinary Analysis and Optimization Conference, Albany, NY*, 2004. AIAA paper 2004-4414.
- [61] G. Farin. *Curves and surfaces for CAD : a practical guide*. Kaufmann, San Francisco, 2002.
- [62] F. van Keulen and J. Booiij. Refined consistent formulation of a curved triangular finite rotation shell element. *International Journal for Numerical Methods in Engineering*, 39(16):2803-2820, 1996.
- [63] G. Kreisselmeier and R. Steinhauser. Application of vector performance optimization to a robust control loop design for a fighter aircraft. *International Journal of Control*, 37:251-284, 1983.
- [64] S. P. Gurav, M. L. Langelaar, and F. van Keulen. Uncertainty-based design optimization of structures by using alternating anti-optimization combined with the nested parallel computing: Application to shape memory alloy microgripper; submitted to. *Computers & Structures*, 2005.

Publications based on present work

S. P. Gurav, K. Vervenne, H. J. Damveld, and F. van Keulen, Bounded-but-unknown uncertainties in design optimization by combining the multipoint approximation method and design sensitivities, *Proceedings of the 43rd AIAA/ASME/ASCE/AHS/ASC Structures, Structural Dynamics, and Materials Conference and Exhibit*, Denver, CO, U.S.A., Paper 1759, 22-25 April, 2002.

S. P. Gurav, M. Langelaar, J. F. L. Goosen, and F. van Keulen, Different approaches to deal with Bounded-But-Unknown uncertainties: Application to MEMS, *Proceedings of the 5th World Conference on Structural and Multidisciplinary Optimization*, Venice, Italy, 19-23 May, 2003.

S. P. Gurav, M. Langelaar, J. F. L. Goosen, and F. van Keulen, Bounded-but-unknown uncertainty optimization of micro-electro-mechanical systems, *Proceedings of the 2nd MIT Conference on Computational Fluid and Solid Mechanics*, MIT, Cambridge, MA 02139, U.S.A., Paper 479, 17-20 June, 2003.

S. P. Gurav, A. Kasyap, M. Sheplak, L. Cattafesta, R. T. Haftka, J. F. L. Goosen, and F. van Keulen, Uncertainty-based Design Optimization of a Micro Piezoelectric Composite Energy Reclamation Device, *Proceedings of the 10th AIAA/ISSMO Multidisciplinary Analysis and Optimization Conference*, Albany, New York, U.S.A., Aug. 31 - Sept. 1, 2004.

S. P. Gurav, J. F. L. Goosen, and F. van Keulen, Uncertainty-Based Design Optimization of Shape Memory Alloy Microgripper using combined Cycle-based Alternating Anti-optimization and Nested Parallel Computing, *Proceedings of the 6th World Congress on Structural and Multidisciplinary Optimization, ISSMO*, Rio de Janeiro, Brazil, May 30 - June 3, 2005.

S. P. Gurav, J. F. L. Goosen, and F. van Keulen, Uncertainty-Based Design Optimization of structures using Bounded-But-Unknown Uncertainties, Design Sensitivities and Parallel Computing: Application to MEMS, *Computers and Structures*, 2005, 83/14, 1134-1149.

S. P. Gurav, M. L. Langelaar, and F. van Keulen, Uncertainty-Based Design Optimization of structures by using Alternating Anti-optimization combined with the Nested Parallel Computing: Application to Shape Memory Alloy Microgripper, *Computers and Structures*, submitted.

S. P. Gurav, and F. van Keulen, Uncertainty-Based Design Optimization of structures using Combined Response Surface for design variables and uncertainties: Application to Piezoelectric Energy Reclamation Device, *Computers and Structures*, will be submitted.



Summary

These days most of the design problems for practical applications involve uncertainties. Some of these uncertainties are of reducible nature and can be influenced by the designer to some extent. Other types of uncertainties are inherent or irreducible. The methods to tackle various types of uncertainties can be classified mainly in three different ways, namely probabilistic approach, fuzzy-sets-based approach, and the anti-optimization. Probabilistic techniques have been developed mainly to deal with random uncertainties described using statistical distributions, fuzzy-sets-based techniques originated from the vague or qualitative description of uncertainties, and anti-optimization is developed to tackle bounded uncertainties. In the present thesis, uncertainties considered are of Bounded-But-Unknwon (BBU) type, i.e., uncertainties are specified with tolerances or bounds on them and exact distribution within the bounds is unknown. The anti-optimization technique looks at the worst case scenario for the responses. It consist of performing numerical searches for the combination of uncertainties, which yields the worst response for a given design and a particular response function. The anti-optimization technique from literature assumes that uncertainties are of convex nature. The anti-optimization technique using vertex checking is computationally efficient, but limits its application to convexity in terms of uncertainties. In the present thesis, the anti-optimization technique is generalized such that convexity and nonconvexity in the uncertainties can be handled easily.

The methods developed in the present thesis rely on use of response surface approximations. The Multipoint Approximation Method (MAM), which is based on response surface approximations, is used as a basis here. The MAM is based on solving a sequence of approximate optimization problems. Each individual approximate optimization problem involves a mathematical programming problem using computationally inexpensive explicit functions for responses. This may result in a substantial reduction of overall computational costs in case of problems involving computationally expensive Finite Element Analysis (FEA).

The generalized anti-optimization technique developed in the present thesis, consists of a two-level optimization approach, where anti-optimization for each of the constraints is carried out for every design within the main optimization. This generalized or *Rigorous* anti-optimization technique can deal with large and non-convex uncertainties safely. However, it requires a large number of computationally expensive function evaluations. In the present thesis, the *Rigorous* anti-optimization technique is enhanced to improve the computational efficiency by using sensitivities, a database technique and Parallel Computing. Additionally, alternative approaches, which can avoid two level optimizations but can tackle non-convex uncertainties as well, are studied in the present thesis. This includes *Cycle-based* alternating anti-optimization and Combined Response Surface (CRS) based anti-optimization technique. The methods are studied on the basis of test examples and applied to practical applications. The practical applications studied in the present thesis, include a car deck floor of a ferry, an embedded measurement structure from MEMS, a piezoelectric energy reclamation MEMS device, and a Shape Memory Alloy (SMA) microgripper.

The *Enhanced* anti-optimization technique developed in the present thesis uses, sensitivity information to construct Gradient Enhanced Response Surfaces. This has resulted in substantially reduction of the overall number of function evaluations making the technique computationally very efficient. Alternately, this incorporation of sensitivities improves the quality of the response sur-

face approximations thus improving the convergence. Secondly, a database technique is developed, which is used here to predict good starting points for anti-optimizations. In this, the worst sets of uncertainties obtained by the anti-optimizations from previous cycles are stored in a database. When there is enough data available in the database, it is used for estimating good starting points for the anti-optimizations. Use of the database technique has improved significantly the overall computational efficiency of the technique. In case of practical applications, where response evaluation is carried out using, e.g., FEA, even with these improvements the anti-optimization technique becomes impractical. Here, a cluster of fast computers is utilized for evaluating expensive FEAs in parallel. A Parallel Computing framework based on PYTHON programming language is used here. Use of Parallel Computing to evaluate expensive function evaluations has significantly improved the overall computational efficiency of the technique. The technique is applied to practical applications such as, a car deck floor of ferry and an embedded measurement structure from MEMS.

In the *Cycle-based* alternating anti-optimization technique developed in the present thesis, instead of nesting anti-optimization within the main optimization, main and anti-optimization are carried out alternately. This technique is inspired from the Lombardi-Haftka approach. In this technique, anti-optimization is carried out only at the sub-optimal point, i.e. the point obtained at the end of each cycle of the main optimization. This *Cycle-based* technique is very computationally efficient as compared to the *Enhanced* anti-optimization. The uncertainty-based design optimization of a piezoelectric energy reclamation device is carried out successfully using the *Cycle-based* technique. In the present thesis, a Nested Parallel Computing scheme is developed to exploit efficient use of available computing power. The Nested Parallel Computing combined with the *Cycle-based* alternating anti-optimization technique provides a very computationally efficient technique. The combined technique is successfully applied to a SMA microgripper problem.

Finally, a CRS-based anti-optimization technique is developed in the present thesis and studied on the basis of a piezoelectric energy reclamation MEMS device. In this, a CRS for design variables as well as uncertainties is used as a basis for the anti-optimization. This technique is quite flexible in dealing with both convex as well as non-convex uncertainties due to the underlying simplicity and ease in implementation of the technique. Like most other response surface based techniques, the method suffers from the 'curse of dimensionality' with the increase in design variables and uncertainties.

S.P. Gurav

Samenvatting

De meeste ontwerproblemen in de hedendaagse praktijk gaan gepaard met onzekerheden. Sommige van deze onzekerheden kunnen tot op zekere hoogte door de ontwerper verminderd of vermeden worden. Andere onzekerheden zijn inherent aan het beschouwde probleem en laten zich niet inperken. De methoden om te gaan met de verscheidene onzekerheden kunnen ingedeeld worden in drie categorieën, te weten de kansrekening-gebaseerde methoden, de zogenaamde 'fuzzy sets' technieken en anti-optimalisatie. Kansrekening - gebaseerde methoden zijn in hoofdzaak ontwikkeld voor toepassingen waar onzekerheden beschreven kunnen worden in termen van kansverdelingen afgeleid van statistieken. Fuzzy sets technieken hebben hun oorsprong in een vage of kwalitatieve beschrijving van onzekerheden. Anti-optimalisatie, is ontwikkeld voor het omgaan met begrensde onzekerheden waarover verder niet veel bekend is. In dit proefschrift worden onzekerheden beschouwd als behorend tot deze laatste categorie, de zogenaamde "Bounded-But-Unknown" (BBU) onzekerheden. Dit wil zeggen dat de onzekere grootheden slechts gekarakteriseerd worden door toleranties of grenzen, en hun statistische verdeling binnen die grenzen is onbekend. De anti-optimalisatie techniek richt zich op het slechtste geval (worst case) voor het beschouwde probleem. Het uitgangspunt is om numeriek te zoeken naar die combinatie van onzekerheden, die resulteert in de slechtste situatie voor een gegeven ontwerp en een gegeven resultaatwaarde. De anti-optimalisatie methode uit de literatuur gaat ervan uit dat de onzekerheden zich convex gedragen. Anti-optimalisatie via de zogenaamde "vertex checking" methode is numeriek efficiënt, maar de toepassing van deze methode beperkt zich tot problemen waar de onzekerheden inderdaad convex zijn. In dit proefschrift wordt de gangbare anti-optimalisatie methode gegeneraliseerd, zodat zowel met convexiteit als niet-convexiteit in de onzekerheden eenvoudig omgegaan kan worden.

De methoden die in dit proefschrift beschreven worden zijn gebaseerd op het gebruik van benaderingen van de resultaatwaarden, de zogenaamde response surface benaderingen. De zogenaamde Multipoint Approximation Method (MAM), tevens gebaseerd op response surface benaderingen, wordt gebruikt voor het uitvoeren van de optimalisatie. De MAM is gebaseerd op het oplossen van een opeenvolgende serie van benaderende optimalisatieproblemen. Elk afzonderlijk benaderend optimalisatieprobleem maakt gebruik van resultaatfuncties beschreven met eenvoudige expliciete wiskundige formules. Deze aanpak leidt tot een aanzienlijke reductie van de totale benodigde rekentijd in het geval van problemen met rekenintensieve modellen, zoals eindige elementen analyses (EEA).

De gegeneraliseerde anti-optimalisatie methode omschreven in dit proefschrift bestaat uit een optimalisatie op twee niveau's, waarbij anti-optimalisatie wordt toegepast voor elke beperkende voorwaarde voor ieder ontwerp binnen het hoofd-optimalisatie probleem. Deze gegeneraliseerde of *Rigoreuze* anti-optimalisatie techniek kan veilig omgaan met grote en niet-convexe onzekerheden. Echter, het benodigde aantal rekenintensieve functie-evaluaties is groot. In dit proefschrift wordt de *Rigoreuze* anti-optimalisatie methode uitgebreid met het gebruik van ontwerpafgeleiden, een database en parallelle rekenmethode, om zodoende de rekenkundige efficiëntie te vergroten. Daarnaast worden in dit proefschrift ook alternatieve benaderingen bestudeerd, waarbij de optimalisatie op twee niveau's vermeden kan worden, maar welke toch in staat zijn om te gaan met niet-convexe onzekerheden. Deze technieken omvatten de *Cyclus-gebaseerde* alternerende anti-optimalisatie en de anti-optimalisatie op basis van een Gecombineerd Response Surface (GRS).

Deze methoden worden bestudeerd op basis van testvoorbeelden, en toegepast op praktische problemen. De praktijktoepassingen die in dit proefschrift gebruikt worden omvatten onder meer een vloerconstructie voor het parkeerdek van een veerboot, een geïntegreerde rekmeetstructuur voor gebruik in microsystemen, een micro-elektro-mechanisch piëzo-elektrisch energie-winnings systeem, en een microgripper gemaakt van geheugenmetaal.

De in dit proefschrift ontwikkelde *Verrijkte* anti-optimalisatie techniek maakt in de eerste plaats gebruik van ontwerpafgeleiden voor het construeren van zogenaamde Gradient Enhanced Response Surfaces. Dit heeft geresulteerd in een aanzienlijke reductie van het totaal aantal functie-evaluaties, en dit maakt deze methode zeer efficiënt. Anderszijds verbetert het gebruik van ontwerpafgeleiden de kwaliteit van de response surface benaderingen, wat resulteert in verbeterd convergentiegedrag. Ten tweede wordt ook een database-techniek toegepast voor het voorspellen van geschikte startpunten voor de anti-optimalisatie. Hierbij worden de slechtste combinaties van onzekerheden uit voorgaande stappen opgeslagen in een database. Wanneer voldoende informatie is verzameld, kan deze gebruikt worden voor het genereren van goede startpunten voor de anti-optimalisatie. De rekenkundige efficiëntie van de totale methode is significant verbeterd dankzij het gebruik van deze database-techniek. Echter, in het geval van praktische toepassingen waarbij de functie-evaluaties gedaan worden via rekenintensieve modellen, zoals bijvoorbeeld EEA, blijkt dat zelfs met deze verbeteringen de anti-optimalisatie methode niet direct bruikbaar is. In deze situatie worden daarom tevens parallele rekentechnieken toegepast op een cluster van krachtige computers, om de rekenintensieve EEA modellen parallel te kunnen evalueren. Hierbij wordt gebruik gemaakt van een besturingsprogramma voor parallel rekenen geschreven in de PYTHON programmeertaal. Met behulp van deze parallele rekenmethoden is de totale benodigde rekentijd voor anti-optimalisatie van problemen met rekenintensieve modellen significant verminderd. De effectiviteit van deze methode wordt in dit proefschrift geïllustreerd aan de hand van een aantal praktische voorbeelden, onder meer de genoemde vloerconstructie voor het parkeerdek van een veerboot en de geïntegreerde rekmeetstructuur voor gebruik in microsystemen.

Bij de in dit proefschrift beschreven *Cyclus-gebaseerde* alternerende anti-optimalisatie methode worden de hoofd- en anti-optimalisatie om en om uitgevoerd, in plaats van de anti-optimalisatie te nesten in de hoofd-optimalisatie. Deze techniek is geïnspireerd op de Lombardi-Haftka methode. In deze *Cyclus-gebaseerde* methode wordt de anti-optimalisatie slechts uitgevoerd voor ieder sub-optimaal ontwerp, dat wil zeggen het ontwerp dat gevonden wordt aan het eind van elke cyclus van de hoofd-optimalisatie. Deze techniek biedt in verhouding tot de *Verrijkte* anti-optimalisatie een nog verdere verbetering van de rekenkundige efficiëntie. De optimalisatie van het micro-elektro-mechanisch piëzo-elektrisch energie-winnings systeem onder onzekerheden is met succes uitgevoerd volgens deze methode. In dit proefschrift wordt tevens een *geneste parallele rekenmethode* ontwikkeld om, in combinatie met de genoemde *Cyclus-gebaseerde* alternerende anti-optimalisatie, de beschikbare rekenkracht zo goed mogelijk te benutten. Hierdoor ontstaat een zeer efficiënte gecombineerde methode, die met succes is toegepast voor het ontwerpen van een microgripper gemaakt van geheugenmetaal.

Tenslotte wordt in dit proefschrift ook een anti-optimalisatie methode op basis van een Gecombineerd Response Surface (GRS) uitgewerkt, en deze wordt geëvalueerd via toepassing op het ontwerp van een micro-elektro-mechanisch piëzo-elektrisch energie-winnings systeem. Hierbij wordt een GRS opgesteld voor zowel ontwerpvariabelen als onzekerheden en gebruikt in de anti-optimalisatie. Deze methode kan omgaan met zowel convexe als niet-convexe onzekerheden, en blijkt relatief eenvoudig te implementeren. Echter, zoals de meeste andere response surface methoden is ook deze techniek niet immuun voor de zogenaamde 'curse of dimensionality' - de vloek der dimensies. Dit houdt in dat met het toenemen van het aantal ontwerpvariabelen en onzekerheden de benodigde rekeninspanning tevens zeer sterk toeneemt.

Acknowledgments

I would like to acknowledge here that this research is supported by the Technology Foundation STW, applied science division of NWO and the technology program of the Ministry of Economic Affairs, The Netherlands.

I would like to acknowledge the endless help of my supervisor Fred van Keulen. You really helped me at some critical moments at the beginning of the Ph.D. work. Its your continuous encouragement and support that helped me to successfully finish this research work in time. You always shared your experiences and knowledge with me, which helped me tremendously to improve myself.

I would like to thank the ADOPT project team for their support during various phases of project. I would like to thank Fred van Keulen, Koen Vervenne, Rene van Rooij, Johan Jacobs, Pascal Etman, Bert Schoofs, Koo Rijpkema, Henk Nijmeijer, and Koos Rooda. Special thanks to Margriet Jansz from Technology Foundation STW for her enthusiastic encouraging and showing interest in the research activities.

I would like to thank Hans Goosen for his very kind guidance and help. Special thanks to Jan Booij and Marianne Stolker for their very kind help and support. Many thanks to Matthijs Langelaar, Gih-Keong Lau, Albert Jan de Wit, Andriy Andreykiv, Peterjan Broomans, Caspar Bolsman, Chiara Cerulli, Javad Fatemi, Gerard Poort, Teun Weustink, and Marten Jan de Ruiter for their kind help in one way or another. They all together created a very enjoyable environment.

I would like to thank Daniel Rixen, Prabhu Kandachar and Jan Spoormaker for their kind help and support during my research at the Industrial Design Department. Special thanks to Jan Spoormaker for his help regarding the VISA procedures for my wife. I would like to thank colleagues from Nedtech Engineering B.V., Hoofddorp for their kind support in the last phase of my thesis. I would like to thank colleagues from AOES Netherlands B.V., Leiden for their kind support.

I would like to acknowledge a very kind support of Mark Sheplak, Lou Cattafesta during my research work at the IMG group of the University of Florida. Additionally, a very friendly guidance given by Rafi Haftka during this project helped me to successfully finish it. I really enjoyed working together with Anurag Kasyap during this project. You all made my stay at Gainesville very enjoyable and memorable.

I would like to thank my elder brother, Pradeep and my father, Prabhakar Gurav for their continuous guidance and encouragement from beginning. I would like to thank my wife, Dipa, for her all time support and help. Finally, thanks to all our friends and relatives who helped us in one way or another.



About the Author

Sham Gurav was born on 6 November 1974 in Rukadi, India. He entered in 1992 engineering college after finishing High School studies. He obtained Bachelor of Engineering (B.E.) degree in Civil Engineering at the Walchand College of Engineering, Sangli, India in 1996. After two years of experience in Civil Engineering practice, he joined Master of Technology (M.Tech.) in Aerospace Engineering at the Indian Institute of Technology, Chennai, India in 1998. During his Master's studies, he carried out research project at the Dresden University of Technology in Germany. After obtaining M.Tech. degree in May 2000, he joined a project work at the Industrial Design department of the Delft University of Technology. In 2002 he started his Ph.D. research at the Structural Optimization and Computational Mechanics Group of the Mechanical Engineering Department of the Delft University of Technology. He carried out this research work until July 2005 under the supervision of Prof.dr.ir. Fred van Keulen. During his Ph.D. research work, he spent three months at the Interdisciplinary Microsystems Group of the University of Florida, Gainesville, U.S.A. as a visiting scholar to work on optimization of a Piezoelectric MEMS energy reclamation device.

